Mapping Super-Relaxed States of Myosin Heads in Sarcomeres using Oblique Angle Fluorescent Microscopy

Matvey Pilagov

A Thesis Submitted to the University of Kent for the degree of

Master of Science in Biochemistry

September 2021

Supervisor: Prof Neil M. Kad

1. Acknowledgements

I would like to sincerely thank my supervisor Neil Kad, my colleagues Rob, Antoine, James and Lorenzo for giving me a chance and teaching me most (everything) I know about life in research.

2. Table of contents

3. Abbreviations

SRX – Super Relaxed State
DRX – Disordered Relaxed State
ATP – Adenosine Triphosphate
ADP – Adenosine Diphosphate
MAVA – Mavacamten
ELC – Essential Light Chain
RLC - Regulatory Light Chain
HMM – Heavy Meromyosin
LMM – Light Meromyosin
MOPS - 3-(N-morpholino) propanesulfonic acid
EGTA - Ethylene glycol-bis(β-aminoethyl ether)-N,N,N',N'-tetraacetic Acid
OAF – Oblique Angle Fluorescence
RPM – Revolutions Per Minute
S1 – Subfragemnt 1 of Myosin Head
S2 – Subfragemnt 2 of Myosin Head
STORM - Stochastical Optical Reconstruction Microscopy
Å – Angstrom
Da – Dalton

4. Abstract

We have utilised modern methods of super-resolution fluorescent microscopy to spatially map fluorescently labelled ATP molecules in relaxed rabbit psoas skeletal muscles. For our imaging process, we have labelled ATP molecules with Rhodamine and Z-lines with Alexa488. Data from imaging these fluorophores have been collected using oblique angle fluorescent microscopy and further analysed to map super relaxed states (SRX) of myosin heads on the thick filament. Our experiments have concluded that most SRX of myosin heads were found in the C-zone of the thick filament, while other zones of thick filament had smaller populations of SRX. Further introduction of mavacamten (MAVA) to our imaging system has revealed an increase in SRX in both D and P zones, while the C zone population of SRX had remained constant. Further experiments must be conducted to establish a clear pattern and further proof our findings.

5. Introduction

A. Muscle composition

i. Muscle Tissue

Muscle is a type of soft tissue found in animals that enables organisms to move. Muscle has importance not only in gross body movement but also permits peristalsis and cardiac contraction. There are two primary types of muscle tissue: smooth and striated. The latter can be either skeletal or cardiac (see Figure 1). As its name suggests, cardiac muscle is found in the heart and is marked by its inability to fatigue despite pumping continuously over the organism's lifetime. In

humans, the amount of blood pumped by the heart is vast, estimated as ~80 Olympic-sized swimming pools in a lifetime (*The Incredible Things We Know about Your Heart and Blood - BBC Future*, n.d.). Skeletal muscle tissue is innervated, the voluntary muscle tissue that exhibits fatigue with high energy requirements. Both skeletal and cardiac tissues are organised into several bundles of myofibers. Myofibers, in turn, are divided into myofibrils which are then divided into a basic cellular unit called sarcomere (see Figure 2) (Mukund & Subramaniam, 2020). By contrast, smooth muscles found in veins and the gut walls are involuntary and activated by adrenergic and cholinergic receptors (J.R.Sellers, 2006). These tissues are much less organised, and each cell has a non-uniform substructure.

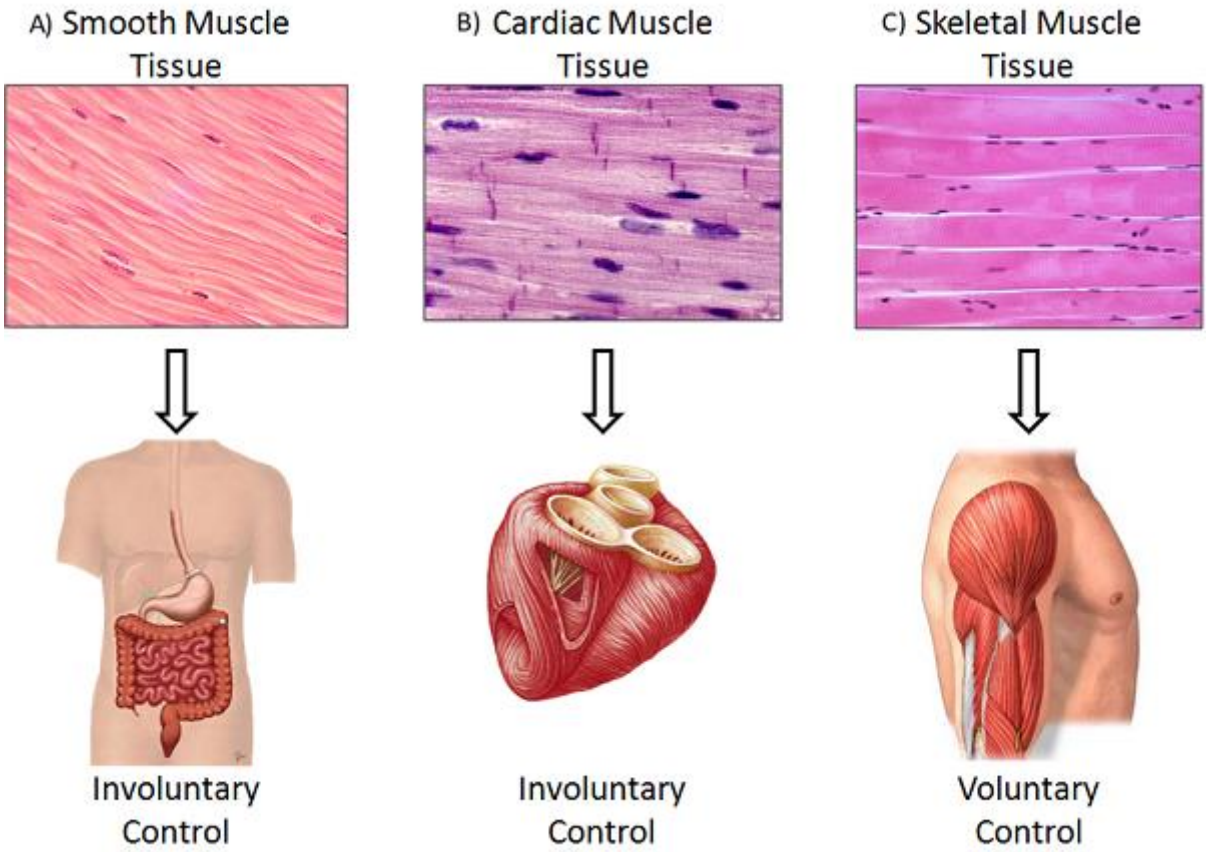

Figure 1.
This figure shows all types of muscle tissue cardiac, skeletal, and smooth as an image of set muscles under the light microscope using different stains for contrast. A) An image of smooth muscle tissue under a light microscope with an example of an organ where this tissue type is present (gut). B) An image of cardiac muscle tissue under a light microscope with an example of an organ where this tissue type is present (heart). An image of skeletal muscle tissue under a light microscope with an example of an organ where this tissue type is present (arm muscles). ("Muscle Types" n.d.)

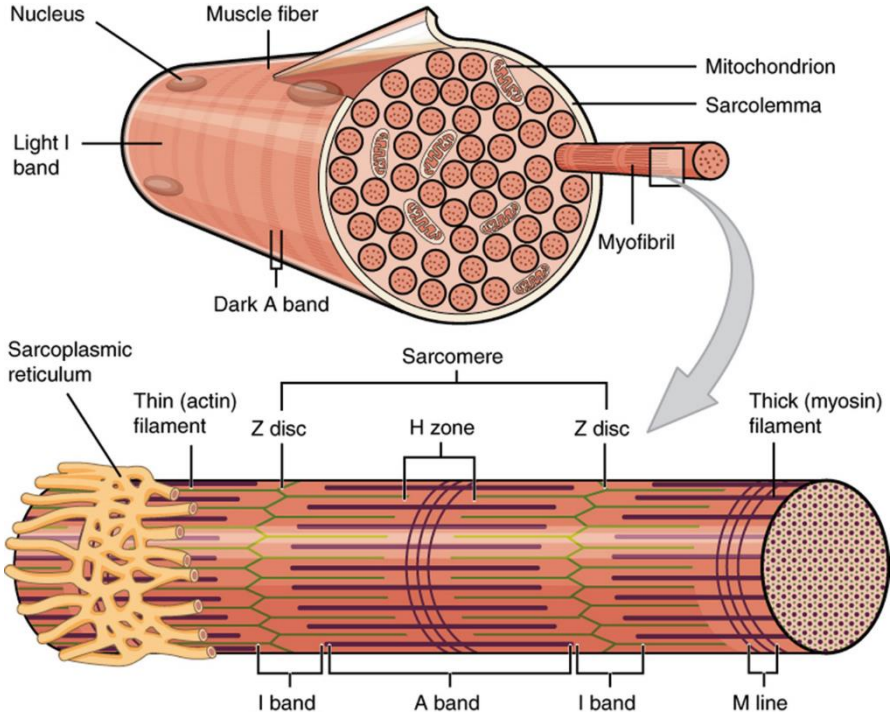

Figure 2.

This figure shows a labelled representation of different levels of striated muscle tissues organisation going down from the largest muscle fibres (myofibers) into myofibrils and further down to sarcomeres. This figure also depicts the observable distinctions of striated muscle that can be seen through a light microscope (i.e. Dark A bands and light I bands). Finally, this figure show structure of the sarcomere with division into different bands, including Z-lines in green with green straight lines representing thin filaments, M-lines in purple with purple lines representing thick filaments. (Samanthi 2017)

ii. The sub-structure of striated muscle

Striated muscle tissue is organised as many fused myocytes with joined cytoskeletons. Sarcomeres are the basic cell structures of striated muscles, which are continuous units of the component thick and thin filaments. Figure 2 shows that each sarcomere is defined at its ends by two Z-lines and an M-line in the middle. Z-lines are multiprotein structures that act as an anchor for the thin filament, which is joined to each Z-line extending towards the M-line. On the other hand, the thick filament is anchored and extends from the M-line in both directions towards the Z-line. The region where two filaments overlay in their extension is called an A band, while the regions where thick and thin filaments are present alone are called the H zone, and I band, respectively (see Figure 3). The reason why thick filament is anchored in M-line and thin filament is anchored in Z-lines is the protein composition of both Z and M lines and protein composition of both filaments.

Alpha-actinin is a primary protein component of the Z-lines which forms the principal crosslinks between actin filaments of opposite polarity originating from adjoining sarcomeres. Alpha-actinin is a rod-shaped protein of length ~35nm, which is an anti-parallel homodimer. The monomer of alpha-actinin comprises an NH2 terminal actin-binding domain composed of two calponin homology domains. The central part of alpha-actinin comprises four tandem sceptrin-like repeats, each comprising a triple alpha-helix anti-parallel bundle. The actin-binding domain of each end of the dimer gives alpha-actinin the ability to crosslink actin filaments (Luther, 2009).

Not unlike Z-lines, M-lines are an anchoring point to the main component of the thick filament – myosin. M-lines are complex proteins that include titin, myomesin, obscurin and Obsl1, crosslinked through interacting Ig domains. In M-band, myosin filaments are crosslinked by a protein network composed of titin and proteins of the myomesin gene family, which comprises three MYOM genes. (Fukuzawa et al., 2008)(Katzemich et al., 2012). The roles of numerous proteins in both Z and M lines will not be discussed further but can be read about here (Knöll et al., 2002; Lange et al., 2020). Moreover, there are costameres, proteins associated with Z-lines that connect the intracellular environment of sarcomeres to the extracellular environment(Srivastava & Yu, 2006). These sub-sarcolemmal proteins are essential to maintain the regular work of contractile apparatus. Compromised costameres are thought to directly contribute to the development of several distinct myopathies(Ervasti, 2003). However, the primary focus should be on the aforementioned proteins – myosin and actin.

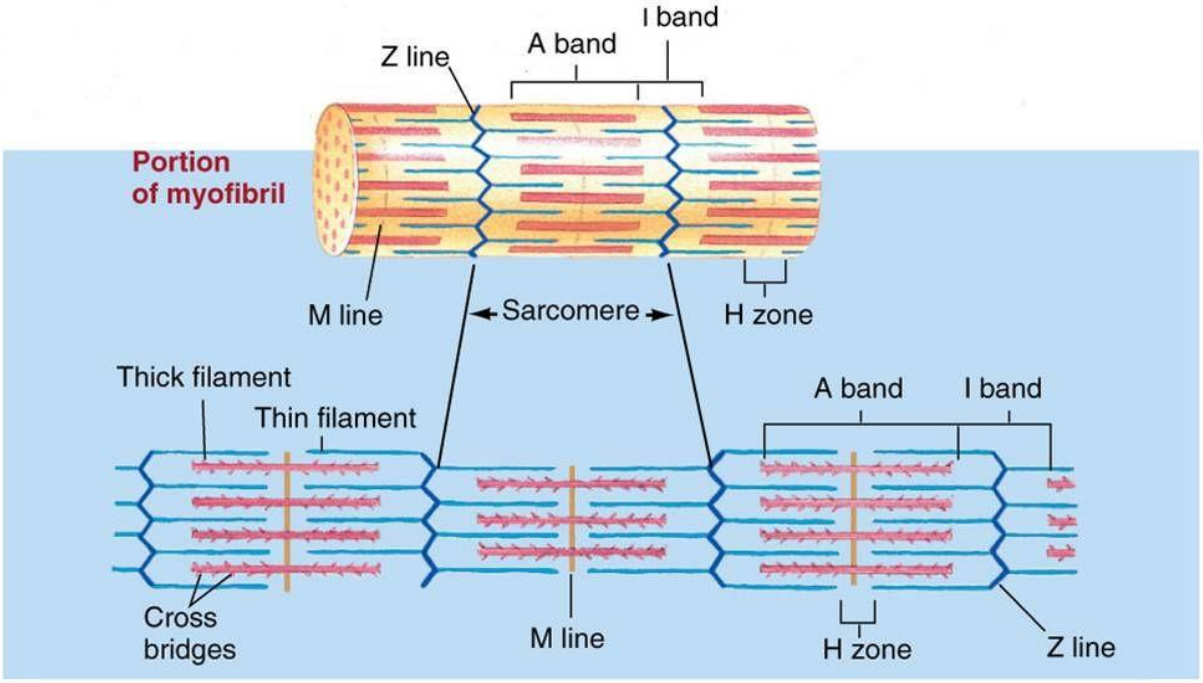

Figure 3.
This figure shows an in-depth dissection of a sarcomere. It includes both thick and thin filaments inside the sarcomere and multiple zones that define such arrangement. Thick filaments are represented by pink coloured lines anchored at M-line, which is represented by a yellow coloured line. Thin filaments are represented by light blue coloured lines and are anchored in Z-lines represented by darker blue coloured lines. (Russell and Edgewise Therapeutics 2021)

iii. Thin filament structure and function

Actin is a highly conserved and highly abundant protein in most eukaryotic cells. Actin in vertebrates can be expressed in three isoforms, including three α-isoforms of skeletal, cardiac, and smooth muscles and the β- and γ-isoforms expressed in both non-muscle and muscle cells (Dominguez & Holmes, 2011). Here we will be focusing on α-isoforms. G-Actin monomers (41,785 Da) are globular proteins that are approximately 67 x 40 x 37 Å in size, has estimated isoelectric point pf 4.8 and net charge of -7 at pH 7 (Elzinga & Collins, 1975)(Elzinga & Collins, 1975)(see Figure 4A). Although the globular structure of G-Actin was established using scanning electron microscopy (SEM), further experiments using X-ray crystallography have shown that G-Actin

consists of two lobes separated by a cleft. The cleft is represented by the ATPase fold, a centre of enzymatic activity that binds ATP and Mg^{2+}. ATP is then hydrolysed into ADP and inorganic phosphate (Pi). G-Actin can only function when either ATP or ADP molecule fills the cleft area, but the ATP molecules have higher affinity than ADP molecules (Graceffa & Dominguez, 2003)(see Figure 4a). The polymerisation of G-Actin forms F-actin, which can be considered a single-stranded helix, rotating anticlockwise with a rotation of 166° around the helical axis and an axial translation of 27.5 Å(Von Der Ecken et al., 2015)(see Figure 4B). The polymerisation process requires ATP/ADP, proteins, and protein complexes to form F-Actin from G-Actin. Arp2/3 is a complex of 220 kDa in size and has seven protein subunits. Arp2/3 initiates actin polymerisation by mimicking G-actin dimer. It attaches to the existing F-actin branch at 70°, allowing another G-actin monomer to attach and form a new F-actin branch (Suraneni et al., 2015). Two proteins that are associated with G-actin polymerisation are thymosin and profilin. Thymosin is a small (5 kDa) protein that binds to the G-actin-ATP complex in a 1:1 ratio and impedes the incorporation of the monomers into the growing polymer(Goldschmidt-Clermont et al., 1992). Profilin is a larger (15 kDa) protein that binds to both G-actin-ATP and G-actin-ADP complexes in a 1:1 ratio instead of impeding the elongation of the filament facilitates the replacement of ADP by ATP(Carlsson et al., 1977). Formation of actin consists of “actin cycle” that adds G-actin-ATP complexes to filament’s barbed end where they “age” (changing ATP into ADP and P_i) while they are going towards the pointed end and simultaneous disassembly of F-actin-ADP at the pointed end where ADP is refined back into ATP, this process of filament formation is known as treadmilling. Due to this process, actin filament remains in constant flux, assembling at the barbed end and disassembling at the pointed end. This process can be regulated, thus allowing for faster/slower assembly/disassembly to increase or decrease actin filament length, respectively(Carlier & Shekhar, 2017)(see Figure 4C).

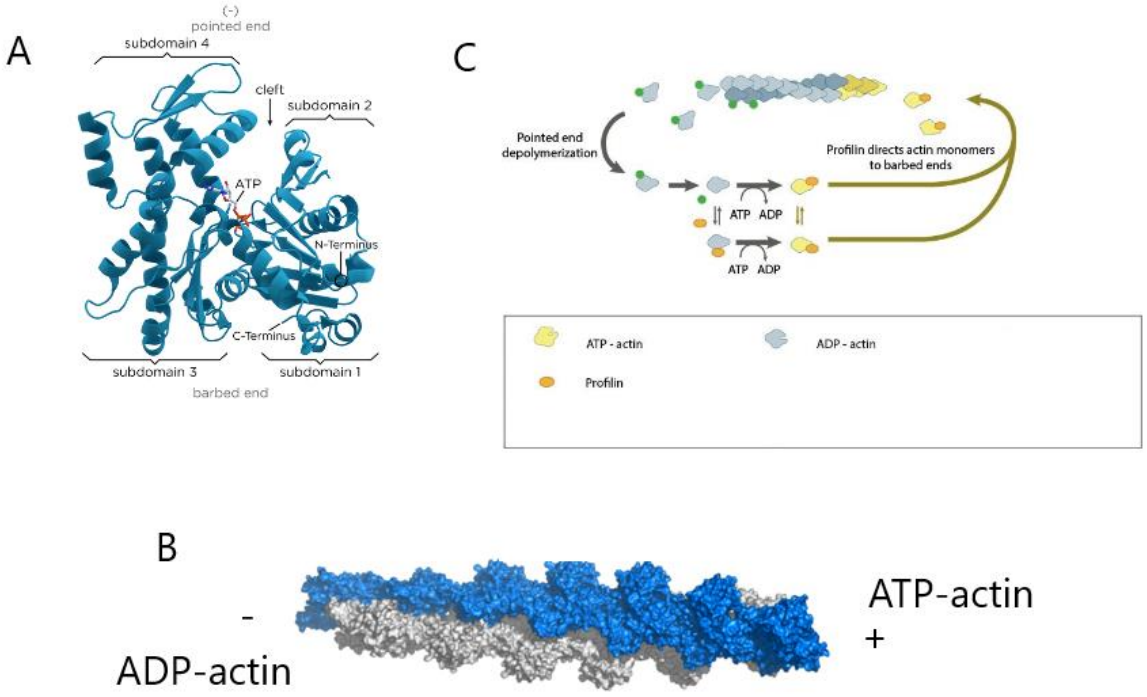

Figure 4.

A) Shows labelled tertiary structure of G-actin with all subdomains, pointed and barbed ends and ATPase cleft("File:G-Actin Subdomains.Png" n.d.). B) Shows a surface representation of repetition of 13 subunits of F-actin filament with pointed (-) end and barbed (+) ends. C) Shows the treadmilling process where polymerisation occurs at the barbed end while simultaneously depolymerisation occurs at the pointed end. ATP-actin is shown in yellow, while ADP actin is shown in grey. Orange circles represent molecules of profilin.

The thin filament is associated with several proteins, including nebulin, polymers of tropomyosin and the troponin complex. During interaction with the S1 fragment of thick filament, actin filaments are capped at the pointed and barded ends by tropomodulin and CapZ, respectively. Titin is the largest know protein which in the human variant contains 34 451 amino acids with a molecular weight of approximately 3816 kDa. Titin extends throughout all sarcomere from M-line to Z-discs. Titin consists of two different protein domains of 244 copies in total. The first domain is the fibronectin type III domain (132 copies). The second is the immunoglobulin domain (122 copies). The exact numbers of set domains may vary from one species to another(Labeit & Kolmerer, 1995). These domains can be further subdivided into two regions: the N-terminal I-band region and the C-terminal A-band region. The I-band region's N-terminal acts as the molecule's elastic part and is composed of two immunoglobulin domains with the PEVK region in the middle. PEVK region is rich in proline, glutamate, valine and lysine(K. Wang et al., 1991). The C-terminal A-band region is thought to act as a protein ruler and is composed of altering fibronectin type III and immunoglobulin domains with super-repeat segments. These domains have been shown to align themselves with 43nm axial repeats of myosin filament to correlate with myosin heads(Bennett & Gautel, 1996) (see Figure 5). Titin is especially important for sarcomeres in the N-terminal I-band region, allowing for elasticity essential for the thin filament's

spring-like motions. Thin filament connects force-generating A-band to Z-lines while also providing a spring-like structure to make the contraction process reversible and mechanically sound, both irreplaceable for constant contractile activity(Clark et al., 2002).

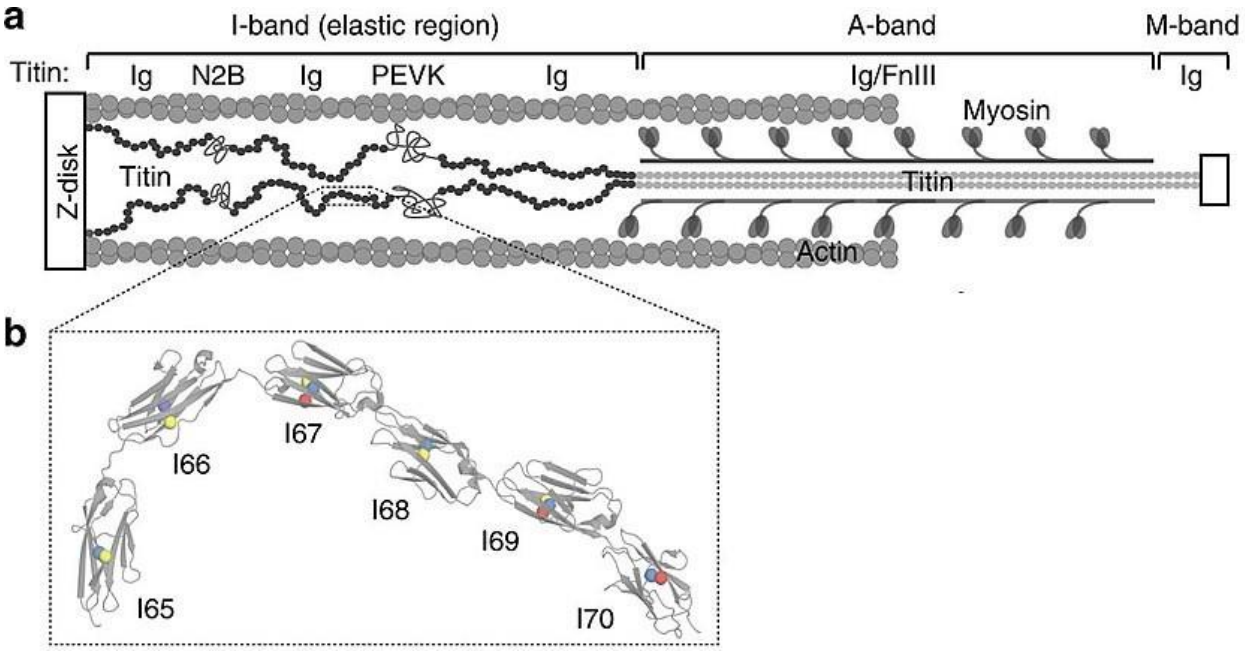

Figure 5.

A schematic representation of one half of the sarcomere where titin is shown in dark-filled circles. Titin is also represented in a more ordered state in A-band by dimmer filled grey circles. They represent the repetition of immunoglobulin and fibronectin II domains in the A-band. All subdomains of titin are shown at the top of the diagram. Ig domains provide elasticity in I-band. Actin and myosin filaments are labelled appropriately. b) A structural representation of titis segment I65-I70. Grey structures represent 566 amino acid sequences divided into 6 immunoglobulin modules. Cysteines locked in beta-strands B, F and G are labelled yellow, blue and red, respectively (Giganti et al., 2018).

In striated muscles, actin filament is also associated with troponin and tropomyosin, which regulates the exposure of myosin-binding sites on thin filament, thus regulating muscle contractions. Tropomyosin is a long, coiled protein with a molecular weight of 65 kDa (about 40nm in length). It binds to the thin filament covering seven adjacent G-actin monomers. Tropomyosin comprises two alpha-helix polypeptide subunits: alpha and beta tropomyosin. Troponin is a protein (80 kDa) that consists of three subunits Troponin C (18kDa), Troponin I (21kDa) and troponin T (31kDa). Each subunit has a function; Troponin C acts as a calcium-binding site which, if activated, deactivates troponin I through a consequent conformational change in troponin T, which acts as a bridge between troponin complex and tropomyosin. When troponin I is deactivated (i.e. calcium ion is attached to troponin C), ATPase activity of actomyosin is reestablished, thus enabling muscle contraction (Lehman & Craig, 2008)(see Figure 6)

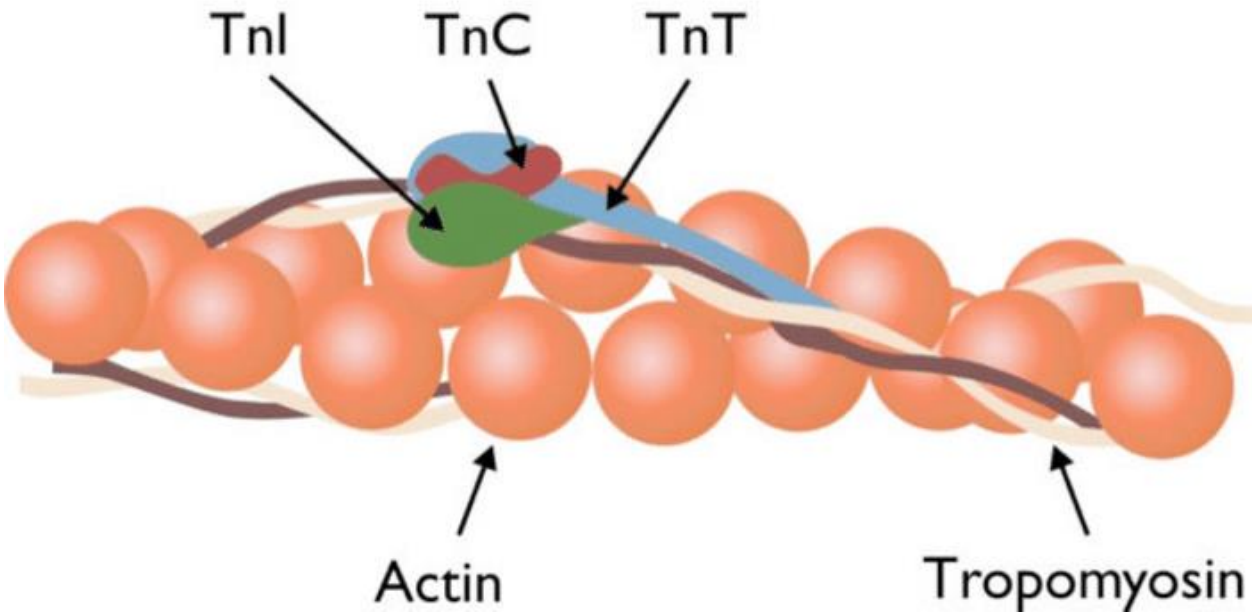

Figure 6.

The schematic architecture of actin filament. Tropomyosin twists around a thin filament with all three troponin subunits attached to actin filament and tropomyosin. Filled orange spheres represent actin. Intertwined brown and beige lines represent tropomyosin. Troponin I is represented by the green subunit, the red subunit represents troponin C, and the blue subunit represents troponin T. (Carrara 2017)

iv. Thick filament structure and function

Myosin is the main component of the thick filament. Myosin has 24 different classes with some structure variation; here, we will discuss Myosin II, which is expressed in animal striated muscles(Lynne M. Coluccio, 2008). Sarcomeric myosin is a hexameric motor protein composed of six subunits. Myosin has a molecular size of approximately 520 kDa. Myosin is composed of two heavy chains (MyHC), each with a molecular size of approximately 220 kDa. Due to their size, MyHC makes up the majority of the overall structure of myosin, two essential light chains (ELCs) which have a molecular size of 17 kDa and two regulatory light chains (RLCs), which have a molecular size of 20 kDa(Aguilar & Mitchell, 2010). Each MyHC comprises a globular motor head domain that bears ATPase activity and binds actin, a converter segment connecting the head domain to the lever arm that binds to ELC and RLC using isoleucine-glutamine (IQ) motifs and a "tail" that consists of the coiled-coil alpha-helix region. For further structural details, please see this review("Myosin Subfragment-1: Structure and Function of a Molecular Motor," 2007). Limited digestion by trypsin MyHC is fragmented into two parts: heavy meromyosin (HMM) and light meromyosin (LMM). LMM region interacts with adjacent LMM regions forming a cylindrical backbone (Lowey et al., 1993). HMM contains the head region, the converter segment, the lever arm, and the NH2-terminal portion of the alpha-helical rod domain (see Figure 7A). LMM contains the COOH-terminal half of the alpha-helical rod domain.

Further digestion of HMM by papain leads to subfragments 1 and 2, S1 and S2, respectively. S1 consists of a head domain, the converter segment, and the lever arm. S2 contains the NH2-terminus of the alpha-helical rod domain(L. Wang et al., 2018)(see Figure 7B). The head region of S1 contains the ATP binding site and can be further subdivided into seven-stranded beta-sheets surrounded by 17 alpha-helices. ATP binding is mainly regulated by the central (~50 kDa)

region of the globular head, which can be further divided into upper and lower subregions(Colegrave & Peckham, 2014) (see figure 7C). The cleft that forms between upper and lower sites contains the ATP binding site(Rayment & Holden, 1993). ATP binding to the ATP-binding domain of S1 is coupled with the opening of the actin-binding cleft. The converter segment is connected to the head domain via relay helix, which is a long alpha-helix. The converter segment and relay helix play an essential role in fine-tuning ATP binding and hydrolysis. Further reding is available here (Bloemink et al., 2016).

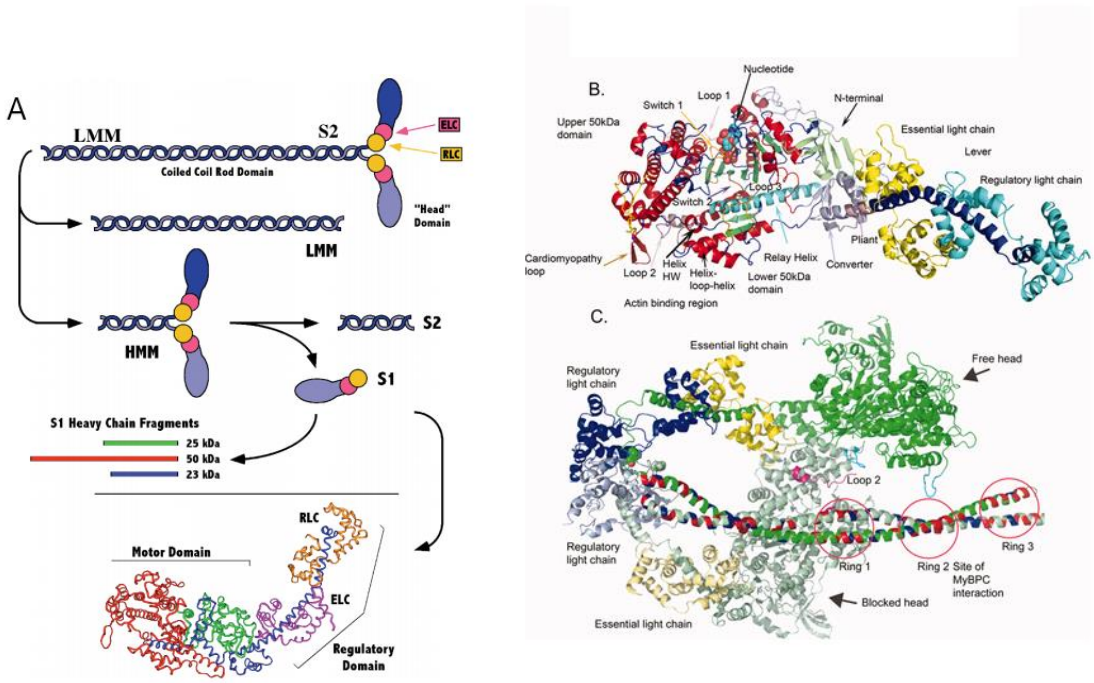

Figure 7.

A structural representation of subsequently proteolyzed Myosin II. MyHC is shown to be broken down into LMM and HMM. HMM is then subsequently broken down into S1 and S2. The amplified structure of S1 is then shown with the motor domain represented in red, green, and blue. ELC and RLC are purple and yellow, respectively (Lynne M. Coluccio, 2008).B) A model representation of striated myosin S1 motor domain. Helices are shown in red, and key functional regions of the motor are ladled(Colegrave & Peckham, 2014). C) A structural representation of the folded form of myosin with two heads (blocked and free) with blocked head folding on the S2 coiled-coil domain of HMM. The three sites of MyBB-C interactions are represented by opened red circles(Colegrave & Peckham, 2014).

Myosin is the main but not the only component of the thick filament. Other essential proteins that compose the thick filament are myosin binding protein-C (MyBP-C), myosin binding protein-H (MyBP-H), myomesin, M-protein and titin. MyBP-C has a molecular weight of 120-140 kDa, and MyBP-H has a molecular weight of ~52 kDa. They were first extracted from striated muscle in 1973 as impurities in myosin preparations. Further studies have demonstrated that they are interaction partners of sarcomeric myosin. They are modular proteins consisting of immunoglobulin and fibronectin-III domains interspersed with unique sequences(L. Wang et al., 2018). The extreme COOH-terminal immunoglobulin 8 – fibronectin-III – immunoglobulin 10

cassette of myosin binding protein-C and myosin binding protein-H supports binding to the LMM portion of myosin heavy chain(Gilbert et al., 1999). Furthermore, the NH2-terminus of myosin binding protein-C, specifically the Pro/Ala rich motif and M-motif flanking immunoglobulin domain C1 region, interact with the S2 fragment of myosin heavy chain(Flashman et al., 2007)(see Figure 8). Myosin binding protein-C is much better defined than myosin binding protein-H. Further reading on myosin binding protein-H can be found here(Bähler et al., 1985), as it will not be discussed further in this thesis. Myomesin and M-protein have molecular weights of 185 kDa and 165 kDa, respectively. They both consist of immunoglobulin and fibronectin-III domains while being localised in the sarcomeric M-band. Myomesin interacts with the central LMM region of myosin heavy chains via the NH2-terminal My1 domain. Such interaction contributes to the assembly and incorporation of myosin into A-bands during myofibrillogenesis(Fukuzawa et al., 2008). Further information is available here (Hu et al., 2015).

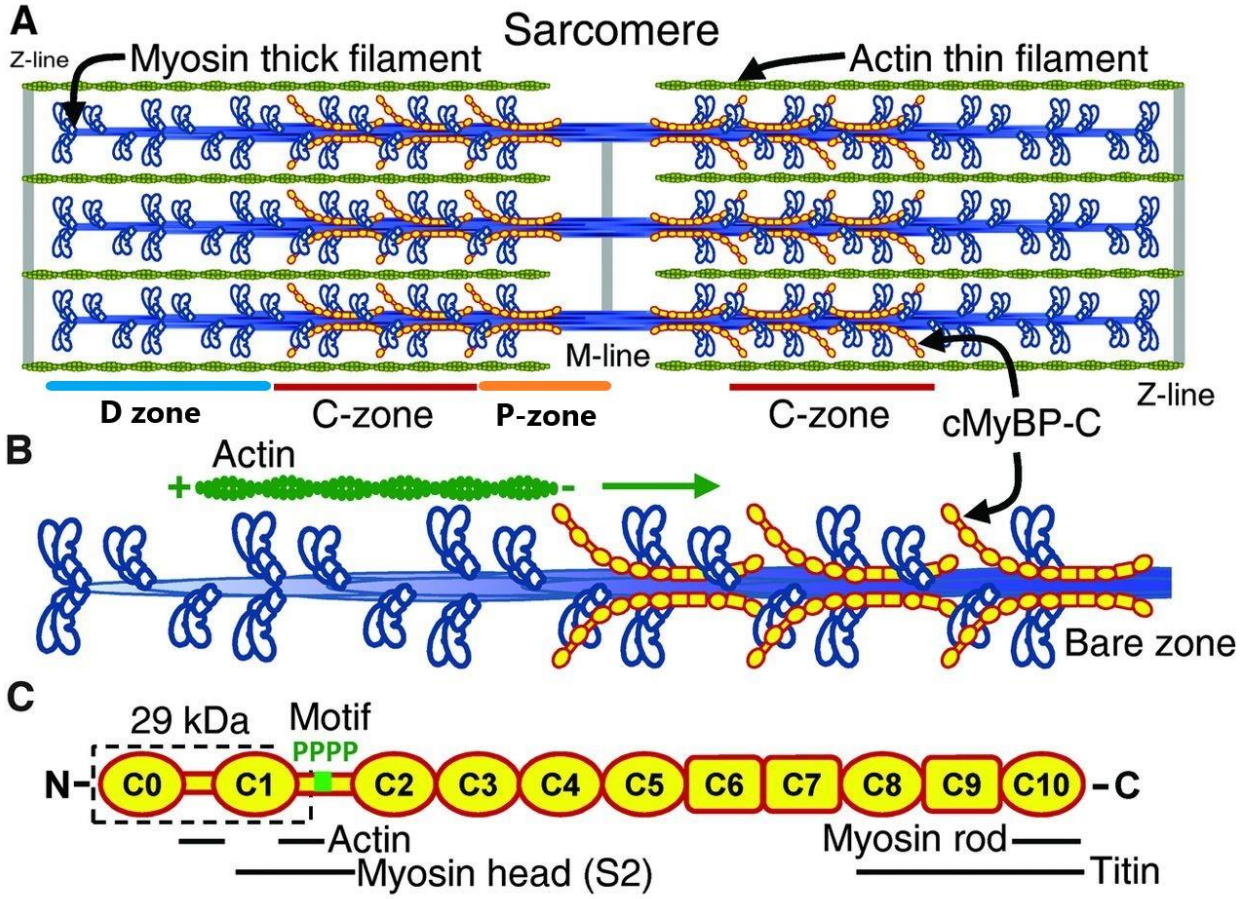

Figure 8.

A) A structural diagram of sarcomere with MyBP-C labelled in yellow. MyBP-C is confined to the C-zone (labelled in red) of the thick filament. D-zone is labelled in bright blue. P-zone is labelled in orange. The thick filament is shown in blue, while the thin filament is shown in greed. M line and Z lines are shown in grey. B) A structural diagram of a half thick filament with MyBP-C is attached to the thick filament and labelled yellow. The thick filament is blue, while the thin filament is labelled in green with pointed (-) and barbed (+) ends shown. C) A structural representation of the entire length of cMyBP-C. C1 and C2 domains are connected by the M-domain, containing an intrinsically disordered N-terminal region with four phosphorylatable serines and a less disordered C-terminal. C0 domain is specific to the cardiac isoform of MyBP-C.

Globular heads of myosin molecules extend from the thick filament's core and interact cyclically with the thin filament in the process referred to as the cross-bridge cycle. The thick filament can be further subdivided into three zones C, D and P. The D-zone is situated on the z-line side of the thick filament, followed by the C-zone, and finally, the P-zone is directly adjacent to the M-line (see Figure 8A (Clark et al., 2002).

B. Muscle contraction mechanics

i. Sliding filament theory

The Sliding filament theory was first proposed simultaneously by two different research teams Huxley & Niedergeke and Huxley & Hanson(A. F. Huxley & Niedergerke, 1954; H. E. Huxley & Hanson, 1954). Huxley & Niedergeke proposed a method using an interference microscope in which the reference beam does not traverse the specimen. Their setup was based on earlier

principles (here and later see references in the main text (A. F. Huxley & Niedergerke, 1954)), but further developments were incorporated to allow water-immersion objective for increased magnification and resolution. Due to the cylindrical shape of the fibre, gross refraction had to be brought to the average value for the fibre contents; this was done by adding serum albumin (a globular blood protein) to Ringer's solution (isotonic buffer imitating body fluid salt concentration) that was used for the imaging. They have employed a constant cone of illumination throughout their experiments under which fibre was completely invisible with ordinary light, but the interference arrangement provided an excellent image of striations. The patter could be controlled to show (highlight) either A or I band as A had a higher reflective index. They have changed sarcomere length using three methods: passive stretch, isometric twitches, and isotonic contractions.

Passive stretch employs stretching a stationary muscle. With this method, they saw an increase in length from 2 um to 4.2 um. According to their observations, the main change occurred in I-band while A-band had a constant length. The isometric twitches method involved keeping the tendon ends stationary while simultaneously measuring the twitch with RCA 5734 transducer. They could not detect any change in band widths using this method. Lastly, isotonic contractions were applied where the muscle could contract freely. They saw various initial lengths up to 3.2 um that would, similarly to their previous observations, only shorten in I-band while A band maintained constant width. With these experiments, Huxley and Niedergerke observed that: striations became very faint on shortening beyond a sarcoma length of about 1.8 um, the dense band narrowed to about half the sarcomere length, after which both bands narrowed in proportion, and at 1.8 um, a very narrow dense band was visible at the centre of the former A-band, and on shortening to 1.7 um additional dense lines appeared midway between these lines (see Figure 9A&B). The hypothesis was proposed that the actin filaments fold into the A-band during contraction, and this folding continues after the I-band has been fully retracted. Unlike Huxley & Niedergeke, Huxley & Hanson (H. E. Huxley & Hanson, 1954) made their observations using high-resolution microscopy in phase-contrast illumination of the blended glycerol-extracted rabbit psoas muscle. They have tested set myofibrils at different conditions. Firstly, they have allowed myofibrils to contract freely at room temperature (22° C) with 0.5 mM ATP, 0.1 M KCl and 1 mM $MgCl_2$. Secondly, they have allowed myofibrils to contract freely at room temperature but this time adding ATP at 5 uM as a series of steps, thus regulating the contraction degree. Thirdly, they allowed myofibrils to contract at low temperatures (about 2° C) with ATP but in the almost complete absence of Mg^{2+}. Lastly, they have allowed myofibrils to contrast as in the first experiment, but myofibrils were held at both ends, so the shortening was controlled. During the first three experiments, they have observed identical changes of band pattern (see Figure 9C). They have also observed that the I band have shortened from 0.8 um to non-existence, while the length of the A-band stayed constant at approximately 1.5 um. Furthermore, they have observed that although the A band did not change in length, it had changed in density. They observed that the H zone that was initially low in density has increased in density, first becoming indistinguishable from the rest of the A band, and then replaced (~85 % rest length) by the zone denser than the rest of the A band. The overall density of the A band decreases as myofibril diameter increases during the shortening. When I bands disappeared at about 65% rest length, contraction bands form at the lines of contact of adjacent A bands. During an isometric contraction, the lengths of both A and I bands do not change; however, a narrow dark zone

appears in the centre of the A band. Huxley & Hanson have arrived at several conclusions from the aforementioned experiments and other experiments exceeding the purpose of this thesis. First, the backbone of the muscle fibre is made up of actin filaments and stretches from Z lines to the H zone, where they are attached to an elastic component; they have named S-fragment. This component was thought to connect all sarcomeres via actin filaments stretching from both ends of Z lines. Second, myosin filaments are stretched from one end of A band, throughout the H zone, to the other end of the A band, and their length is unaltered by stretch or by contraction down to the point where the sarcomere length is equal to the length of the A band. Third, in the absence of ATP, myosin and actin filaments are interlocked in a permanent state of cross-linkage. Finally, they have proposed a possibility of driving force for contraction to be provided from the formation of actin-myosin linkages in the presents of ATP.

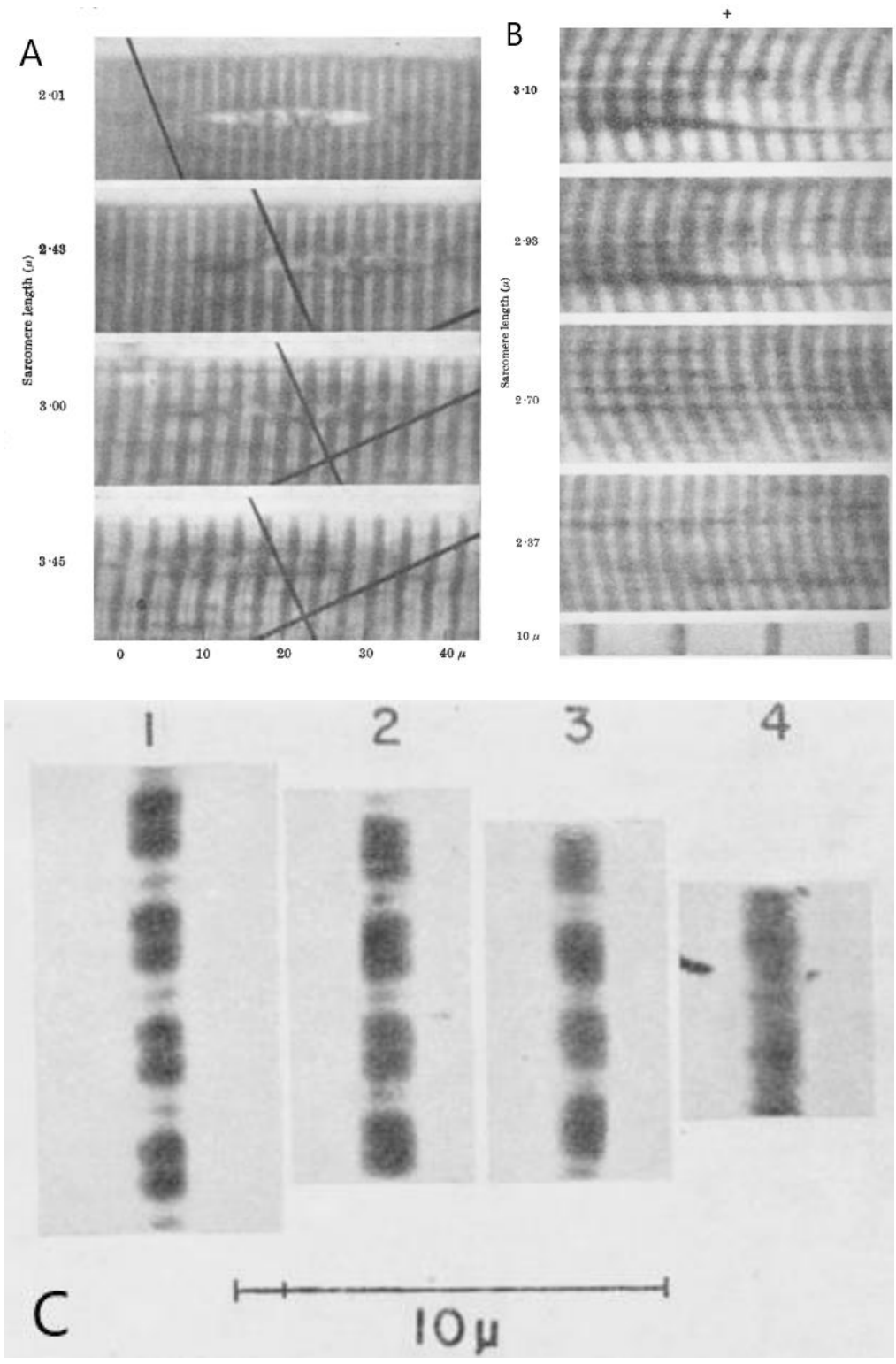

Figure 9.

A passive stretch of muscle fibre. Positive contrast (A band dark). Scale is provided of x-axis in um. Almost all changes can be observed in lighter regions (I bands). B) Muscle fibres during short isotonic tetanus. Positive contras (A band dark). Again, A bands have a constant length while I bands (light) change. C) The same four sarcomeres of one myofibril photographed during contraction induced by ATP from rest length to 50 % rest length when contraction bands have formed.(Huxley and Niedergerke 1954)

The conclusion that was drawn from both papers presented above was the sliding filament theory which states that a decrease in the length of a sarcomere during contraction can be attributed to thin filament moving along the thick filament towards the M line, thus shortening H and I bands while A band remain at a constant length. Similarly, only I band and H zones increase in length during muscle relaxation, whereas A maintains its length and moves further away from the Z-liens (see figure 10). Also, the fact that only A band does not shorten means that the only place of myosin-actin interactions is the A band which, in the absence of ATP, do not form any active cross-linkages and therefore provides no movement of thin filament as was shown above and below.

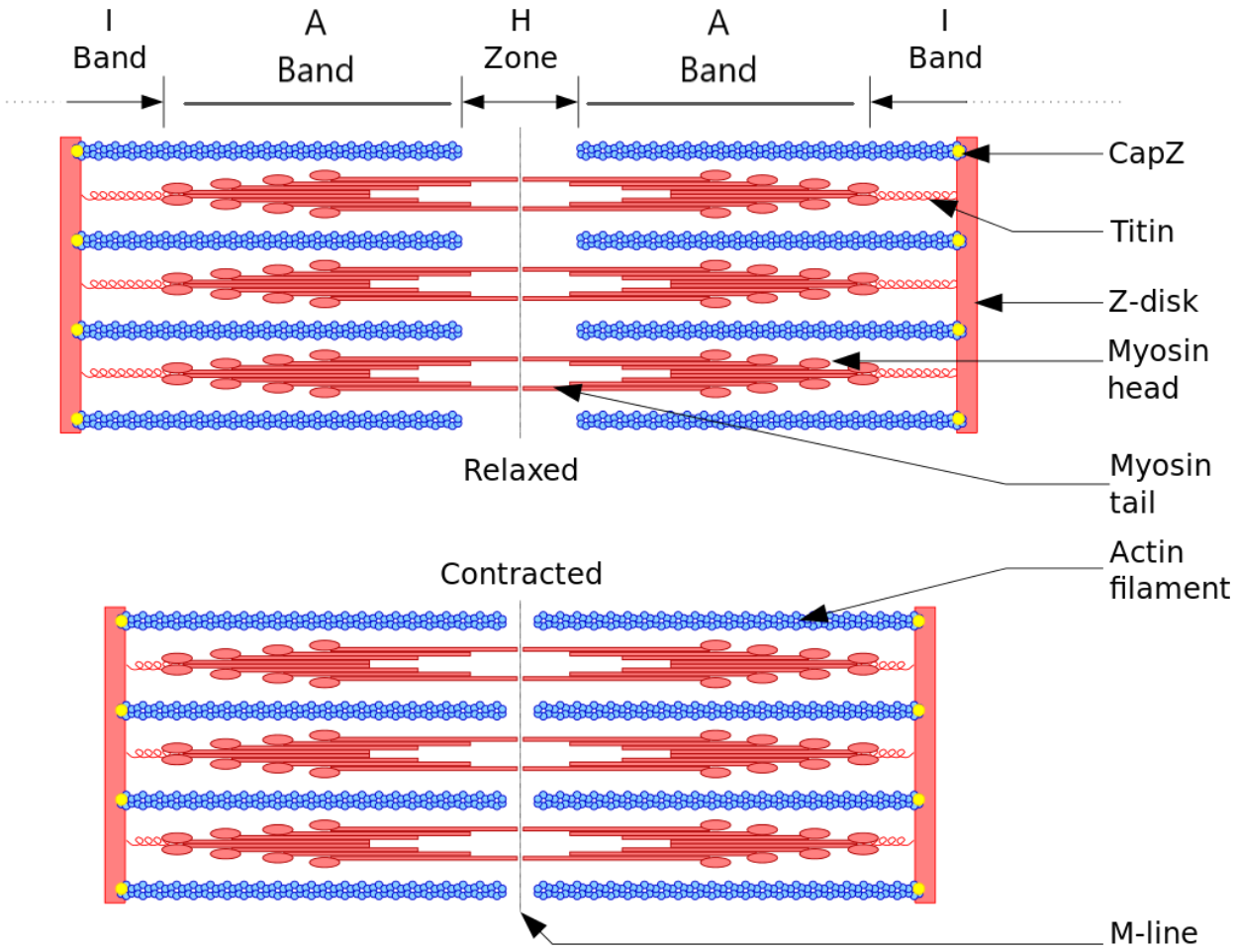

Figure 10.

A labelled structural representation of a sarcomere shows the change in all zones and bands during the contraction of a sarcomere. Blue filaments represent thin filaments. Pink filaments represent the thick filament. Zones and bands are labelled accordingly(Wikipedia contributors 2021).

ii. Myosin heads cross-bridge cycle

The myosin cross-bridge cycle is the process that involves myosin heads and actin filament interacting in A band to create the movement of the thin filament observed in sliding filament theory. Subfragment I of myosin heads consists of the motor domain and two light chain domains. The motor domain contains a nucleotide-binding site of the P-loop variety closely associated with switch-I and switch-II helices (see Figure 7A). ATP binding domain is located toward the end of a large cleft that separates two actin domain binding sites. ATP binding domain is also close to the P-loop and two switches that make myosin a part of a larger family of P-loop containing ATP and GTPases. Due to the ATP binding domain location, binding of ATP and subsequent release of ADP does not occur in the cleft directly but rather in a small pocket at the end of the cleft, where ATP molecule enters, Pi group first, followed by the main body of the ATP molecule thus blocking the exit of the hydrolyzed Pi molecule (M. A. Geeves et al., 2005)(Michael A. Geeves & Holmes, 2005). The nucleotide-binding site and actin-binding site communicate through the switch-I and switch-II helices, which move in response to the state of the nucleotide-binding domain. Nucleotide-binding domain changes conformation depending on the present or absence of P_i in the active site (see figure 11 A). Other side of the motor domain (C-terminus) consists of a long alpha-helix stabilised by calmodulin or calmodulin-like light chains (the number of chains depends on the myosin isoform). This light chain binding domain is better known as the lever arm because it can swing through the angle of ~60° during the Lymn-Taylor contraction cycle (see Figure 11B). The myosin cross-bridge (Lymn-Taylor contraction cycle) cycle was first proposed by Lymn-Taylor in 1971 (Lymn & Taylor, 1971). During the Lymn-Taylor contraction cycle, the lever arm moves 5-20 nm in relation to the actin-binding site. (Wittinghofer & Geeves, 2016).

The Lymn-Taylor contraction cycle major events and conformation changes in the actin-myosin ATPase are described in Figure 11C. During Lymn-Taylor contraction, ATP acts as an inhibitor for actin-myosin interaction. By positioning itself in the cleft and forcing actin-binding regions on either side of the cleft apart, ATP reduces the affinity of myosin for actin by about 1000 fold. When ATP binds to ATP binding pocket, SW1 region closes first, thus opening large cleft region and releasing actin. This is followed by the closure of the SW2 region. Closure of the SW2 region is linked to the recovery stroke in which the converter domain and lever are repositioned into the pre-power or working-stroke conformation. The order of the events involving SW1 and SW2 are precisely timed. SW1 closure and actin dissociation take ~ 1 ms. ATP hydrolysis occurs about 10 times slower (~ 10 ms). The resulting complex is stable for ~ 20 s unless it encounters an actin-binding site, resulting in the completion of the rest of the cycle in ~ 20 ms(Wittinghofer & Geeves, 2016).

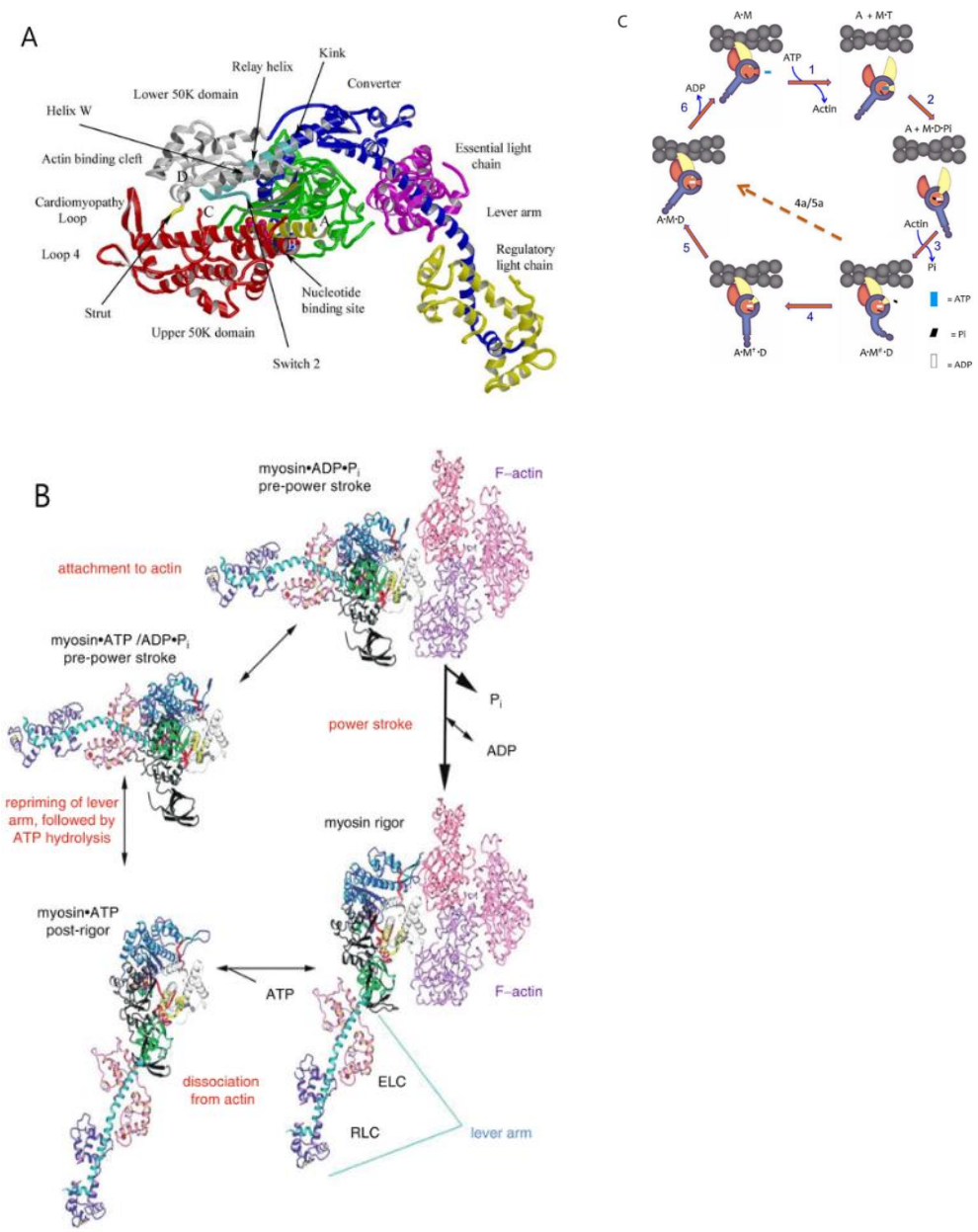

Figure 11.

A) A labelled structural representation of post-rigor myosin motor domain. This representation is shown from the pointed end of ancient at the point of attachment of S1 to actin. P-loop and adjacent helices are shown in yellow, while the N-terminus is shown in green. The upper 50 kDa domain of the motor domain is shown in red, while the lower 50 kDa domain is shown in grey. The disordered loop 1 that is comprised of the upper 50 kDa domain N-terminus is marked by letters A and B. Disordered loop 2, which connects upper and lower 50 kDa domains, is marked by points C and D. Dark blue ribbon represents the C-terminal long helix which carries two calmodulin-like light chains and joins the thick filament. Relay helix is shown as a separate domain for clarity, but it is a part of the upper 50 kDa domain. (Wittinghofer & Geeves, 2016). B) Structural representation of myosin power stroke, showing high-resolution structures of myosin and actin in the pre-power stroke state, the rigour state and the post-rigor state(Dilson E. Rassier, 2013). C) A representation of ATP-driven actin-myosin mechanical cycle. The myosin cross-bridge is shown to consist of three major components. 1. The central core of the myosin head (filled red circle) with the lower 50 kDa domain projecting up to make contact with a single actin monomer (filled grey circle). The myosin head remains a fixed reference point throughout the cycle. 2. The upper 50 kDa domain with SW1 is shown in yellow, which is drawn as two parts: the upper jaw of the major cleft that splits the actin-binding site and a ring with SW1 projecting into the centre of the myosin head (both yellow). 3. A dark blue ring represents SW2 projecting to the centre while the converter domain and the lever arm stretches out of the ring (also dark blue). The nucleotide pocket

is represented by a red space inside two circles (yellow and dark blue). The nucleotide pocket has an entrance point represented by openings in two rings (blue and yellow). A-M at the top left represents the rigor actin-myosin complex, and the starting point with the upper 50 kDa domain cleft closed to allow both sides of the cleft to connect with actin. Both SW1 and SW2 circles are opened for ATP to enter the nucleotide pocket. The following numbers represent the numbers on the diagram indicating the step about to be described.

1. ATP binds into the nucleotide pocket, and the yellow circle rotates to close SW1 ATP inside the pocket. During that process, the major cleft follows the movement of the SW1 circle, thus opening the major cleft, leading to dissociation from actin.
2. The dark blue segment rotates to bring SW2 into contact with ATP. The motor domain restores its position before the power stroke. After both SW1 and SW2 circles are closed, ATP is hydrolysed to form a stable M-ADP-Pi complex.
3. After ATP hydrolysis lower 50 kDa part of the cleft returns to its original position, thus rebinds to actin, the cleft closes, and both upper and lower 50kDa domains bind actin. The rebinding involves the rotation of the SW1 circle, thus triggering both Pi release and the rotation of the blue segment generating a force; a distortion of a converter domain represents the produced force. There is, however, no consensus on the ordering in which cleft closure, Pi release and powers stroke occur. The location of the elastic component within the cross-bridge is not defined.
4. When/if enough force is generated in the previous step, the thin filament is moved 5-20 nm by the cross-bridge working stroke. This is shown as a relative displacement of the motor domain relative to the actin filament. Once the working stroke is finished, the blue segment shifts to allow ADP to escape the cleft in step 6.
4a/5a. In a case where the force provided by the converter region is too small to move the thin filament, no sliding is taking place, and the further rotation of the blue SW2 ring is inhibited. The degree of set inhibition is defined by the load sensitivity of the myosin (~ 5-100 fold inhibition depending on the type of myosin)(Wittinghofer & Geeves, 2016).

iii. Regulation of contraction

There are two different regulatory systems. In actin-linked regulation, Ca^{2+} concentration regulates troponin, which regulates tropomyosin, which in turn regulates contraction by blocking myosin heads attachment sites on the actin filament. The three-state model was later proposed to state that calcium alone does not fully stimulate mechanical contraction (McKillop & Geeves, 1993a). Similarly, a myosin-linked regulation system will block sites on the thick filament, preventing two filaments from attachment. Muscles of different species may have different regulation systems (Szent-Györgyi, 1975).

iv. Thin filament regulation

Muscle contractions are regulated by intracellular Ca^{2+} concentration. Calcium ions concentration affects the thin filament conformation, thus controlling the myosin heads attachment and muscle contractions. Parts of the thin filament that are important for contraction regulation are tropomyosin, troponin, and actin. They exist in thin filament in 1:1:7 stoichiometry. Troponin can be further subdivided into troponin C, troponin I and troponin T (Ebashi et al., 1969). During the resting muscle state, intracellular calcium ion concentration is lower than uM level. This concentration is maintained by Ca^{2+} ATP driven pump that is located on the sarcoplasmic reticulum (SR) membrane, which pumps Ca^{2+} into the SR. With such low calcium concentration, most regulatory Ca^{2+} are dissociated from troponin C, thus driving thin filament into the inactive Ca^{2+} - off state. This state is defined by myosin heads disability to bind

to the actin filament. During muscle contraction, however, Ca^{2+} is released from the SR, allowing them to rebind to troponin C, which causes a conformational change in troponin and thus a shift in an azimuthal position of tropomyosin on the actin filament. The shift in tropomyosin allows actin-myosin interactions driving the thin filament into Ca^{2+} - on the state (Lehman et al., 1994).

It has been shown (Moss et al., 1985) that removal of tropomyosin C from skinned muscle inhibits force production by preventing Ca^{2+} activation of the thin filament. Troponin C has two globular regions, COOH and NH_2 terminals, connected by a long central helix. There are two possible Ca^{2+} binding sites on each region: helix-coil-helix E-F hands (see Figure 12 C). Under relaxed conditions, COOH-terminal sites (III-IV) have high (~10^7 M^{-1}) Ca^{2+} affinity and sufficient Mg^{2+} affinity so that Mg^{2+} binds normally. COOH terminal sites are named structural sited due to their ability to enhance troponin C – troponin I interactions during Mg^{2+}- Ca^{2+} binding and consequent binding of troponin C to the thin filament(Potter et al., 1995). The NH_2 terminal site is a physiological Ca^{2+} trigger site; it lowers the affinity for Ca^{2+} and has a high selectivity for Ca^{2+} over Mg^{2+}(Potter & Gergely, 1974). Further reading on tropomyosin C structure are available here (Sorenson et al., 1995)(van Eerd & Takahashi, 1976)(H. L. Sweeney et al., 1990). Tropomyosin interaction with actin is influenced by troponin and myosin that significantly increase tropomyosin binding to actin. These interactions can be found in 14 quasi-equivalent repeats of consequent regions of charged and uncharged amino acid side chains of tropomyosin(McLachlan & Stewart, 1976). These electrostatic interactions of tropomyosin and actin can be divided into two different states(Phillips et al., 1986). Images of tropomyosin on F-actin taken with X-ray support the electrostatic binding on the periphery of the actin filament(Lorenz et al., 1995). Further reading on different isoforms of tropomyosin and their properties are available here (Mak & Smillie, 1981)(Landis et al., 1997)(Hitchcock-DeGregori & An, 1996)(Chandy et al., 1999)(Swenson & Stellwagen, 1989). Three-state (blocked, closed, and open) dynamic steric model (see Figure 12 D, E&F) was proposed for tropomyosin states during actin-myosin interactions(McKillop & Geeves, 1993b). Multiple studies (Vibert et al., 1997)(Lehman et al., 1994, 1995) on the negatively stained thin filament and stained frog muscle have shown that tropomyosin in the absence of Ca^{2+} occupies the position that blocks most myosin-binding sites (blocked) on the actin filament. After Ca^{2+} attaches to troponin, tropomyosin moves ~25° around the surface (closed) of thin filament from its previous position exposing several more myosin-binding sites(Vibert et al., 1997; C. Xu et al., 1999). Troponin was moved further 10° (open) upon the addition of S1 but in a total absence of MgATP. Further biochemical evidence supporting the three states theory had shown that open state was only present at rigor but required Ca^{2+} and strong binding of myosin heads (Vibert et al., 1997). Further reading on blocked, opened and closed states are available here (Poole et al., 2006)(McKillop & Geeves, 1993a)(Pirani et al., 2005). Another very recent paper has shown the conformational change of troponin due to Ca^{2+} binding by utilising new methods of cryoEM and image analysis (Yamada et al., 2020). In this study, they have shown the entire length of actin filament with detailed structures of troponin core, the entire length of tropomyosin with the head-tail junction, the N-terminus extension of troponin T and the C-terminus extensions of troponin I below and above the troponin core, respectively. Troponin core structure has been shown before(Takeda et al., 2003) and is coherent with results from this study. The inhibitory role of the C-terminus of the troponin I chain, which is located downstream of Gly 137, has been well characterised by biochemical studies (M. A. Geeves et al., 2000)(Farah et al., 1994)(Tripet et al., 1997) (see Figure 12 A&B).

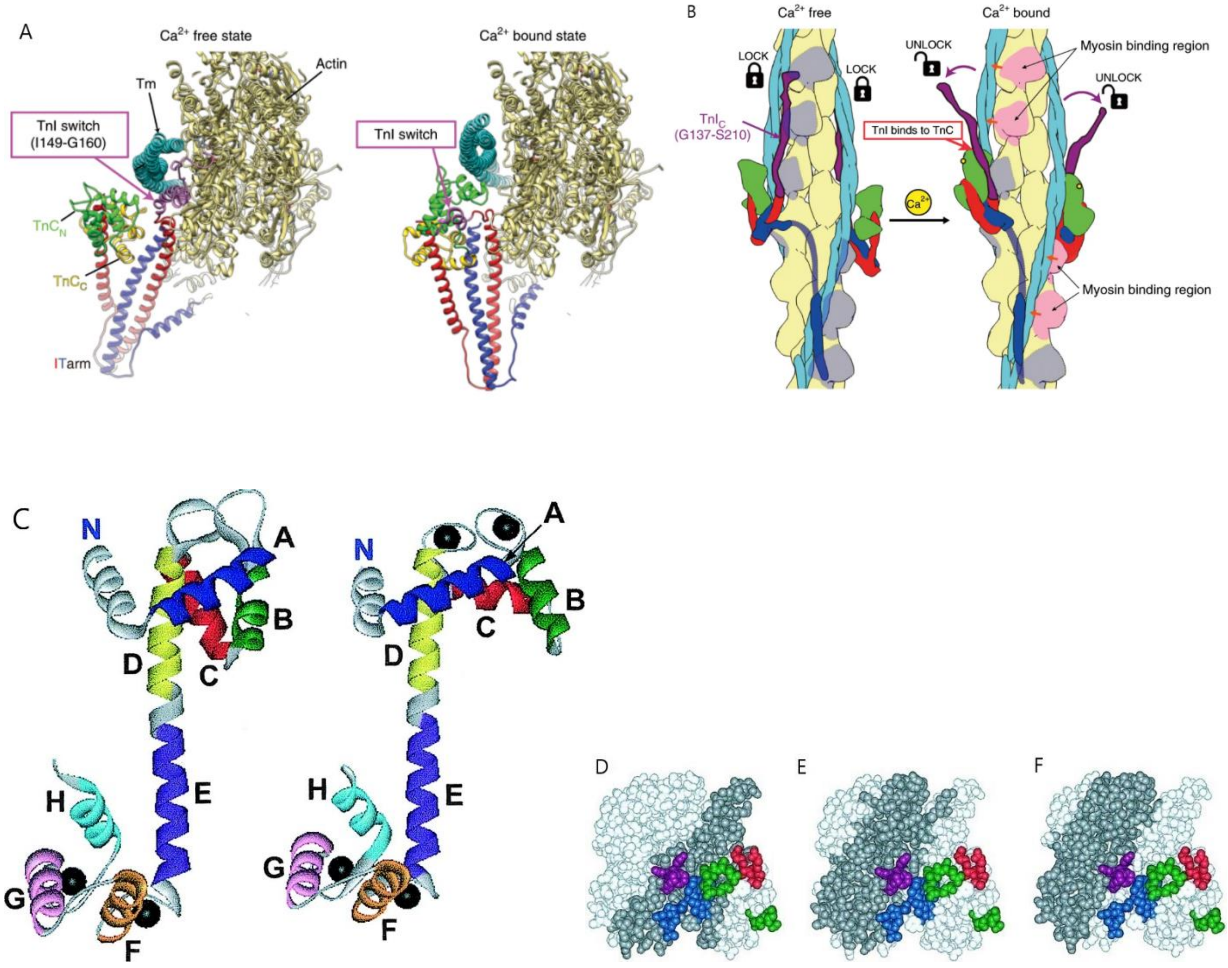

Figure 12.

A) A 3D model of an actin filament viewed from the pointed end shows a conformational change in troponin and tropomyosin that occurred before, and after Ca^{2+} binding to troponin C. Troponin C N-terminus is labelled in greed while C-terminus is labelled in yellow. Tropomyosin is represented in bright blue. Troponin I switch is represented in purple. Actin is represented in pale yellow. Troponin I and T arms are represented by red and blue helices, respectively (Yamada, Namba, and Fujii 2020).

B) A schematic diagram of a change in troponin and tropomyosin during the Ca^{2+} binding and consequent effects that unlock myosin heads binding sites. Troponin I C-region is represented in dark purple. Tropomyosin I is represented in light blue, while actin is represented in pale yellow. Troponin core is represented in green, red and blue. Myosin binding sites are represented in grey (closed) and pink (opened) (Yamada et al., 2020).

C) Left: a structural representation of troponin C crystal structure with Ca^{2+} bound only to NH_2 terminal. Solid circles represent Ca^{2+}. Letters represent 8 helices of NH_2 terminal showing their orientation. Right: a structural representation of troponin C crystal structure with Ca^{2+} bound to NH_2 and COOH terminals. In this model, helices are oriented more parallel to each other compared to the previous model (Yamada, Namba, and Fujii 2020). D) A representation of the actin-troponin complex in a blocked position. Here and further, tropomyosin is represented in see-through green. Actin is represented in pale green. Bright colours (green, red, blue and purple) represent potential myosin-binding sites on the actin filament. Actin residues are coloured: 1-4,24-28 green, 144-148,340-346 blue, 332-336 purple and 93-96 red. E) A representation of the actin-troponin complex in the closed position. F) A representation of actin-troponin complex in the open position(Gordon et al., 2000).

V. Thick filament regulation

1. Super Relaxed State & Disordered Relaxed State of myosin heads in striated muscle

Super Relaxed state (SRX) and Disordered Relaxed state (DRX) can be defined as states of myosin heads that have a slower nucleotide turnover than active myosin head turnover rate (~ 1-4 s). DRX was shown to have an ATP turnover rate of ~20 s, while SRX was shown to have an ATP turnover rate of ~230+-24 s(Hooijman et al., 2011);(McNamara et al., 2014). The structure proposed to associate with SRX and DRX is called interactive head motif (IHM). Closed (IHM) state of myosin heads was shown to be a favourable state of myosin heads which was observed in both purified myosin(Burgess et al., 2007; Hyun et al., 2008; Jung et al., 2011; Wendt et al., 1999, 2001) and in isolated thick filaments from striated muscles(Woodhead et al., 2005; Zoghbi et al., 2008) (see Figure 13 A & B). The initial discovery of SRX was made in rabbit skeletal muscle, but shortly after, it was shown to exist in rabbit cardiac, tarantula exoskeletal, mouse skeletal and human cardiac fibres(Hooijman et al., 2011)(Alamo et al., 2016; Cooke, 2011; Wilson et al., 2014)(Anderson et al., 2018). Sarcomeric proteins like myosin binding protein-C (MyBP-C) have been shown to control over SRX and DRX states of myosin heads(McNamara et al., 2019). In IHM, the interaction between myosin heads and myosin-binding regions of the actin filament is inhibited by interactions of myosin heads with each other and their fold back on the myosin tails (Irving & Craig, 2019). Further proof has been shown to underline the relation between SRX and IHM (Zhao et al., 2008)(Wilson et al., 2014). SRX and DRX coexist in a constant state of dynamic equilibrium. Such an equilibrium exists to create a more energy-favourable system in which less energy is used due to a larger part of myosin heads being in SRX rather than DRX. If all heads were to be in DRX, metabolic intake of an additional ~1000 Cal per day (~50% increase in metabolic rate) would be needed to compensate for energy requirements(Cooke, 2011). In skeletal muscle, SRX was shown to convert to DRX in times of extreme stress, which would make sense due to the instant contraction force that is required from skeletal muscles (Linari et al., 2015). Interestingly, several pharmaceutical companies are currently pursuing pharmaceutical agents that would initiate a decrease in SRX in favour of DRX to produce a drug for treating obesity and type two diabetes by increasing a patient's metabolic rate (Nogara et al., 2016). Studies performed on both skeletal and cardiac fibres revealed a difference in SRX states in different started muscles. During the addition of excess ADP to the muscle tissue, the proportion of SRX was fully turned into an active state in skeletal muscles while cardiac muscles retained some SRX(Hooijman et al., 2011). Several mechanisms that would explain the sudden change from SRX to the active state were proposed for skeletal muscles. First, an unproven but straightforward explanation is that a myosin head brought out of SRX disrupts SRX in adjacent myosin heads, thus bringing them all into the active state(Moss & Fitzsimons, 2010). Second, a theory proposes that since myosin MyHC (in tarantula thick filament) has two heads of which one is strongly bound to the core of the thick filament and has no affiliations with actin and the second one which can extend towards thin filament and interact with actin, it is possible that configuration of vertebrate skeletal muscle also has a similar structural configuration which allows actin-binding head to cooperatively activate thick filament (Brito et al., 2011)(Sulbarán et al., 2013). The cardiac muscle “not-complete” decrease in SRX during ADP addition is associated with the difference in the physiological functions of set muscle tissues(McNamara et al., 2014). The ultrastructures of thick filament have been solved (Crowther et al., 1985) and improved by

using cryo-EM and improved image processing (Roger Craig & Woodhead, 2006; Woodhead et al., 2005). The structural interactions in adjacent myosin heads have been shown in tarantula thick filament (Woodhead et al., 2005).

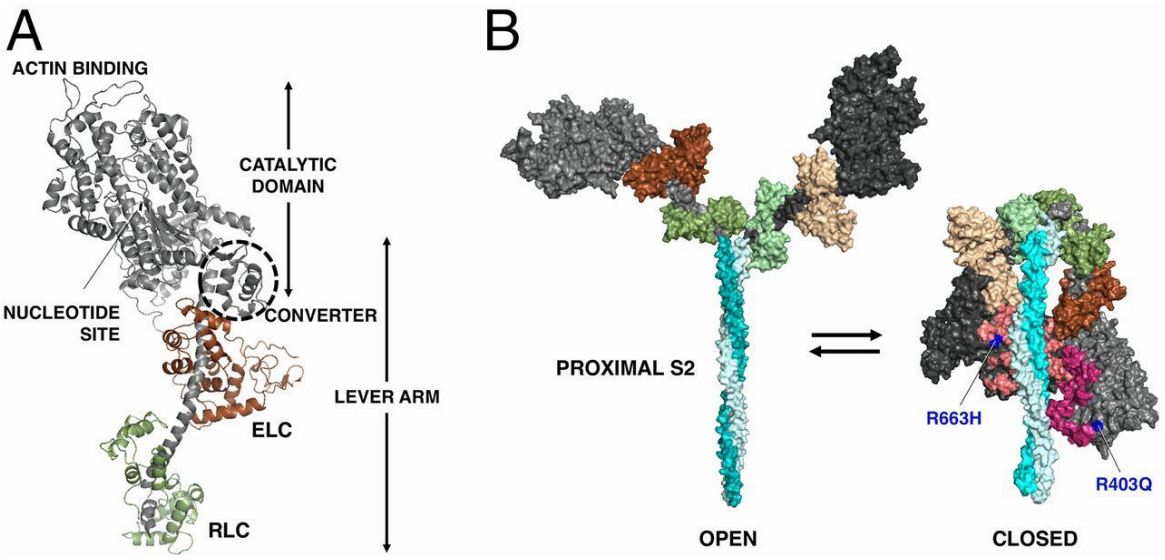

Figure 13.

A) A structural representation of myosin head subfragment 1 in the pre-stroke state. The ELC is shown in brown, while RLC is shown in green. B) A structural representation of open and closed IHM states of myosin head HMM. The motor domains are coloured black (blocked head) and grey (free head). The ELCs are shown in brown, while RCLs are shown in green. S2 helix is shown in pale blue. R663H and R403Q mutations associated with hypertrophic cardiomyopathies (HCM) are shown by blue dots (Anderson et al., 2018).

a. Myosin Binding Protein-C

Myosin binding protein-C is a myosin filament associated protein that modulates cross-bridge formation and kinetics (Koretz, 1979; McClellan et al., 2001). There are three isoforms of MyBP-C: slow skeletal, fast skeletal, and cardiac. MyBP-C can only be found in the C-zone of the thick filament, and it is regularly patterned in 7-9 transverse parallel stripes approximately 43 nm apart. MyBP-C can be described as polymer protein approximately 40 nm in length and 3 nm in width with a molecular weight of about 140 kDa. MyBP-C has 10 domains C1-C10, the actual binding motif is situated between C1 and C2 subdomains. In the cardiac isoform of MyBP-C, there is also an immunoglobulin domain in the C0 subdomain and 4 serine residues in the M-domain (Yasuda et al., 1995) (Gautel et al., 1995). With C-terminus, myosin binding, protein-C binds to the thick filament, while with its N-terminus, it can interact with both the actin filament and myosin heads(Moos et al., 1978; Shaffer et al., 2009). The aforementioned serine residues can be phosphorylated by several kinases (Barefield & Sadayappan, 2010). Experiments have shown that mice trabeculae treated with protein kinase A (PKA) had demonstrated increased contractility. PKA mimics beta-adrenergic activation, which enables the release of myosin heads from the thick filament, thus enabling them to move closer to the thin filament(Colson et al., 2008, 2010). Further reading on mice experiments (Colson et al., 2007, 2008, 2012). A more recent study (McNamara et al., 2019) (also on mice) aimed to determine the mechanism by which cardiac myosin binding protein-C phosphorylation increases contractile kinetics. This study tested the hypothesis that phosphorylated cardiac myosin binding protein-C increases the number of active myosin heads by releasing them from SRX into a more active state. In this study, mice with different (alanine or aspartic acid) substitutions for three main phosphorylatable serines (273,282 and 302) of cMyBP-C were used to establish the relation between cMyBP-C and SRX. Their experiments had shown that phosphomimetic cMyBP-C destabilized SRX, while phosphor-ablated cMyBP-C was stabilising SRX. Serine 282 sites were found to play a critical role in SRX regulation. Experiments with PKA were also conducted in this study on wild type mice samples. They have shown a reduction in SRX, thus confirming the results from previous studies. They have also added PKA to non-phosphorylatable cMyBP-C samples where there was no detectable effect. During other experiments, they added recombinant myosin S2 to their samples, where they saw a significant decrease in the SRX population, thus increasing force generation and rate of tension redevelopment in skinned fibres. Interaction between cardiac isoform of myosin binding protein-C and RLC was proposed in 1985 (Margossian, 1985). It was suggested that such an interaction might be via the cardiac-specific domain C0 of cardiac myosin binding protein-C (Ratti et al., 2011). This suggestion is supported by the results (Harris et al., 2004; Herron et al., 2006; Kunst et al., 2000) obtained from experiments with short, N-terminus MyBP-C fragment as it contains C0 domain. It must also be added that genetic mutations in the MYBPC3 gene that encodes for myosin bind protein-C constitute a significant cause of hypertrophic cardiomyopathy (HCM) comprising ~ 40 % of all known mutations (Van Dijk et al., 2009). Together with mutations in other major thick filament binding proteins that include ELC, RLC and titin, they make up >70 % of HCM cases with an identified genetic cause (Konno et al., 2010).

b. Regulatory light chain and phosphorylation

Regulatory light chain (RLC) is a part of myosin HMM, essential in converting chemical energy into mechanical work. It was shown that by removing light chains, the sliding velocity of actin filament in motility assays has decreased by 10 without affecting ATPase activity (Lowey et al., 1993). In human cardiac muscle, RLC is phosphorylated at Ser-15 by the Ca^{2+}/calmodulin-dependent myosin light chain kinase (MLCK) (Scruggs et al., 2010). The phosphate group that binds to RLC has a negative charge, thus repelling RLC with myosin head from thick filament core (H. Lee Sweeney et al., 1994)(Levine et al., 1996). The repulsion was shown to reduce the proportion of myosin heads in SRX through the electron micrographs and X-ray diffraction studies of the tarantula thick filament. This study had shown MLCK treatment disorders myosin heads in the relaxed state (R. Craig et al., 1987; Padrón et al., 1991). Further studies in tarantula have shown that phosphorylated RLC reduces the proportion of SRX via disorder in the helical structure of the thick filament (Alamo et al., 2008). Studies in vertebrate cardiac muscle treated with MLCK have shown an increase in density of cross-bridges near the thick filament, which indicated a high level of thick filament disorganisation (Colson et al., 2010). The treatment of RLC with MLCK increases resting and maximum force, the rate of force development and Ca^{2+} sensitivity in cardiac trabeculae, thus allowing phosphorylated RLC to shift myosin heads from SRX into DRX. The increase in Ca^{2+} would precipitate the changes in actin filament described before, which, together with changes to RCL, would result in increased resting and active forces (McNamara et al., 2014). Studies in rat trabeculae have shown that MLCK phosphorylated recombinant RCL have increased maximum power output and shortening velocity compared to while type (Toepfer et al., 2013). Rats in which RLC was either dephosphorylated or non-phosphorylatable have experienced a 4-fold decrease in isometric force and reduced maximum power compared to phosphorylated and wild type RLC mice (Scruggs et al., 2009; Toepfer et al., 2013). The transgenic mice have also experienced a presence of systolic impairment without any change in end-diastolic volume, thus leading to the conclusion that RLC dephosphorylation may reverse myosin heads from DRX back into SRX, resulting in reduced force production (Stewart et al., 2010b)(Naber et al., 2011). Studies of human heart failures associated with HCM have been shown to relate to RLC coding sequence mutations and a general increase in RLC phosphorylation (Toepfer et al., 2013) (Yuan et al., 2015)(Sa et al., 2018)(Kampourakis et al., 2018).

C. Hypertrophic Cardiomyopathy

i. General Information and significance

HCM is the most common genetic heart condition with a mutational prevalence of 1 in 500 (*Hypertrophic Cardiomyopathy (HCM) | American Heart Association*, n.d.; *Hypertrophic Cardiomyopathy (HCM) | BHF*, n.d.). Physiological manifestations of HCM may vary considerably, and pathophysiology is not always closely linked to outcome (Marian & Braunwald, 2017). Overall, HCM results in a thickening of the left ventricular wall up to >=13 mm in adults (Maron et al., 1995). HCM can be defined as an archetypical single gene disorder with an autosomal

dominant inheritance pattern (Greaves et al., 1987). In other words, a single mutation is usually a cause of HCM. The large variability in the phenotype of HCM is mainly due to the other genetic and non-generic influences (Marian & Braunwald, 2017). The link with the X-linked model (sex-related) is documented but rare (Hartmannova et al., 2013)(Branzi et al., 1985). Good examples of mutations that have been shown to link with HCM are Atg403Glu mutation in the MYH7 gene, which encodes a beta-myosin heavy chain and mutations in MYBPC3 that codes for myosin binding protein C (Geisterfer-Lowrance et al., 1990). These two mutations are the most common mutation causes for HCM and are responsible for about 50 % of HCM cases(Millat et al., 2010)(Richard et al., 2003). HCM is a genetically related disease; thus, family history of HCM or genetic testing may reveal the presence of this disease. Apart from genetic testing, an increase in left ventricle wall thickness to greater than 13 mm will cause HCM diagnosis if there is no other cardiac or systemic disease capable of explaining this thickening. HCM diagnosis in most often established with non-invasive cardiac imaging (e.g. echocardiography, cardiac magnetic resonance imaging). Physical manifestations of HCM are highly variable. Some of them may manifest into arrhythmias (atrial fibrillation and malignant ventricular arrhythmias) or may be asymptomatic all together (Cirino & Ho, 1993). Full list of symptoms includes exertional dyspnea, fatigue, palpitations, light-headedness, syncope, atypical chest pain and sudden cardiac death (SCD). The degree of severity of symptoms highly depends on the degree of left ventricle hypertrophy (LVH) and severity of left ventricular outflow track obstruction (LVOTO). Large proportion of young patients with HCM remain asymptomatic or minimally symptomatic throughout life. The most devastating complication that may occur with HCM patients is SCD. SCD triggers remain poorly understood (Teekakirikul et al., 2019).

ii. HCM association with mutations in the components of the thick filament

MYBPC3 gene encompasses more than 21 kbp and comprises 35 exons, including 34 coding (see Figure 14)(Carrier et al., 1997). MYBPC1-3 codes the three isoforms of myosin binding protein-C for slow skeletal, fast skeletal, and cardiac, respectively. At this moment, more than 350 individual mutations in MYPBC3 were identified in patients with inherited HCM. This number represents 40-50 % of all HCM mutations, making it the most frequently mutated gene in HCM (Behrens-Gawlik et al., 2014; Schlossarek et al., 2011). More than 60 % of MYBPC3 are truncating mutations. They include nonsense mutations, insertion, deletion, splicing and branch point mutations. These mutations lead to COOH-terminally truncated cMYBP-C, which lacks the major myosin and/or titin binding sites (Behrens-Gawlik et al., 2014). MYBPC3 associated HCM mutations are primarily heterozygous, thus resulting in late disease onset (Carrier et al., 2015). Founder mutations have been identified in multiple studies (Adalsteinsdottir et al., 2014; Calore et al., 2015; Christiaans et al., 2010; Jääskeläinen et al., 2004; Kubo et al., 2005; Niimura et al., 1998) and can all be underlined by truncating mutations that result in shorter cMyBP-C which lacks phosphorylation M motif and/or major binding domain to other sarcomeric proteins. For a complete review, see (Carrier et al., 2015).

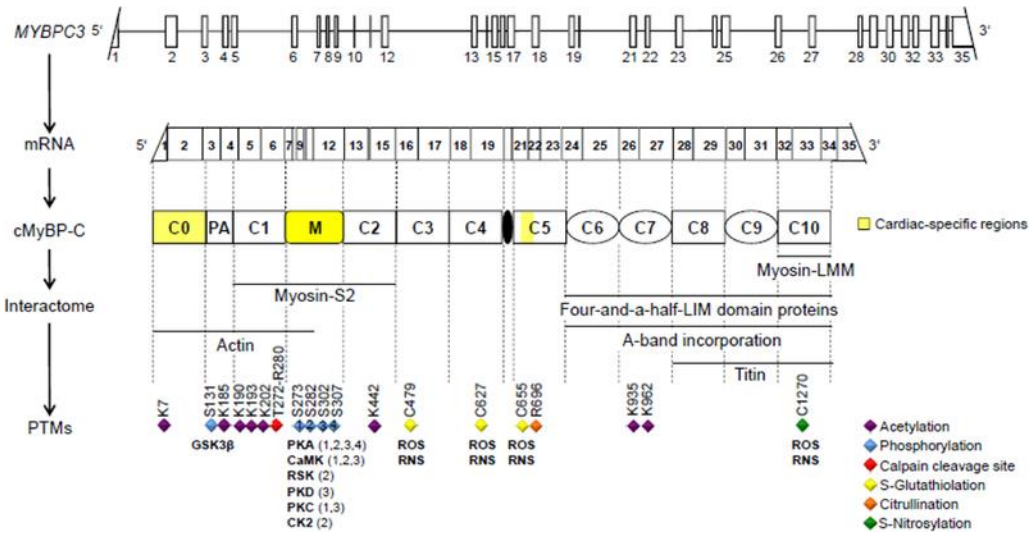

Figure 14

A schematic representation of myosin binding protein-C coding gene MYBPC3 with mRNA, protein structure, interactome (interaction partners) and PTMs (sites of posttranslational modifications. Cardiac isoform-specific regions are labelled in yellow. Different posttranslational modifications are labelled in different colours with legend provided (Carrier et al., 2015).

Mutations in RLC and ELC coding genes can also cause HCM. In early research, the analysis of RLC gene MYL2 and ELC gene Myl3 for 186 unrelated individuals with HCM had precipitated two mutations in MYL2 that may associate with HCM. These missense mutations we very different. One was associated with early stages with no clinical manifestation, while the other was associated with early onset of clinical manifestation and premature SCD. The conclusion was drawn that mutations in MLC are very rarely (about 1 %) the cause of HCM (Kabaeva et al., 2002). A more recent study shows that R58Q mutation in RLC is associated with HCM. They show that R56Q mutation promotes an OFF state of the tick filament by increasing the number of SRX states of myosin heads, thus reducing ATP turnover rate and slowing interaction between actin and myosin filaments in A-band. They also show that the phosphorylation of R58Q mutated RCL to normal physiological levels restores the thick filament's regulatory state and increases calcium sensitivity. They concluded that missense mutation in R58Q is associated with HCM and that this signalling pathway offers a promising target for pharmaceutical development (Kampourakis et al., 2018). Further reviews of different musicians in RLC causing HCM are available here (Huang & Szczesna-Cordary, 2015). Mutations in titin coding genes like TNNT2, TNNI3 and TPM1 are a less common cause of HCM. They cause less than 10 % of cases (Erdmann et al., 2003; Kimura et al., 1997; Richard et al., 2003; Thierfelder et al., 1994). Mutations in other coding genes like cardiac alpha-actin (ACTC1), cysteine and glycine-rich protein 3 (CSRP3) are a cause of HCM, although these are even less common (Geier et al., 2008; Mogensen et al., 1999).

D. Pharmacology

i. Mavacamten and omecamtiv mecarbil

Mavacampten (MAVA), formerly known as MYK-461, is a selective allosteric inhibitor of cardiac myosin ATPase, which causes a decrease in contractile activity of the left ventricle in both healthy

and HCM patients. Currently, this drug is in phase 3 clinical trials. MAVA acts directly by interacting with human beta-cardiac myosin and normalizing its power output. MAVA was identified during the actin-activated myosin ATPase inhibitors trial as it could lengthen the total cycle time of the ATPase cycle by pushing myosin heads into SRX state. MAVA was shown to drive myosin heads into the state of SRX by adding it to purified human beta-cardiac myosin. In this experiment, 10 uM MAVA in the presents of 25-hep HMM at both 25 mM and 100 mM potassium acetate was shown to be approaching 100 % SRX. Although it is known that MAVA inhibits the actin-myosin cross-bridge formation, the precise mechanism of inhibitions is unknown (Anderson et al., 2018). Further figures should be provided to indicate the success that MAVA achieved during the last phase of its pharmaceutical trials. Fifty-nine participants with the mean age of 54 years and 58 % women were subjected to 200 ng/ml,500 ng/ml and 0 ng/ml of MAVA. Serious adverse events in patients occurred in 10 % of >0 ng/ml participants and 21 % of participants on placebo. Five MAVA(>0ng/ml) participants were observed to have a reversible reduction in LVEF by <=45 %(Ho et al., 2020).

Omecamtiv Mecarbil (OM), formerly known as CK-1827452, is a selective cardiac myosin activator. OM specifically binds to the S1 domain of the cardiac myosin head without any specific effect on other types of muscle tissue (i.e. skeletal and smooth). Unlike MAVA, OM has a clear mechanism of action. OM has a binding site in a narrow cleft between the N-terminus 25-K domain and the lower portion of the 50 kDa domain. OMs attach to serine 148, which is ~6.5 nm from the actin-binding site of the myosin head and ~3 nm from the ATP binding site. The conformational change produced by OM attachment results in increased speed of ATP hydrolysis by myosin heads that consequently increase the speed of Pi release, thus accelerating the transition from weakly bound to strongly bound force-producing state (Kaplinsky & Mallarkey, 2018). Essentially OM in opposition to MAVA drives myosin heads from SRX into DRX and DRX into active attachments.

E. Other recent sarcomeric imaging studies

A recent study (Pandzic et al., 2020) showed a new method of observing and analysing data recorded by treating cardiac muscle with blebbistatin and comparing pre-blebbistatin with post-blebbistatin treated muscle. Blebbistain is a myosin inhibitor most specific for myosin II. In their experiment, two types of ATP-Alexa-647 attachments were measured. First was free (unbound) ATP molecules; these attachments could be characterised as ATP molecules that are not bound to the myosin heads but instead exist free in sarcomeric space. The second type was bound ATP molecules; these are ATP molecules bound to myosin heads. By measuring, normalising, and plotting the binding of these two types of ATP molecules, they have shown that the addition of blebbistatin increased the binding times of bound ATP molecules and decreased the number of unbound ATP molecules. They have concluded that blebbistatin pushed myosin heads into the SRX, thus increasing the attachment time for bound ATP and reducing the number of free ATP molecules as more of them were stuck in SRX. Stochastic Optical Reconstruction Microscopy (STORM) is one of the super-resolution (SR) fluorescent microscopy technics that are used to increase the diffraction-limited resolution(Heilemann et al., 2008; Rust et al., 2006). Other SR techniques include structured illumination microscopy (SIM) (Gustafsson, 2000), stimulated emission microscopy (STED) (Hell & Wichmann, 1994) and photo-activated localization (fluorescent) ((f)PALM) (Betzig et al., 2006; Hess et al., 2006). STORM resolution is advantageous to other SR techniques as it uses organic dyes and has a resolution of ~20 nm. STORM utilises optically switchable fluorophores, which are switched between fluorescent and non-fluorescent states in each frame. With a large number (typically 5, 000 – 40, 000 frames) of frames taken localization algorithm determined the centre positions of each fluorescent event at a nanometre scale. Finally, with an overwhelming number of fluorophore centres analysed, the final images are reconstructed with resolution improved by 10 times (J. Xu et al., 2017). Multiple reviews have been written for general principles of STORM and detailed labelling of photo-switchable fluorophores (Bates et al., 2013a, 2013b; Endesfelder & Heilemann, 2014; Van De Linde et al., 2011).

Another recent study (Nelson et al., 2020) was conducted to investigate the spatial arrangement of ATP molecules in relaxed striated muscle and the effects of MAVA on myosin heads in set muscles. In this study, STORM was used to determine the spatial arrangement of BODIPY-ATP attaching to each zone of the thick filament with both frequency and duration of ATP attachments. Data analysis that followed produced two distinctive lifetimes of ATP molecules fitted to two exponentials. These two exponentials are believed to represent DRX and SRX states of relaxed myosin heads. ATP molecules were separated into C, D, and P zones with both position and durations. The zones were determined using anitimyomesin-labelled M lines. After separating events into different zones, the amount of SRX myosin heads were determined for each zone using the durations of ATP attachments. Experiments were repeated with presents of MAVA (MAVA+) and without MAVA present (MAVA-). The results indicate that in MAVA- a condition, the largest portion of SRX states were localised in the C zone, while the D and P zones had mainly DRX. Upon the addition of MAVA, all zones appear to have the same amount of SRX with a slight (negligible) decrease in C-zone and a massive rise in D and P zones (see Figure 15).

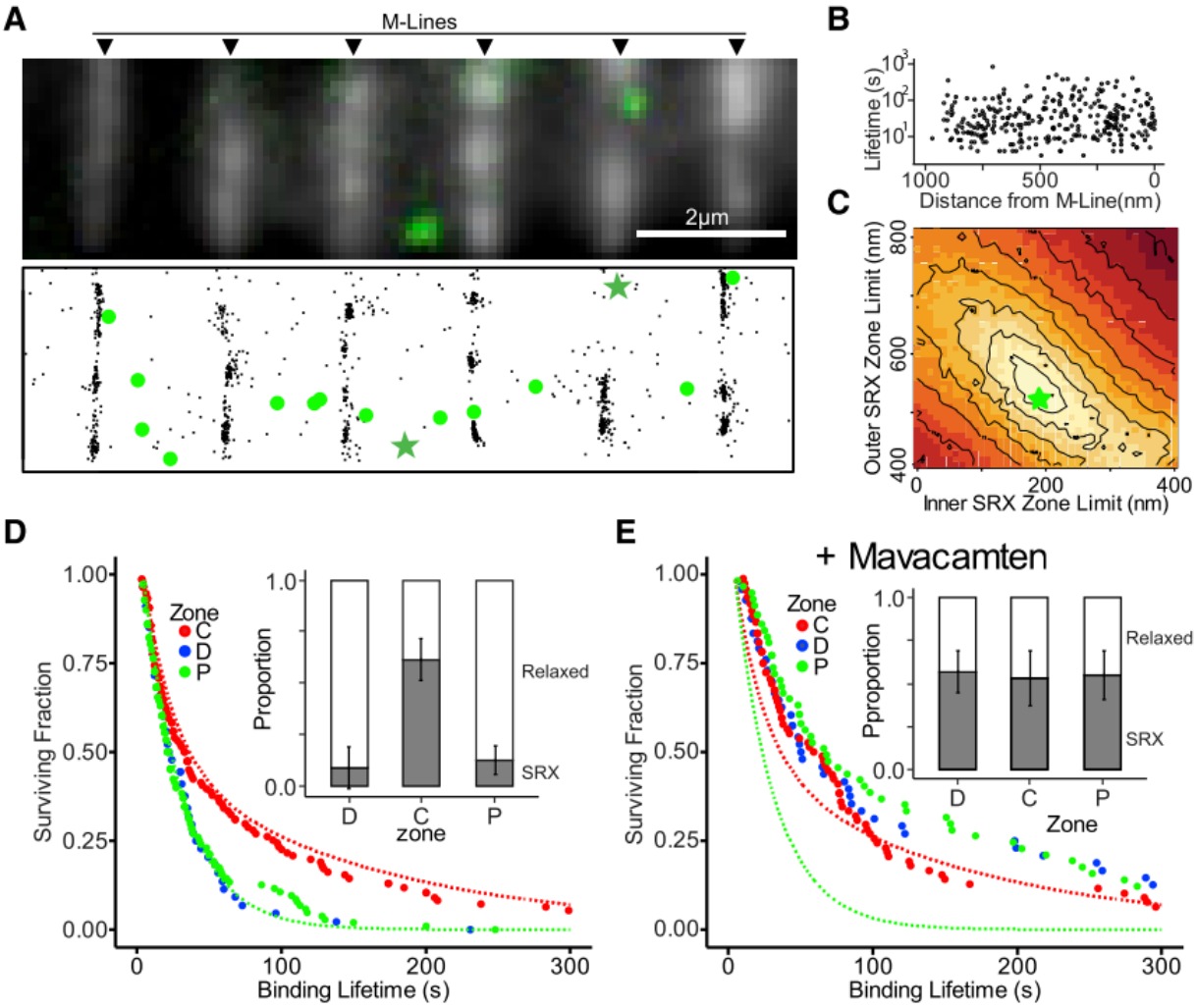

Figure 15.

A) Top image shows fluorescently illuminated M-lines and fluorescently labelled ATP molecules shown in green. Bottom images Bottom panel shows the top image that was colour and drift corrected using subpixel localisation. Myomesin-labelled M-lines are shown as black dots. Fluorescently labelled ATP molecules are still shown in green. Green stars represent ATP attachments observed in the top panel. B) A graph representing time versus distance from the M-line of fATP binding events. C) A root mean-square deviation heatmap that compares predicted SRX-containing zones of variable width to experimental data. D) A survival plot representing lifetimes of events D, C and P zones acquired in experiments without MAVA. The dotted red line represents a simulated zone with all myosin heads in SRX, while the green one represents a simulated zone with all myosin heads in DRX. The bar chart at the top-right corner of the graph represents the proportion of SRX (shaded-SRX, non-shaded DRX) in each zone. E) Same as D) but for experiments with MAVA (Nelson et al. 2020).

F. Aim of this thesis

This thesis will describe our way of preparing, imaging, and analysing spatial arrangement of Rhodamine-labelled ATP molecules with anti-alpha-actinin labelled Z-lines for the goal of determining the SRX arrangement in C, D and P zones of the thick filament, as well as using MAVA+ experiments for comparison with MAVA- conditions and further proof of MAVA effectiveness in inhibition of myosin heads. Much like the two studies described above, we aim to establish a methodology for single-molecule muscle analysis's experimental and analytical parts. Although at this stage of this thesis will be focusing exclusively on skeletal muscles, we would like to hope that in the future, it will be possible to expand our attempts into healthy cardiac muscles and cardiac muscles from HCM affected patients.

7. Materials and Methods

A. Buffers and Reagents

All buffers were diluted using purified water at an 18.2 mΩ/cm resistance from a Synergy ultrapure water (Type 1) system at room temperature. Sodium-azide was added to long-term storage buffers for microorganism growth control.

Fibre preparation buffer:

6 mM Imidazole, 8 mM Mg-acetate, 70 mM Propionate pH 7.0, 5 mM EGTA, 7 mM ATP, 1 mM Na-azide

Fibre skinning buffer:

6 mM Imidazole, 8 mM Mg-acetate,70 mM Propionate pH 7.0, 5 mM EGTA, 7 mM ATP, 1 mM Na-azide, 0,5 % $HO(C_2H_4O)_{20}C_{16}H_{33}$

Fibre storage buffer:
6 mM Imidazole, 8 mM Mg-acetate, 70 mM Propionate pH 7.0, 5 mM EGTA, 7 mM ATP, 1 mM Na-azide, 50 % Glycerol

Fibre buffers contained Imidazole Mg-acetate Propionate and ATP to imitate conditions in relaxed conditions living muscle tissue. EGTA was added to deprive tissues of any Ca^{2+} and thus prevent contractions. $HO(C_2H_4O)_{20}C_{16}H_{33}$ was added for chemical skinning. Glycerol was added to prevent water in muscle tissues from freezing while allowing for storage at -20 °C.

Wash Buffer:
6 mM Mg Acetate, 10 mM EGTA, 54 mM Na Acetate, 18 mM Na2SO4, 10 mM MOPS, 1 mM DTT*
*Add on the day of experiment

Wash Buffer (relaxed):
6 mM Mg acetate, 10 mM EGTA, 54 mM Na Acetate, 18 mM Na2SO4, 10 mM MOPS, 5 mM ATP**, 1 mM DTT*
*Add on the day of the experiment
** Added on the day and varied depending on experimental requirements

250uM dATP wash buffer:
10 uM dATP, 1 mg/ml BSA, 50 nM PEP, 1 ul PK, 6 mM Mg Acetate, 10 mM EGTA, 54 mM Na Acetate, 18 mM Na2SO4, 10 mM MOPS, 1 mM DTT*
*Add on the day of experiment

50nM RdATP imaging buffer:
50 nM RdATP, 1 mg/ml BSA, 50 nM PEP, 1 ul PK, 6 mM Mg Acetate, 10 mM EGTA, 54 mM Na Acetate, 18 mM Na2SO4, 10 mM MOPS, 1 mM DTT*
*Add on the day of experiment

Wash and imaging buffers contained Mg Acetate, Na Acetate, Na2SO4 and MOPS to imitate conditions in relaxed conditions living muscle tissue. PEP and PK were added as part of the Regeneration system. RdATP, BSA and dATP were added for imaging purposes.

Stopped Flow buffer
25 mM KCl, 20 mM MOPS, 5 mM MgCl2, 1 mM Na-azide

B. Muscle preparation

i. Chemical skinning of rabbit psoas skeletal muscles

Rabbit psoas skeletal muscles were dissected from tissues using the following skinning method. First, 3-4 cm long and 1-2 mm in diameter muscle fibres were dissected from flash-frozen psoas muscle. Second, they were tied to the toothpick with a strong thread by each end of the fibre, so the middle part of the fibre remained loose while the ends were fixed to the toothpick. Third, sample sticks were equilibrated in 25 ml of Fibre preparation buffer by adding 50 ml Fibre preparation buffer to the 50 ml tubes containing toothpicks with the sample; the sample was kept on ice during equilibration. Fibre preparation buffers were changed four times every 30 minutes. Fourth, fibres were skinned for 2 hours by adding 50 ml Fibre skinning buffer to the 50 ml tube containing sample sticks. Finally, sample sticks were equilibrated with 50 ml fibre storage buffer at 4°C for 2 hours before moving them to permanent storage at -20°C.

ii. Myofibril preparation of skinned rabbit psoas skeletal muscles

On the day of the experiment, a small part of the skinned skeletal muscle was cut for myofibril preparation. Skeletal muscle stick was placed into Wash buffer, and a piece of a muscle: 2-3 cm

long, 2-3 mm thick was cut from set muscle stick. The rest of the stick was placed back into a fibre storage buffer and stored for future use. All muscle cutting and dissections were performed on ice. A long piece of tissue cut from the stick was further cut into smaller pieces, each ~0.75-1 cm long. Smaller pieces were then stripped into smaller strips. It was found that smaller strips provided better myofibrils during imaging. It was also found that strips that were unbroken during stripping have also provided better images. Strips were then transferred into 800 ul Washing Buffer one by one to prevent them from sticking together and forming knots that would later decrease the quality of obtained images. Buffer containing strips were then homogenized (Tissue Ruptor II, Qiagen) twice using the following template: high speed for 20 sec followed by slow speed for 10 sec with a 30-sec break on ice in between. Homogeniser has moved around while homogenising to ensure complete homogenisation of the sample. The homogenised sample was then observed under the light microscope under max magnification (x400) for quality control purposes. Under a light microscope, myofibrils should appear long, thin-medium thick (~1 uM), striated filaments. Further quality control was established by measuring OD600 using a spectrophotometer. Measuring OD600 provided a rough estimate of the density of the myofibrils in the sample, thus allowing all experiments to have approximately the same myofibril density. Wash buffer was used as a blank for the spectrophotometer, and the optimal OD600 was found to be ~0.85 ±0.1.

C. Preparation of flow cell chamber

Flow cells are an assembly of standard microscope slides, gaskets, and coverslips. Microscope slides were modified by drilling two 3 mm diameter holes followed by shaking at 150 rpm on an SK-0180-Pro overnight in a 100 % ethanol bath. Gaskets were created from double-sided tape cut into 10x15 mm (inner dimensions) rectangles with a hollow centre. Coverslips were also cleaned in 100 % shaking (same conditions as above) ethanol bath overnight. To further ensure that slides and coverslips were clean, each was plasma cleaned (PDC-32G-2, Harrick Plasma) for 5 minutes on the max setting. After coverslips were plasma cleaned, one of their sides was coated in 5 ul of 15 ug/ml poly-l-lysine. Another plasma cleaned coverslip was then used to spread poly-l-lysine evenly on the surface of other coverslips. Poly-l-lysine covered coverslips were allowed 30 min to dry before assembling the flow cell by attaching gasket atop the slide followed by the coverslip, poly-l-lysine covered side facing the slide. When combined with other parts of the flow cell gasket produced an enclosed 30ul space between the coverslip and the slide surface (see Figure 15).

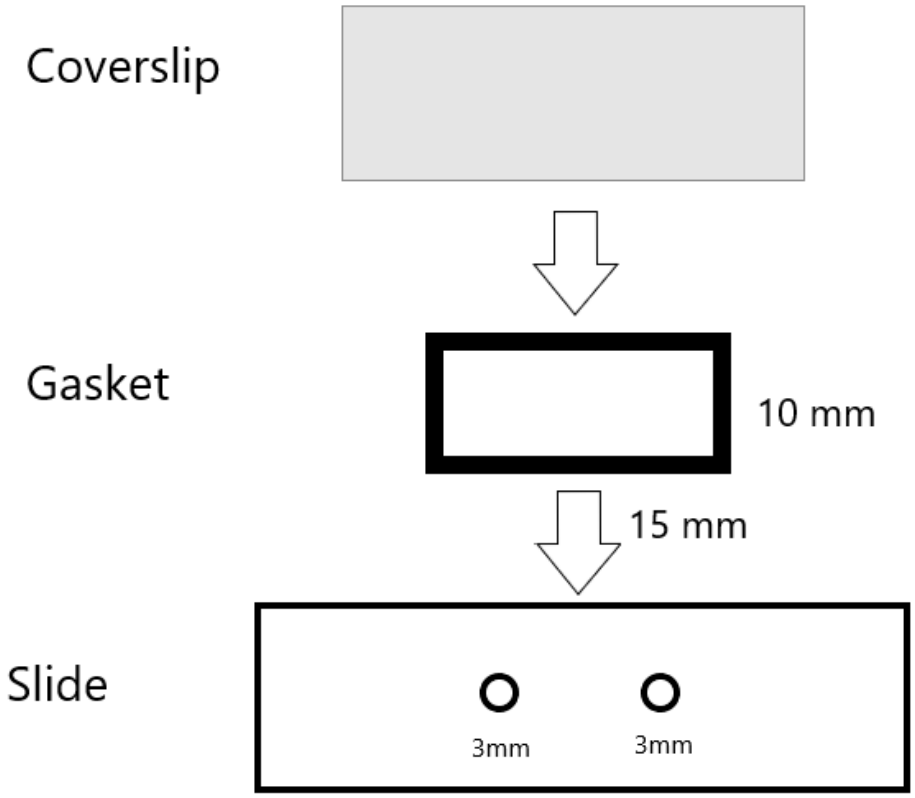

Figure 15.
Representation of assembly of the flow cell. A 10 mm x 15 mm gasket is placed on the slide with holes (3 mm in diameter). The gasket is then covered by a coverslip creating ~30 ul space between the coverslip and the slide surface.

D. Rigor conditions experiments

i. Rigor conditions experiments without MAVA

Following myofibril preparation in rigor conditions, 30 ul were taken from the prepared myofibrils sample and incubated with 30 ul 50 nM RdATP Imaging Buffer. 200 nM anti-alpha-actinin (Monoclonal Anti-α-Actinin (Sarcomeric) antibody produced in mouse, A7811, Sigma) and 200 nM Alexa 488 (Goat anti-Mouse IgG (H+L) Cross-Adsorbed Secondary Antibody, Alexa Fluor 488, A11001, ThermoFisher) were both diluted in 30ul Wash buffer and also added to the sample. This sample was allowed to incubate for 2 h on ice and wrapped in tin foil for fluorophore preservation. 50nM RdATP in imaging buffer containing an ATP regeneration system (described below) enabled any ADP molecules to be converted into ATP over 30 mins. The regeneration system was also added to the 250 uM dATP Wash Buffer to maintain the regeneration process after the final wash. After a 2 h incubation, sufficient fluorescently labelled ATP was exchanged onto the myosin heads such that 1 in 1e6 molecules was labelled. A further 30 min incubation followed the introduction of the myofibrils into the flowcell to permit attachment to the poly-l-lysine coated coverslip. Following the 30 min incubation, 100 ul of 250 uM dATP Wash Buffer (final wash) was flowed into the flow cell to remove the excess RdATP, thus decreasing the

background noise during imaging. Imaging the first myofibril was started <2 min after the 250 uM dATP Wash Buffer was introduced.

ii. Rigor conditions experiments with MAVA

Mavacamten was diluted in 100 % DMSO to 3uM and added to 250 uM dATP wash buffer. Previous investigations (Mariano et al., 2001) show DMSO may have an inhibitory effect on contractile proteins above 5 %; therefore, the concentration of DMSO to which the myofibrils were exposed was kept below 5 % at all times.

E. Relaxed conditions experiments

i. Muscle preparation conditions

Prior to the rigor approach, the relaxed approach was used. In this approach, relaxed (5 mM dATP) conditions were maintained throughout myofibril preparation and throughout all flow cell setup steps except for the last one. During the last step, dATP concentration varied depending on desired fATP/dATP ratio but was never dropped low enough to drive myofibrils into the rigor state.

ii. Flow chamber setup for imaging

Flow cell preparation in relaxed conditions was done very differently from rigor preparation. During the following explanation, Washing Buffer (relaxed) was made with different dATP concentrations that depended on the RdATP/dATP ratio used for different experiments. First, the flow cell was washed with 3x100 ul washing buffer relaxed followed by 30 min incubation. While the flow cell was incubating, Alexa-488 (200 nM) and anti-alpha-actinin (200 nM) were conjugated and left to incubate for 1 h. Second, freshly prepared myofibrils (30 ul) in relaxed conditions were flown into the flow cell and further incubated for 30 min. Following 30 min incubation period, excess myofibrils were washed away with 100 ul wash buffer relaxed. BSA (100 ul,10 mg/ml) was then flown in and left to incubate for 2 min to be swiftly removed by 100 ul wash buffer relaxed. Conjugated Alexa 488 and anti-alpha-actinin were diluted in 30 ul washing buffer relaxed and flown into the flow cell. The flow cell was incubated for 1 h with additional coverage for photobleaching protection. There was some variation for the next step depending on the RdATP/dATP ratio. If RdATP/dATP ratio provided too much background noise during imaging an additional 100 ul wash buffer, the relaxed wash was introduced to reduce set background noise. However, if the background did not interfere with obtaining attachment reading, the last 100 ul wash was not applied. In Mavacamten experiments, mavacamten was introduced either with final 100 ul wash or second-to-last wash, again, depending on the background and RdATP/dATP ratio. Mavacamten had the same 3 uM concentration, 1.5 %DMSO and was incubated for 10 min.

F. Stopped flow experiments

The stopped-flow spectrometer used throughout this thesis was an SF-61 DX2

manufactured by HiTech Scientific, which was capable of double mixing but only used for single mixing. The stopped-flow contained two 700 µL sample syringes driven by air pressure from an external air pressure pump. Both syringes were triggered simultaneously, pushing the reactants into an observation cell in the optical light path of a high-intensity light source. The light source used for these experiments was a LED lamp (290 nm) (ocean optics). The fluorescence of the sample was detected via a photomultiplier placed at a right-angle to the incoming light. When the samples reached the observation cell, they were mixed in a 1:1 ratio resulting in the concentration of both reactants being halved. As the solution left the observation cell, it filled the empty stop syringe, forcing the syringe to hit a back-stop, which immediately ceased the flow. The samples syringes were temperature controlled by an external water bath.

i. RdATP experiments [ATP/ADP]

To determine if Rhodamine labelled ATP we have used contained acceptable ATP/ADP ratio following stopped-flow experiment was conducted. Myosin head sub-fragment 1 (S1) was mixed with Rhodamine ATP. S1 concentration was decreased throughout the experiment from 2.5 uM to 39 nM while RdATP concertation was kept constant at 1 uM. Similarly, S1 was mixed with RdATP that was mixed with regeneration system (PEP/PK). Data obtained from two experiments were then compared to determine if the regeneration system in pace was working. This regeneration system will be described in further detail in the next section of this thesis. All concentrations stated in this section are pre-mixing concentrations. 320 nm filter was used for both experiments. A stopped Flow buffer was used for both experiments.

G. ATP Regeneration system

ATP regeneration system was kept constant throughout all experiments. ATP was regenerated using a mixture of pyruvate kinase (PK) and lactate dehydrogenase enzymes as well as phosphoenol pyruvate (PEP), which had provided inorganic phosphate (P_i) to convert ADP into ATP (see Figure 16). The PEP concentration for the regeneration process was kept at the same concertation as the RdATP concertation to ensure the excess of Pi in the solution. 1 ul of PK was added to each reaction. All reagents (PEP, PK and RdATP) were mixed and allowed to incubate for 30 min. The process of incubation was introduced to allow ample time for RdADP to regenerate into RdATP. Following the incubation, dATP was added to the mixture. dATP concentration was adjusted according to desired RdATP/dATP concentration ratio. All dilutions were made with Wash buffer.

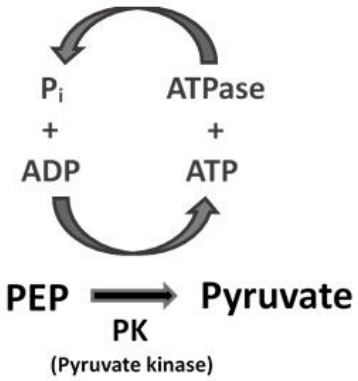

Figure 16.

A schematic reaction of what occurs during the ATP regeneration process. PEP is broken down into pyruvate and inorganic phosphate. P_i is released and can be taken up by ADP to create ATP. PK catalyses this transfer of Pi. ATP is then broken down into ADP with a release of energy, and the process is repeated until no PEP is left.

8. Results

Before we began our imaging and consequent analysis, a simple question was asked. How much of our RdATP stock is ATP, and how much has deteriorated into ADP? Stopped flow experiments were created to determine the exact concentration of ATP in our RdATP stock solution. Once the first experiment was conducted, and it was established that our RdATP mainly was consistent with ADP (>50 %), the Regeneration system was introduced to increase ATP concentration. Stopped flow analysis was then conducted on Regenerated RdATP to confirm the increase in ATP concentration. To determine the spatial arrangement of myosin heads in each zone of thick filament and compare SRX and DRX states from obtained videos, we have utilised the TrackMate plugin of ImageJ and a series of excel spreadsheets. Trackmate was used to track fluorescent ATP attachments to different zones, and Alexa488 labelled anti-alpha-actinin attachments to Z-lines. X and Y coordinates, as well as the duration of each track, were recorded. The data from TrackMate was then transferred into a series of spreadsheets that would place each track in different zones of the sarcomere, thus producing each sarcomere is a list of tracks for each zone in the thick filament. Data from each zone would be then fitted to three exponentials, representing three different states of myosin heads, to determine the proportions of each state in each zone.

A. Data Analysis

i. Stopped flow analysis

Data collected from stopped-flow experiments were analysed using the following method. The fluorescent measurements collected during experiments were plotted against S1 concentrations for both Regenerated and non-regenerated RdATP samples (see Figure 16). Fluorescent emission was measured for tryptophan(*ATP Binding and Hydrolysis by MX-S1 in the Absence of Actin. A,... | Download Scientific Diagram*, n.d.) on S1 (ex=290 nm, em=340 nm) that was bound to RdATP but not for Rhodamine fluorophore (ex=570 nm, em=590 nm). The fluorescence of Rhodamine was cut out by using a 320 filter. Fluorescents produced by tryptophan would increase with the increase of RdATP+S1 complexes. As RdATP concentration was kept constant at 1 uM throughout the experiments while S1 concentration was changed, the fluorescent reading would increase with the increase of S1 concentration until all S1 molecules would be coupled in RdATP+S1 complexes. At this point, the fluorescent intensity would reach the maximum value (Amax) and plateau. It must be said that the concentrations that are stated above are pre-mixing concentrations; thus, although the Amax would be observed at S1 concentration ~1 uM, the actual concentrations of S1 and RdATP inside the mixing chamber at this moment will be halved (~500 nM at 100% ATP). The actual RdATP concentration was derived from the Michaelis-Menten plot (see Figure 17). From Michaelis-Menten equation K_m=½ V_{max} or K_m=½ A_{max} in this case, where ½ A_{max} is half of the maximum amplitude change for each fit. Comparing K_m of each plot to the theoretical [RdATP] at ½ A_{max} indicated the contamination of RdATP with RdADP. The analysis indicated that more than 90% purity was achieved with the regeneration system, while the unregenerated sample has shown <50% purity.

A

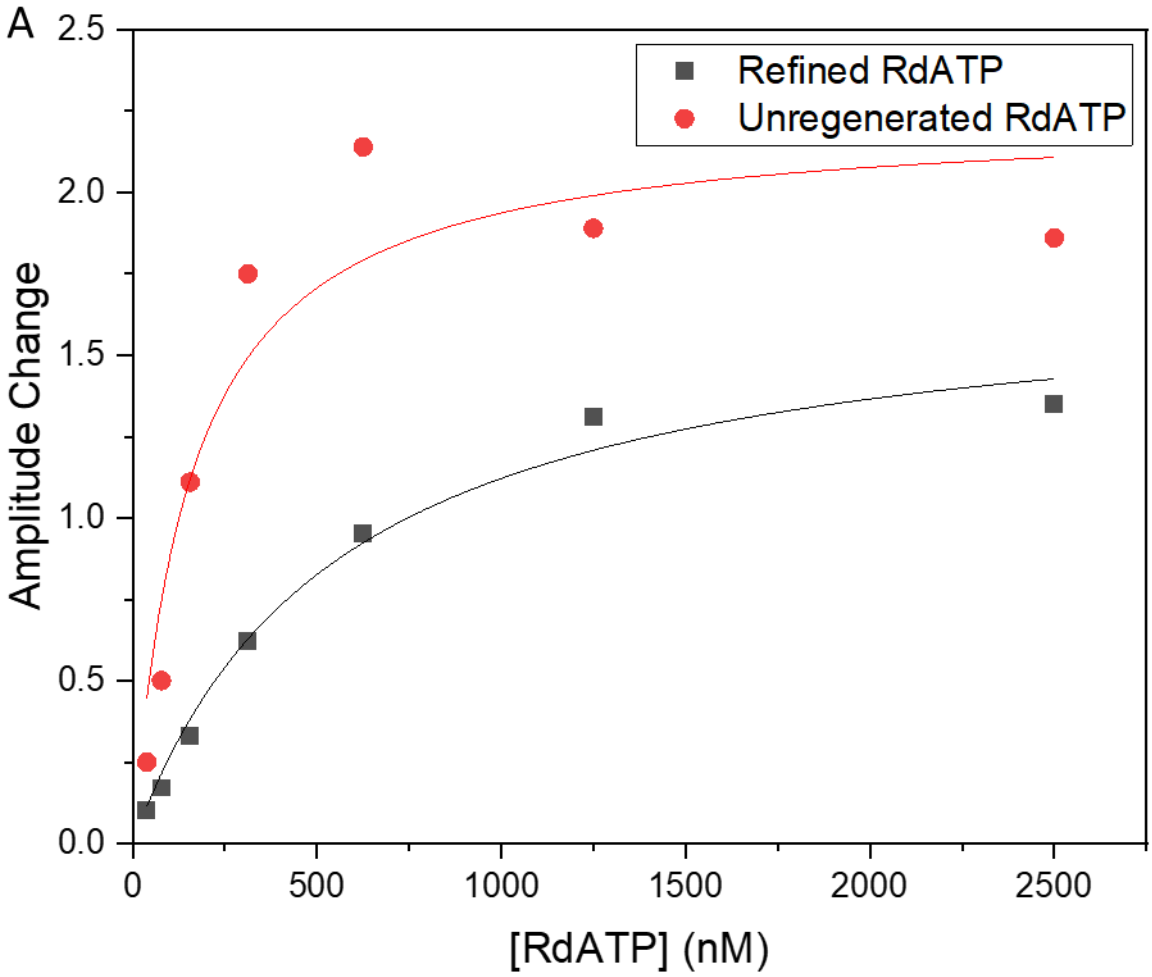

B

Model	MichaelisMenten
Equation	y = Vmax * x / (Km + x)
Vmax	2.23937 ± 0.2346
Km	156.10807 ± 61.28491
Reduced Chi-Sqr	0.07173
R-Square (COD)	0.89215
Adj. R-Square	0.87058

C

Model	MichaelisMenten
Equation	y = Vmax * x / (Km + x)
Vmax	1.74472 ± 0.11289
Km	555.46219 ± 96.10488
Reduced Chi-Sqr	0.00445
R-Square (COD)	0.98644
Adj. R-Square	0.98373

Figure 17.

An output of OriginPro (“Origin 2022 Feature Highlights” n.d.) including a graph and two tables with Km and Vmax values specific to an S1 ATPase affinity for RdATP calculated from stopped-flow experiments.

A) A graph plotted to compare Unregenerated and Refined RdATP. Black dots correspond to experimental data with the ATP regenerating system, whereas red dots correspond to experiments without such a system. Both data sets were fitted to Michaelis-Menten equations (see Figure 17 B and C). The black and red lines correspond to refined and unrefined RdATP data, respectively. B) A table showing OriginPro output for unrefined data. C) A table showing OriginPro output for refined data. Stopped flow experiments were not repeated (n=1).

ii. Image acquisition using OAF microscopy and microscope setup

All experiments involving flow cells were conducted using custom-built oblique angle fluorescent (OAF) microscope, described here (Desai et al., 2015). Rhodamine ATP was excited using a 561 nm diode OBIS LS laser (coherent, USA) at 20 mW, and Alexa-488 labelled antibodies were excited using Oxxius 488 nm also at 20 mW. All images were acquired using the OrcaFlash 4.2 camera (Hamamatsu, pixel size 63.2 nm) using 1x1 binning. Flow cells were placed on a microscope stage and fixated. Brightfield camera (Swann, C500 CCD Colour Camera) was then used to establish an approximate focus of appropriate (see 8.B.ii) myofibril. Imaging was then switched from brightfield to fluorescent (OrcaFlash 4.2), and a 488 nm laser was switched on. Images were displayed in the live feed using ImageJ. During video acquisitions, the 488 nm laser was turned on initially to establish a clear focus without risking photobleaching of the RdATP. Images of Alexa-488 labelled Z-lines were acquired for the first 30 seconds, after which the 488 lasers was switched off, and 561 lasers were switched on to image ATP attachment (see Figure 18). The laser ON time was 200 ms during stroboscopic imaging, including laser pre-exposure time (10 ms). These two parameters were kept constant throughout all experiments while laser OFF times was changed depending on the desired time frame (i.e. overall time 5 s,2 s,1 s etc.). Stroboscopic illumination was set using a custom-written program (Arduino). Once imaging of a single myofibril was done, the microscope was switched to brightfield again to find a new myofibril for further imaging. Ordinarily, up to three myofibrils were imaged per one flow cell.

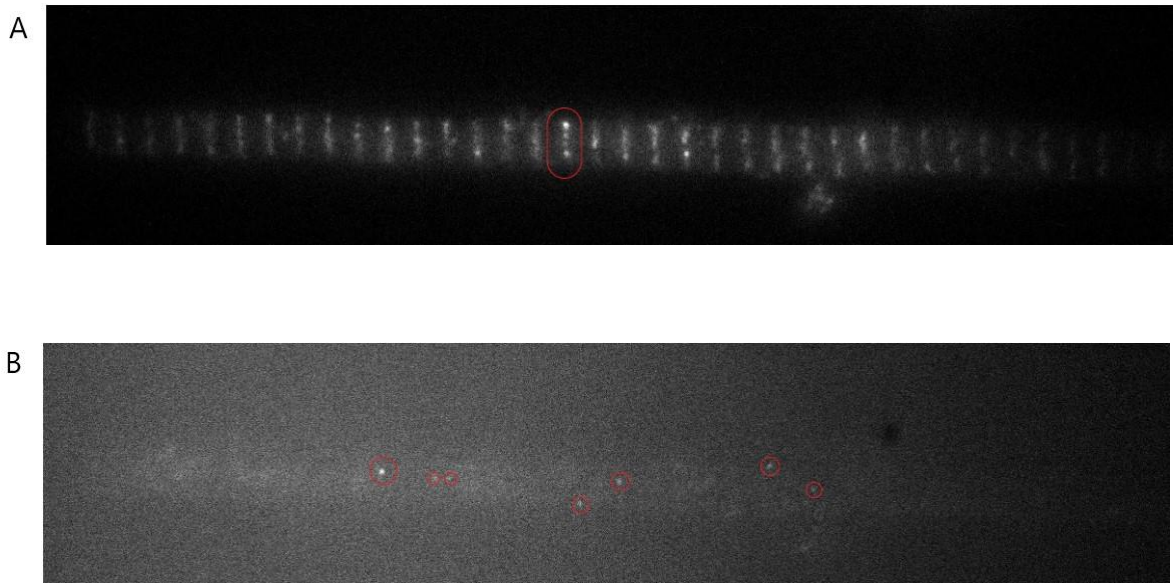

Figure 18.

Images were collected using ImageJ, Orca and lasers described above during stroboscopic illumination with a time frame of 5 sec in MAVA- conditions.

A) Shows the image that was collected during 488 lasers ON time. Alexa488 bound to alpha-actinin is visible, thus marking all z-lines of the selected myofibril. The red oval represents one of many z-lines present in this image.

B) A period of imaging once the 488 lasers were switched OFF and 561 lasers were switched ON. Some rhodamine ATP attachments are visible and labelled with red circles.

These are both images of the middle (605 nm) channel

iii. Single-molecule fluorescent microscopy

1. TrackMate settings and analysis

TrackMate analysis was divided into two parts. During the first part, only Alexa488 fluorophores were tracked as only 488 nm laser was on, and thus only z-line were illuminated. 488 nm laser was switched off after 30 seconds of illumination, and 561 nm laser was switched on for the rest of the acquisition. Only RdATP fluorescence was analysed during the second part as 561 nm laser excites Rhodamine but does not excite Alexa488. The 488 nm illuminated part of the video will be referred to as the first part of the video, and the 561 nm illuminated part of the video will be referred to as the second part of the video. A z-line stack (max intensity) of horizontal slices was made for each second part of the video to ensure that all tracks were correctly recorded. In some cases, tracking was interrupted due to the fluorophore being too dim or moving too far away from the initial binding. With the z-line stack, this problem was eliminated as clear lines of RdATP attachments were visible with a naked eye (see Figure 19). The first part of the video was loaded onto the ImageJ, and the TrackMate plugin was loaded. The video properties were altered to represent the microscope setup (i.e. the number of frames, pixel characteristics and frame

interval). LoG detector was then used with an estimated fATP attachment diameter of 390 nm. The threshold was established through trial and error to only labelled z-lines excluding other random fluorescence. Following the detection, HyperStack Displayer was chosen for view representation. No additional filters were established during any steps of TrackMate analysis. A simple LAP Tracker was chosen to track the fATP attachment. Both Linking max distance and Gap-closing max distance were set to 100 nm, while the Gap-closing max frame gap was set to 20 frames. Some variation in Gap-closing max frame gap was allowed to ensure the entire length of attachments were recognised as a single attachment. Data was then extracted in two excel spreadsheets showing X and Y positions of each track and the duration of each track. Analysis with the same parameters was conducted in the second part of the video.

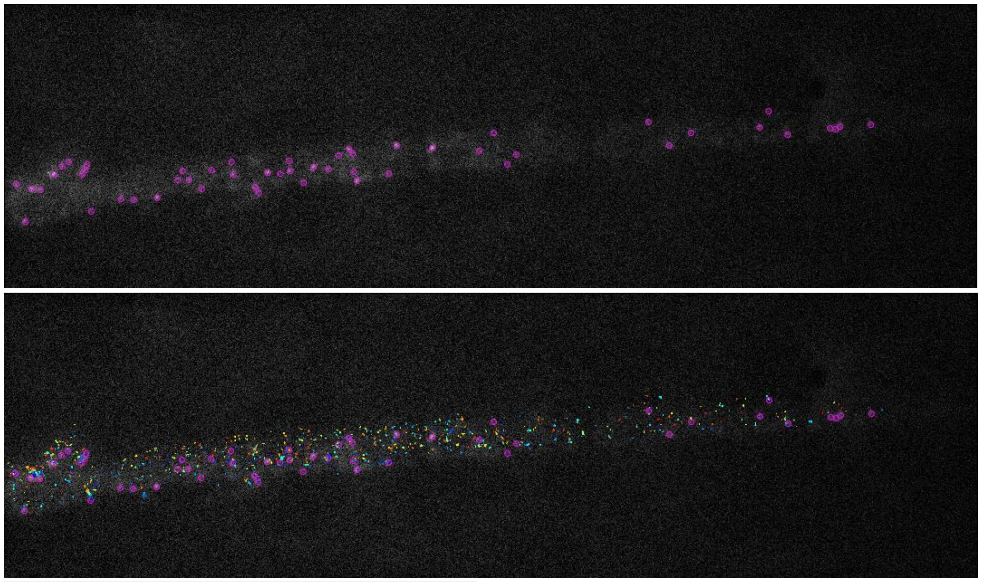

	TRACK_X_LOCATION (nm)	Duration of track(sec)
1	252.417	5
2	277.688	5
3	349.937	5
4	381.182	5
5	387.307	40
6	454.713	20
7	504.356	5
8	582.764	5
9	601.925	5
10	603.874	100

	TRACK_X_LOCATION (nm)	Y Location (mean)(nm)
1	252.417	11721.471
2	277.688	13071.832
3	349.937	13881.901
4	381.182	12435.225
5	387.307	12620.535
6	454.713	12018.138
7	504.356	11966.276
8	582.764	12187.966
9	601.925	12479.059
10	603.874	13277.908

Figure 19.

The following images show the process TrackMate analysis of a single stroboscopic 5 s video as an example of set analysis. Only ATP attachments are shown here, but Z-lines were analysed using the same principal
The first image shows the determination of the threshold and fATP attachment diameter. Although fATP attachment diameter was not changed throughout all analyses, the threshold changed each video. Purple circles represent tracks on that frame that TrackMate is going to follow.
The second image shows the same frame and purple tracks but with all other frames added to this frame. These new tracks are represented in multicoloured dots. The dot's colour depends on how long this particular track has stayed on the myofibril before de-attaching.
The last two images represent typical data that was obtained from each video. This data provided us with the exact x and y positions of each track and tracks duration.

2. Correcting tilted z-lines and ATP position extraction for each sarcomere

As stated above, at the end of the TrackMate analysis, we were left with each track's x and y positions and track durations. It was decided that ATP attachment data should be extracted from one sarcomere at the time so we could first recalculate each x-position into relative position between two z-lines (disused in more detail in next section) and then allocate each ATP track into C, D or P zones of the thick filament. As not all z-lines were perpendicular to the x-axis, it was vital that we devised a method to make them so and at the same time correct ATP positions in a way that would move them together with corrected z-lines. The tilted z-lines correction was done due to the following argument. If z-lines were corrected, we would be able to pick up all ATP tracks between them using the x position of Z-lines at each end of the sarcomere and search the spreadsheet for ATP tracks that had x-values between two z-line x-values. If we were to proceed with z-lines analysis in tilted positions, we would not be able to extract ATP tracks in a way that

utilises x coordinates of Z-lines as we would be excluding or adding some ATP tracks that would otherwise lay within other sarcomeres. With this argument in mind following method was used to correct tilted z-lines. Data obtained from TrackMate analysis was transferred into the excel spreadsheet where both ATP and z-line positions were plotted. The x coordinates of the beginning and the end of one z-line were used to search all z-line tracks that lay between these two coordinates, essentially selecting only the z-line tracks that make up singular z-line. The tilt was corrected by fitting the Z-line to the left of the sarcomere and then correcting all of the positional data to that fit. The same was then applied to ATP positions (see Figure 20). This method was carried out with all sarcomeres one by one to produce a fully untilted myofibril.

Before:

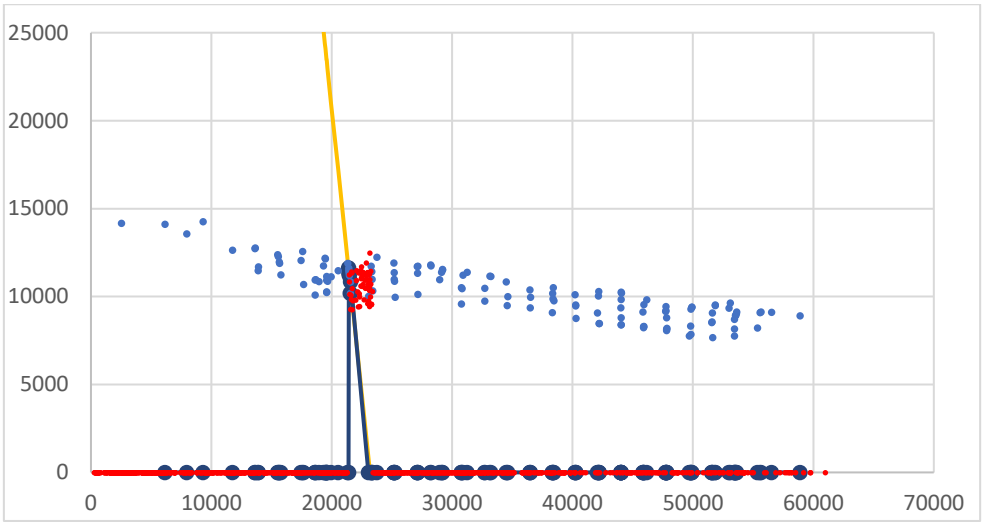

After:

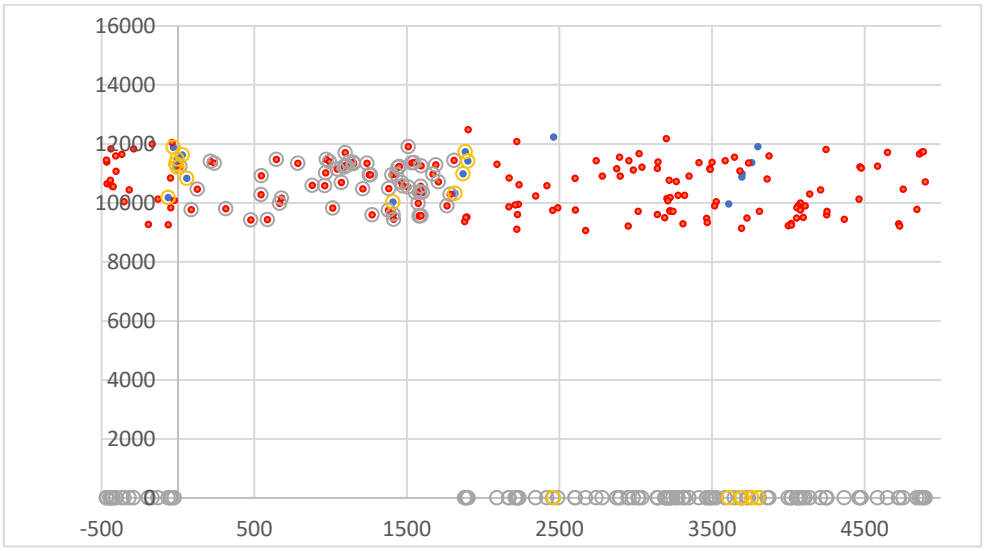

Figure 20.

A graphical representation before and after tilted Z-line correction for a single relaxed, stroboscopic (5 sec) video. These graphs show that although the z line was tilled at the top graph (a bit to the left), it appears to be straight on the second graph. Z-lines are represented by blue dots, while red dots represent RdATP attachments. Circled (yellow circles), red or blue dots represent the dots that are currently being corrected. Scales on both graphs are a representation of x and y coordinates of dots and should be disregarded.

3. Relative ATP positions in sarcomere

The next difficulty that presented itself after the tilted z-lines fix was that all sarcomeres had different lengths, and thus the plan of overlaying them to create a meaningful pattern was impossible. Myofibrils and, consequently, sarcomeres differ in sizes naturally, which was observed throughout our experiments. If we overlay sarcomere with a more considerable distance between Z-lines and sarcomere with a smaller distance between Z-line, obtained, data would be inaccurate. Thus, the solution was devised to overcome this problem. The solution was to create a relative position of ATP x coordinated. We have judged that even though the length of each sarcomere may differ, the ATP positions relative to that distance will be the same

throughout sarcomeres. For that reason, we have calculated the mean position of each z-line (in the x-axis) to then use (a+b)/c, where a is the mean position of the first z-line, b is the ATP coordinate on the x-axis, and c is the mean position of the second z-line. With his formulae, x positions of ATP were corrected to become relative to the whole length of the sarcomere while ignoring the actual length making it possible to overlay all sarcomeres with ease. Relative positions were then binned using C, D and P zones of the thick filament as bins to accurately represent attachment frequency for the whole myofibril neatly overlayed in one graph.

4. Determining the ratio of myosin heads states with regards to different zones

After relative ATP positions were established, thus providing us with both frequency and the duration for each zone, durations of set tracks were taken and plotted onto separate graphs, each representing a different zone. All graphs were set to a logarithmic scale to better represent data fitted to two-three exponentials depending on which experimental data was represented. Relaxed experiments were best fitted by three exponentials, while two exponentials better represented newer rigor experiments. Rigor method of experimentation was established very close to the end of this project and thus did not have ample time to be developed into a working condition; thus, data from these experiments will not be presented in this thesis. The fitting was done by an inbuilt tool in excel - “solver”, thus rendering human error to a minimum. Relative ratios of myosin heads states were calculated using amplitudes and rate constants provided by fitting three/two exponentials. Amplitudes that were derived from exponentials were corrected in relation to each other. A correction was necessary as all states have different rates. States with slower rates will show smaller amplitudes during the analysis than states with faster rates. The slower state will process fewer ATP molecules than faster states in the same amount of time; thus, the correction must be made to equilibrate the difference in ATP molecules to better represent the actual state's ratio. The correction was done using a simple equation, (kB/ kA)*ampA = ampcorrA, where kB is the rate constant of DRX, kA is the rate constant for SRX, ampA is the uncorrected amplitude for SRX, and ampcorrA is the corrected amplitude for SRX. SRX rate constant and uncorrected amplitude in this equation was then swapped with active state rate constant and uncorrected amplitude to determine corrected amplitude for the active state. These calculations related SRX and active state to DRX; thus, DRX uncorrected amplitude and DRX corrected amplitude had the same value. It must be said that although it was chosen to relate all states to DRX, it could have been any other states with the same result. Finally, the relative percentage of myosin heads for each state was calculated. It was done by dividing each corrected amplitude by the sum of all amplitudes (e.g. ampcorrSRX / (ampcorrDRX + ampcorrActive + ampcorrSRX) = rel% SRX, where ampcorrSRX is the corrected amplitude for SRX, ampcorrDRX is the corrected amplitude for DRX, ampcorrActive is the corrected amplitude for active state and rel% is the relative percentage of heads in SRX state).

B. Relaxed State experiments

Experiments that were done for this thesis can be divided into two categories: relaxed state experiments and rigor state experiments. Although rigor experiments had given us better

preliminary outcome, we were not able to do an appropriate number of biological repeats to say with any confidence that data from rigor experiments can be used in this thesis without further work. On the other hand, relaxed state experiments were conducted in amplitude, and thus this data will be presented in full. Relaxed state experiments were conducted with and without MAVA for both 2000 ms and 5000 ms intervals. RdATP was regenerated using the regeneration protocol provided above, and RdATP/dATP concentration was kept at 5 nM/5 mM throughout all experiments. The following graphs (see Figures 21-24) represent different zones of the thick filament. From Figure 21-22, we have observed that with the introduction of MAVA to the system, all zones have a decrease in SRX states. The experiments were done in consequent succession as follows: 2 sec, 2 sec + MAVA, 5 sec, 5 sec + MAVA using the same tissues and reagents as well as flow cells that were prepared in the same batch. Data from 2-sec experiments had to lead us to conclude that although these experiments were done in three biological repeats, they will have to be regarded as anomalous, as the addition of MAVA was shown to increase SRX %, the effect that we have not observed here (in fact, the opposite is was observed). 5-sec experiments (Figure 23-24) had much more expected results than 2-sec experiments. Experiments without MAVA have shown a clear distinction in relative SRX% between C-zone and D- and P- zones, where C-zone had a much larger relative SRX % than the other two zones. Comparing experiments with and without MAVA had shown an increase in relative SRX % in D and P zones.

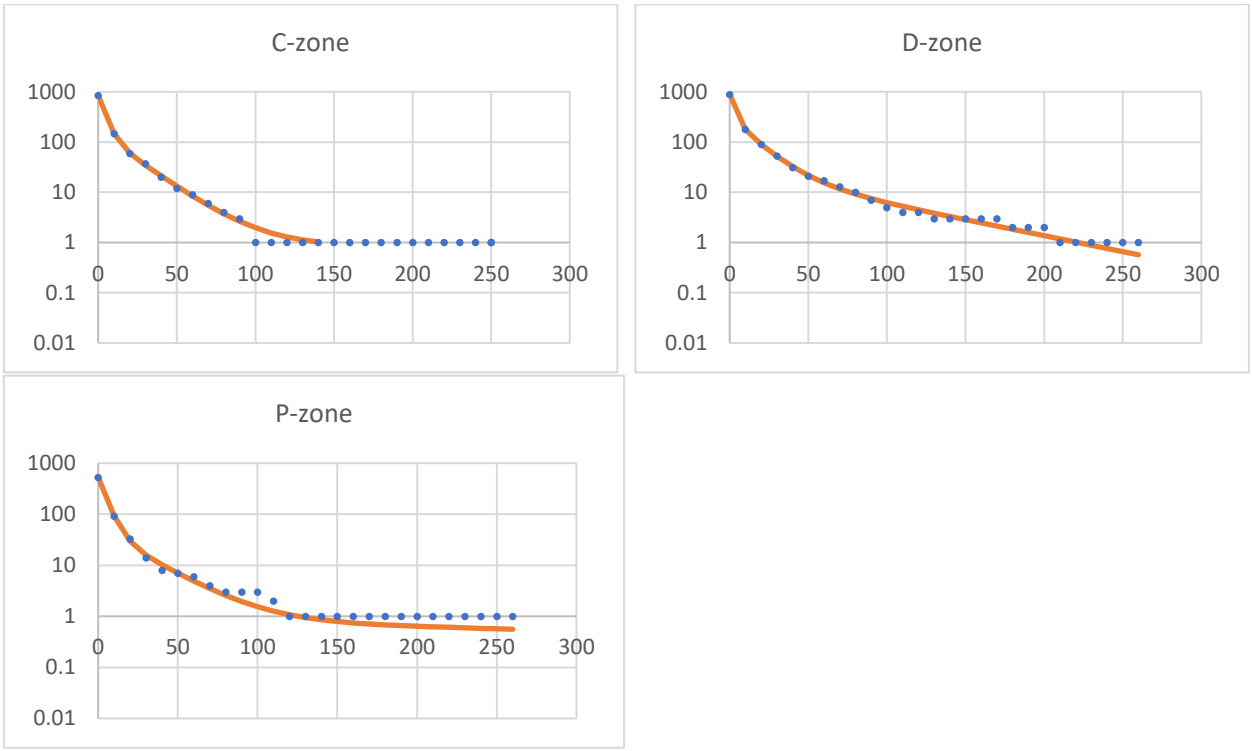

Figure 21.

Represents experiments done in 2 sec stroboscopic illumination, no MAVA conditions. In the above graphs, the active state is represented by a grey line, DRX with green and SRX with dark blue. The orange curve represents the sum of these three lines and thus the sum for rates and amplitudes of all three exponentials. Blues dots represent ATP duration attachments that were binned in 10 sec bins. Data presented here comes from three separate experiments (n=3). The relative ratio of myosin heads states for each zone was calculated to be:

C-zone SRX - 10 %, DRX - 47 %, Active – 43 %

D-zone SRX - 23 %, DRX - 52 %, Active – 25 %

P-zone SRX - 11 %, DRX - 30 %, Active – 59 %

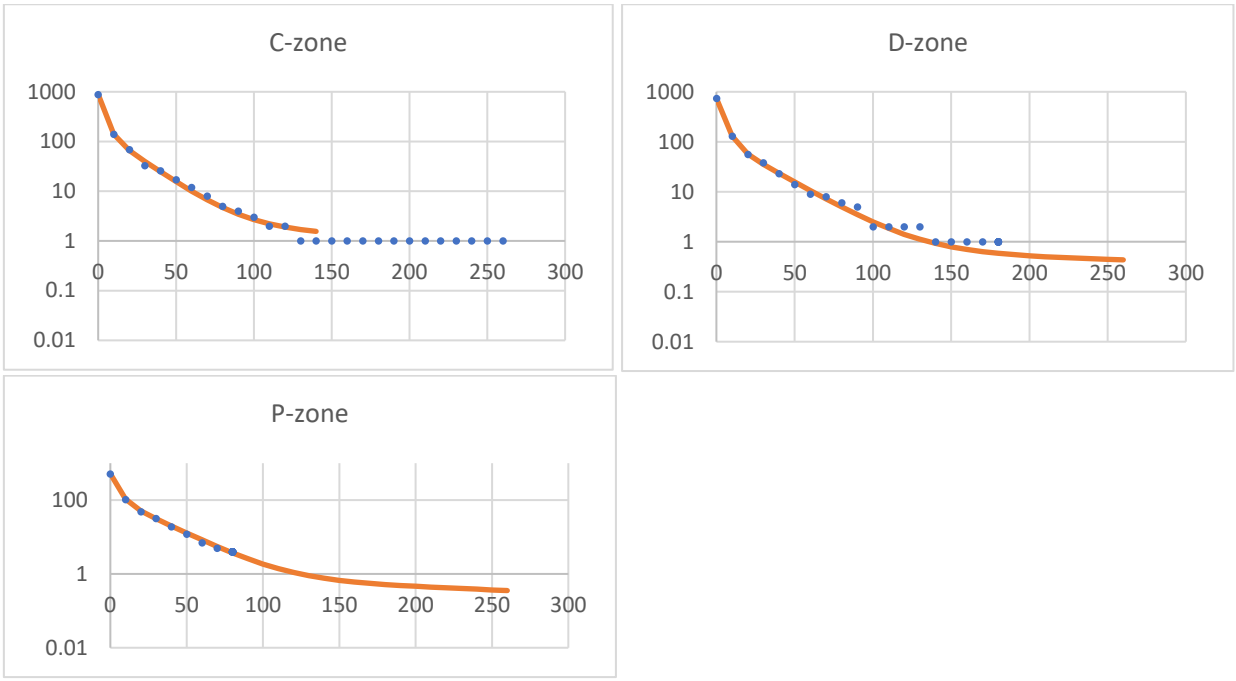

Figure 22.

Represents experiments done in 2 sec stroboscopic illumination, with the addition of MAVA. In the above graphs, the active state is represented by a grey line, DRX with green and SRX with dark blue. The orange curve represents the sum of these three lines and thus the sum for rates and amplitudes of all three exponentials. Blues dots represent ATP duration attachments that were binned in 10 sec bins. Data presented here comes from three separate experiments (n=3). The relative ratio of myosin heads states for each zone was calculated to be:

C-zone SRX - 10 %, DRX - 53 %, Active – 37 %

D-zone SRX - 6 %, DRX - 51 %, Active – 43 %

P-zone SRX – 6 %, DRX - 60 %, Active – 34%

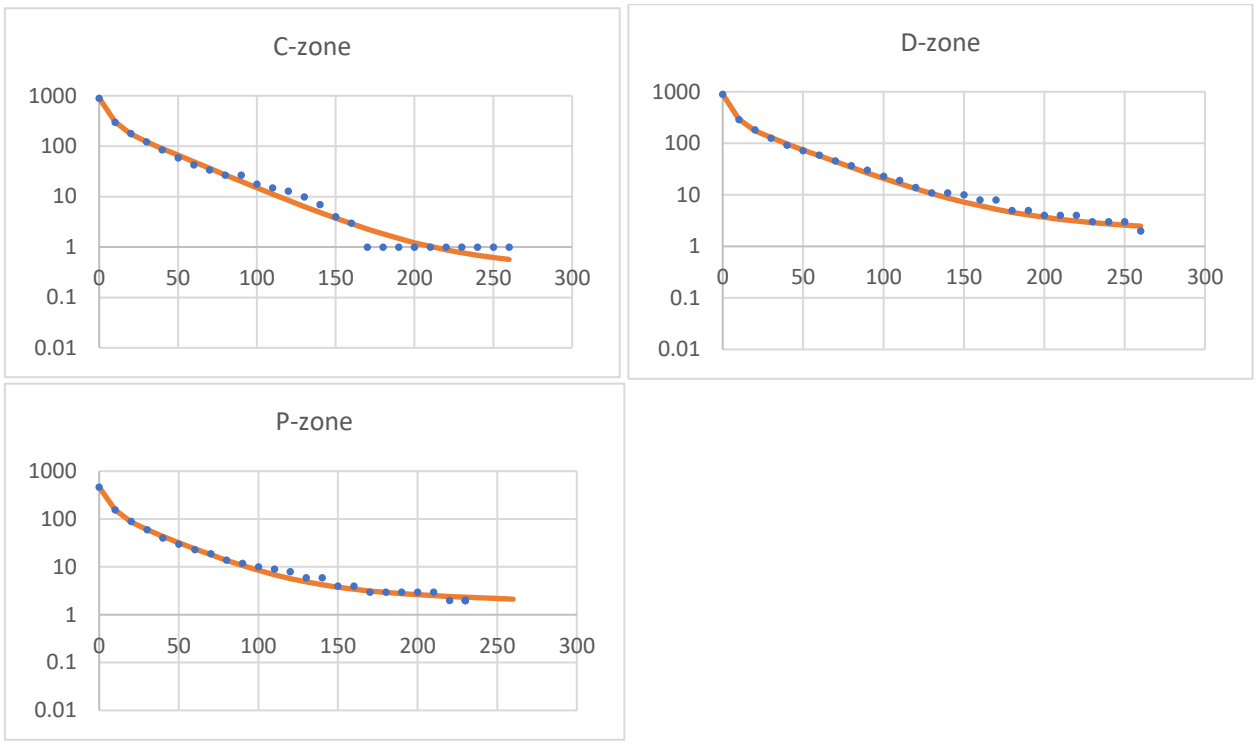

Figure 23.

Represents experiments done in 5 sec stroboscopic illumination, no MAVA conditions. In the above graphs, the active state is represented by a grey line, DRX with green and SRX with dark blue. The orange curve represents the sum of these three lines and thus the sum for rates and amplitudes of all three exponentials. Blues dots represent ATP duration attachments that were binned in 10 sec bins. Data presented here comes from three separate experiments (n=3). The relative ratio of myosin heads states for each zone was calculated to be:

C-zone SRX - 50 %, DRX - 38 %, Active – 12 %

D-zone SRX - 13 %, DRX - 68 %, Active – 19 %

P-zone SRX – 21 %, DRX - 59 %, Active – 20%

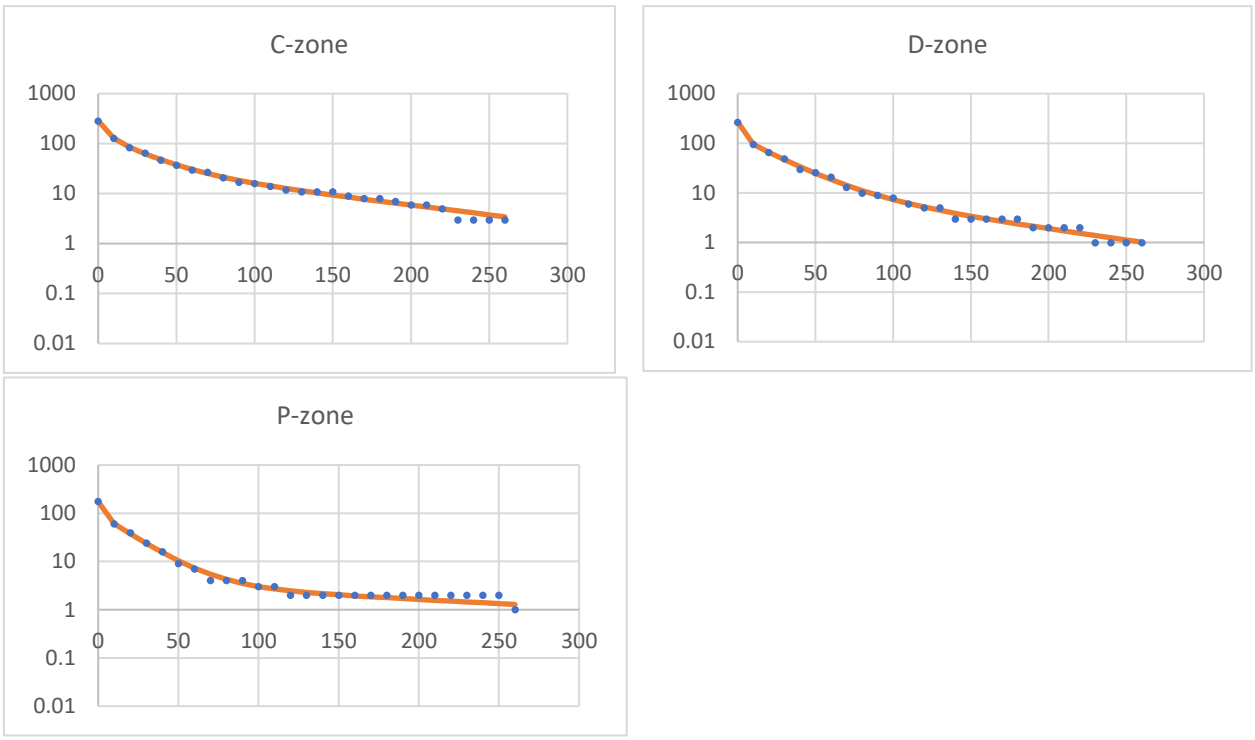

Figure 24.

Represents experiments done in 5 sec stroboscopic illumination, no MAVA conditions. In the above graphs, the active state is represented by a grey line, DRX with green and SRX with dark blue. The orange curve represents the sum of these three lines and thus the sum for rates and amplitudes of all three exponentials. Blues dots represent ATP duration attachments that were binned in 10 sec bins. Data presented here comes from three separate experiments (n=3). The relative ratio of myosin heads states for each zone was calculated to be:

C-zone SRX - 52 %, DRX - 41 %, Active – 7 %

D-zone SRX - 30 %, DRX - 64 %, Active – 6 %

P-zone SRX – 32 %, DRX - 66 %, Active – 2%

9. Discussion

Before discussing the results and advantages of our methods, we would like to present a mathematical model, which calculates a theoretical approximation of the percentage of SRX heads in a thick filament.

A. Theoretical probability calculations

Here we would like to propose a statistical construct to calculate an approximate number of fluorescently labelled ATP molecules that would bind to myosin heads with regards to fluorescently labelled ATP concentration, dATP concentration, the theoretical number of thick filaments in a sarcomere, the centre-to-centre distance between thick filaments, myofibril diameter and the number of myosin heads on the thick filament. As stated above, all relaxed experiments were conducted with 5 nM RdATP/5 mM dATP. According to the literature, the centre-to-centre distance between thick filaments was calculated to be ~43 nm(Millman, 1998). Also, according to other literature, rotational symmetry for the thick filament was shown to be 3-fold which would mean that there are 9 myosin heads per 42.9 nm of the thick filament.

Furthermore, the same literature indicated that the diameter of myofibril could vary between 1-2 um while the whole length of the thick filament was shown to be ~1600 nm(Al-Khayat, 2013). With these values, established calculations can now be made to estimate the statistical probability of observing the fluorescent event.

The total number of thick filaments in one sarcomere was estimated by dividing myofibril diameter by centre-to-centre distance between thick filaments. The highest possible values were taken for the estimates to determine the largest possible outcome for the whole statistical analysis. 2000 nm/43 nm=46. There were 20-30 sarcomeres in each myofibril, so with that in mind multiplying the number of thick filaments for a sarcomere by the number of sarcomeres would provide us with the total number of thick filaments in the myofibril. 46*30=1380. The total number of myosin heads per thick filament was then established by dividing an approximate length of the thick filament by spacing of myosin heads repeat sequence and multiplying produced values by the number of myosin heads that were present in this sequence. 1600/42.9*9=335. Now that we had both the total number of myosin heads per tick filament and the total number of tick filaments per myofibril, we were able to calculate the total number of myosin heads in myofibril by multiplying two values together. 335*1 380=462 300. To make it easier to count, let us round it up to 500 000. Statistical analysis of 500 000 myosin heads in one myofibril then continued using imaging buffer concentrations. 5 nM RdATP/5 mM dATP essentially states that for every 1 RdATP molecule, there are 1 000 000 dATP molecules present in the imaging buffer; thus, the chances of RdATP molecule binding to a myosin head instead of dATP molecule are $1e10^{-4}$ %. As we have calculated the approximate number of myosin heads in myofibril to be ~500 000, multiplication of these two values would produce the chances of one RdATP molecule to be seen on the image. 500 000 * ($1e10^{-4}$) = 50 %. The probability of seeing a single RdATP at any particular point in time of the imaging process is 50 %. This value is a gross overestimation as we also must consider the fact that not all myosin heads are available for attachments at all times. Some of them might be undergoing SRX with dATP molecules attached and thus would be incapable of receiving RdATP. The same case can be made for DRX and active attachments. It is must also be remembered that we have taken the highest possible estimations for all values in previous calculations. Even then, this RdATP molecule that has attached to one myosin head has only 40 - 50 % (Stewart et al., 2010a;(Anderson et al., 2018)of being in SRX. 0.5*0.5=0.25. There is only a 25 % chance that the RdATP molecule will attach to a single myosin head that is in SRX. If we were to say that we are considering only 50 % of myosin heads to be the inactive state and thus only 50 % are available for potential attachment of RdATP molecule per frame, then the chance of RdATP attachment to SRX drops to 12.5 %. Results from 5-sec experiments concur with that mathematical model and places overall myosin heads SRX % at 11%. Please note that this percentage was calculated using uncorrected amplitudes as the mathematical model did not consider relative ATP turnover rates of different states.

B. The spatial arrangement of SRX in all zones of the thick filament

Analysis of our data had shown that myosin heads in SRX are largely located in the C-zone of the thick filament. Some SRX is present in both P and D zones but in much smaller quantities. This is consistent with some recent experiments (Nelson et al., 2020). Our values from 5-sec experiments can partially concur with work done by other groups where the population of SRX

in C, D and P zones without MAVA was found to be 61+-12 %, 9+-12 % and 13+-8 %, respectively, which fits our results. However, some variations with the same group concerning data acquired during an experiment with the addition of MAVA. Both our and Nelson et al. data have shown an increase in SRX % in P and D zones. Our increase (P-zone 11 %, D-zone 17 %), however, was not as large in comparison to Nelson el al (P-zone 42 %, D-zone 48 %). From this pattern of the spatial arrangement of SRX, a question may be asked: why C-zone has the largest SRX concentration? Myosin binding protein-C was connected (Li et al., 2019) with modulation myosin heads into SRX state. It can only be found in the C-zone of the thick filament. Mutations in a coding gene of MyBP-C were shown (see 6.C.) to cause SRX-related diseases. Striated muscle was only recently reported to have SRX (McNamara et al. 2014), and thus much information is still under debate about all aspects involving SRX of myosin heads. For example, the difference between isoforms of muscle tissue and SRX states associated with these isoforms were shown to have different reactions to activation (Hooijman, Stewart, and Cooke 2011). Are there any other differences between isoforms? Where does SRX appear in the sarcomere, and why there specifically? Do neighbouring myosin heads in SRX affect the states of adjacent heads? Some studies have shown that myosin heads interact and induce SRX in adjacent myosin heads if they are in SRX themselves in thick tarantula filament (Woodhead et al. 2005) and later was shown to be the case in skeletal muscle (Brito et al. 2011; Sulbarán et al. 2013). Although we could not answer all of these questions, we aimed to determine the spatial arrangement of myosin heads in the A-band. Not many single-molecule studies were conducted in skeletal muscles, the most recent one being (Nelson et al. 2020), differences and similarities of which were discussed above.

C. Advantages of our current methodology

Although some of our experiments (2 sec) presented above provided us with some anomalous results, we are confident that other experiments (5 sec) have shown the advantages of our current methodology. First, our RdATP regeneration system has ensured that all attachments that we have observed can be attributed to RdATP, not RdADP attachments, as the regeneration system was present throughout interactions between RdATP molecules and myofibrils. Second, stroboscopic illumination has not only decreased the photobleaching effects of the lasers but have also provided us with the opportunity to calculate the rate of photobleaching. Unfortunately, not enough usable data was collected to implement set calculation, but it is a possibility for future experiments. Finally, keeping myofibrils in relaxed conditions throughout the experiment allows us to be certain that all myosin heads are not in rigor when images are taken.

D. Future Projects

Unfortunately, the time allocated for this project was not long enough to complete all goals put before us at the beginning of this project. First and foremost, this project was aimed to study cardiac muscle and mutations causing HCM. Thus, it is imperative for the future of this project to move from skeletal muscle onto cardiac and then, potentially, onto mutated cardiac muscle. To further develop our understanding of mechanics behind different states of activity in myosin heads and their connection to MyBP-C and its role in inducing SRX in myosin heads, we were planning to involve Protein Kinase A (PKA), which is thought to phosphorylate slow isoform of MyBP-C (Colson et al. 2012; Lim and Walsh 1986; Ackermann and Kontrogianni-Konstantopoulos 2011).

10. Conclusion

A multitude of experiments has provided us with a working methodology of preparation for rabbit psoas skeletal myofibrils and consequent analysis. Set analysis has allowed us to determine the spatial arrangement of myosin heads in a super-relaxed state on the thick filament. However, although methods were established, much more work is required to produce more meaningful results for both relaxed and rigor conditions.

11. References

Adalsteinsdottir, B., Teekakirikul, P., Maron, B. J., Burke, M. A., Gudbjartsson, D. F., Holm, H., Stefansson, K., DePalma, S. R., Mazaika, E., McDonough, B., Danielsen, R., Seidman, J. G., Seidman, C. E., & Gunnarsson, G. T. (2014). Nationwide study on hypertrophic cardiomyopathy in iceland evidence of a MYBPC3 founder mutation. *Circulation*, *130*(14), 1158–1167. https://doi.org/10.1161/CIRCULATIONAHA.114.011207

Aguilar, H. N., & Mitchell, B. F. (2010). Physiological pathways and molecular mechanisms regulating uterine contractility. *Human Reproduction Update*, *16*(6), 725–744. https://doi.org/10.1093/humupd/dmq016

Al-Khayat, H. (2013). Three-Dimensional Structure Of The Human Cardiac Myosin Thick Filament - Clinical Implications. *Qatar Foundation Annual Research Forum Proceedings*, *2013*, BIOP 073. https://doi.org/10.5339/qfarf.2013.biop-073

Alamo, L., Qi, D., Wriggers, W., Pinto, A., Zhu, J., Bilbao, A., Gillilan, R. E., Hu, S., & Padrón, R. (2016). Conserved Intramolecular Interactions Maintain Myosin Interacting-Heads Motifs Explaining Tarantula Muscle Super-Relaxed State Structural Basis. *Journal of Molecular Biology*, *428*(6), 1142–1164. https://doi.org/10.1016/j.jmb.2016.01.027

Alamo, L., Wriggers, W., Pinto, A., Bártoli, F., Salazar, L., Zhao, F. Q., Craig, R., & Padrón, R. (2008). Three-Dimensional Reconstruction of Tarantula Myosin Filaments Suggests How Phosphorylation May Regulate Myosin Activity. *Journal of Molecular Biology*, *384*(4), 780–797. https://doi.org/10.1016/j.jmb.2008.10.013

Anderson, R. L., Trivedi, D. V., Sarkar, S. S., Henze, M., Ma, W., Gong, H., Rogers, C. S., Gorham, J. M., Wong, F. L., Morck, M. M., Seidman, J. G., Ruppel, K. M., Irving, T. C., Cooke, R., Green, E. M., & Spudich, J. A. (2018). Deciphering the super relaxed state of human β-cardiac myosin and the mode of action of mavacamten from myosin molecules to muscle fibers. *Proceedings of the National Academy of Sciences of the United States of America*, *115*(35), E8143–E8152. https://doi.org/10.1073/pnas.1809540115

ATP binding and hydrolysis by mX-S1 in the absence of actin. A,... | Download Scientific Diagram. (n.d.). Retrieved December 15, 2020, from https://www.researchgate.net/figure/ATP-binding-and-hydrolysis-by-mX-S1-in-the-absence-of-actin-A-tryptophan-fluorescence_fig1_8026674

Bähler, M., Eppenberger, H. M., & Wallimann, T. (1985). Novel thick filament protein of chicken pectoralis muscle: the 86 kd protein. I. Purification and characterization. *Journal of Molecular Biology*, *186*(2), 381–391. https://doi.org/10.1016/0022-2836(85)90112-3

Barefield, D., & Sadayappan, S. (2010). Phosphorylation and function of cardiac myosin binding protein-C in health and disease. In *Journal of Molecular and Cellular Cardiology* (Vol. 48, Issue 5, pp. 866–875). https://doi.org/10.1016/j.yjmcc.2009.11.014

Bates, M., Jones, S. A., & Zhuang, X. (2013a). Stochastic optical reconstruction microscopy (STORM): A method for superresolution fluorescence imaging. *Cold Spring Harbor Protocols*, *8*(6), 498–520. https://doi.org/10.1101/pdb.top075143

Bates, M., Jones, S. A., & Zhuang, X. (2013b). Preparation of photoswitchable labeled antibodies for STORM imaging. *Cold Spring Harbor Protocols*, *8*(6), 540–541. https://doi.org/10.1101/pdb.prot075168

Behrens-Gawlik, V., Mearini, G., Gedicke-Hornung, C., Richard, P., & Carrier, L. (2014). MYBPC3 in hypertrophic cardiomyopathy: From mutation identification to RNA-based correction. In *Pflugers Archiv European Journal of Physiology* (Vol. 466, Issue 2, pp. 215–223). Pflugers Arch. https://doi.org/10.1007/s00424-013-1409-7

Bennett, P. M., & Gautel, M. (1996). Titin domain patterns correlate with the axial disposition of myosin at the end of the thick filament. *Journal of Molecular Biology*, *259*(5), 896–903. https://doi.org/10.1006/jmbi.1996.0367

Betzig, E., Patterson, G. H., Sougrat, R., Lindwasser, O. W., Olenych, S., Bonifacino, J. S., Davidson, M. W., Lippincott-Schwartz, J., & Hess, H. F. (2006). Imaging intracellular fluorescent proteins at nanometer resolution. *Science*, *313*(5793), 1642–1645. https://doi.org/10.1126/science.1127344

Bloemink, M. J., Melkani, G. C., Bernstein, S. I., & Geeves, M. A. (2016). The relay/converter interface influences hydrolysis of ATP by skeletal muscle myosin II. *Journal of Biological Chemistry*, *291*(4), 1763–1773. https://doi.org/10.1074/jbc.M115.688002

Branzi, A., Romeo, G., Specchia, S., Lolli, C., Binetti, G., Devoto, M., Bacchi, M., & Magnani, B. (1985). Genetic heterogeneity of hypertrophic cardiomyopathy. *International Journal of Cardiology*, *7*(2), 129–133. https://doi.org/10.1016/0167-5273(85)90352-3

Brito, R., Alamo, L., Lundberg, U., Guerrero, J. R., Pinto, A., Sulbarán, G., Gawinowicz, M. A., Craig, R., & Padrón, R. (2011). A molecular model of phosphorylation-based activation and potentiation of tarantula muscle thick filaments. *Journal of Molecular Biology*, *414*(1), 44–61. https://doi.org/10.1016/j.jmb.2011.09.017

Burgess, S. A., Yu, S., Walker, M. L., Hawkins, R. J., Chalovich, J. M., & Knight, P. J. (2007). Structures of Smooth Muscle Myosin and Heavy Meromyosin in the Folded, Shutdown State. *Journal of Molecular Biology*, *372*(5), 1165–1178. https://doi.org/10.1016/j.jmb.2007.07.014

Calore, C., De Bortoli, M., Romualdi, C., Lorenzon, A., Angelini, A., Basso, C., Thiene, G., Iliceto, S., Rampazzo, A., & Melacini, P. (2015). A founder MYBPC3 mutation results in HCM with a high risk of sudden death after the fourth decade of life. *Journal of Medical Genetics*, *52*(5), 338–347. https://doi.org/10.1136/jmedgenet-2014-102923

Carlier, M. F., & Shekhar, S. (2017). Global treadmilling coordinates actin turnover and controls the size of actin networks. *Nature Reviews Molecular Cell Biology*, *18*(6), 389–401. https://doi.org/10.1038/nrm.2016.172

Carlsson, L., Nyström, L. E., Sundkvist, I., Markey, F., & Lindberg, U. (1977). Actin polymerizability is influenced by profilin, a low molecular weight protein in non-muscle cells. *Journal of Molecular Biology*, *115*(3), 465–483. https://doi.org/10.1016/0022-2836(77)90166-8

Carrier, L., Bonne, G., Bährend, E., Yu, B., Richard, P., Niel, F., Hainque, B., Cruaud, C., Gary, F., Labeit, S., Bouhour, J. B., Dubourg, O., Desnos, M., Hagège, A. A., Trent, R. J., Komajda, M., Fiszman, M., & Schwartz, K. (1997). Organization and sequence of human cardiac myosin binding protein C gene (MYBPC3) and identification of mutations predicted to produce truncated proteins in familial hypertrophic cardiomyopathy. *Circulation Research*, *80*(3), 427–434. https://doi.org/10.1161/01.res.0000435859.24609.b3

Carrier, L., Mearini, G., Stathopoulou, K., & Cuello, F. (2015). Cardiac myosin-binding protein C (MYBPC3) in cardiac pathophysiology. *Gene*, *573*(2), 188–197. https://doi.org/10.1016/j.gene.2015.09.008

Chandy, I. K., Lo, J. C., & Ludescher, R. D. (1999). Differential mobility of skeletal and cardiac tropomyosin on the surface of F-actin. *Biochemistry*, *38*(29), 9286–9294. https://doi.org/10.1021/bi983073s

Christiaans, I., Nannenberg, E. A., Dooijes, D., Jongbloed, R. J. E., Michels, M., Postema, P. G., Majoor-Krakauer, D., van den Wijngaard, A., Mannens, M. M. A. M., van Tintelen, J. P., van Langen, I. M., & Wilde, A. A. M. (2010). Founder mutations in hypertrophic cardiomyopathy patients in the Netherlands. In *Netherlands Heart Journal* (Vol. 18, Issue 5, pp. 248–254). Bohn Stafleu van Loghum. https://doi.org/10.1007/BF03091771

Cirino, A. L., & Ho, C. (1993). Hypertrophic Cardiomyopathy Overview. *GeneReviews®*, 1–16. http://www.ncbi.nlm.nih.gov/pubmed/20301725

Clark, K. A., McElhinny, A. S., Beckerle, M. C., & Gregorio, C. C. (2002). Striated muscle cytoarchitecture: An intricate web of form and function. *Annual Review of Cell and Developmental Biology*, *18*, 637–706. https://doi.org/10.1146/annurev.cellbio.18.012502.105840

Colegrave, M., & Peckham, M. (2014). Structural implications of β-cardiac myosin heavy chain mutations in human disease. *Anatomical Record*, *297*(9), 1670–1680. https://doi.org/10.1002/ar.22973

Colson, B. A., Bekyarova, T., Fitzsimons, D. P., Irving, T. C., & Moss, R. L. (2007). Radial Displacement of Myosin Cross-bridges in Mouse Myocardium due to Ablation of Myosin Binding Protein-C. *Journal of Molecular Biology*, *367*(1), 36–41. https://doi.org/10.1016/j.jmb.2006.12.063

Colson, B. A., Bekyarova, T., Locher, M. R., Fitzsimons, D. P., Irving, T. C., & Moss, R. L. (2008). Protein kinase a-mediated phosphorylation of cmybp-c increases proximity of myosin heads to actin in resting myocardium. *Circulation Research*, *103*(3), 244–251. https://doi.org/10.1161/CIRCRESAHA.108.178996

Colson, B. A., Locher, M. R., Bekyarova, T., Patel, J. R., Fitzsimons, D. P., Irving, T. C., & Moss, R. L. (2010). Differential roles of regulatory light chain and myosin binding protein-C phosphorylations in the modulation of cardiac force development. *Journal of Physiology*, *588*(6), 981–993. https://doi.org/10.1113/jphysiol.2009.183897

Colson, B. A., Patel, J. R., Chen, P. P., Bekyarova, T., Abdalla, M. I., Tong, C. W., Fitzsimons, D. P., Irving, T. C., & Moss, R. L. (2012). Myosin binding protein-C phosphorylation is the principal mediator of protein kinase A effects on thick filament structure in myocardium. *Journal of Molecular and Cellular Cardiology*, *53*(5), 609–616. https://doi.org/10.1016/j.yjmcc.2012.07.012

Cooke, R. (2011). The role of the myosin ATPase activity in adaptive thermogenesis by skeletal muscle. In *Biophysical Reviews* (Vol. 3, Issue 1, pp. 33–45). https://doi.org/10.1007/s12551-

011-0044-9

Craig, R., Padron, R., & Kendrick-Jones, J. (1987). Structural changes accompanying phosphorylation of tarantula muscle myosin filaments. *Journal of Cell Biology*, *105*(3), 1319–1327. https://doi.org/10.1083/jcb.105.3.1319

Craig, Roger, & Woodhead, J. L. (2006). Structure and function of myosin filaments. In *Current Opinion in Structural Biology* (Vol. 16, Issue 2, pp. 204–212). https://doi.org/10.1016/j.sbi.2006.03.006

Crowther, R. A., Padrón, R., & Craig, R. (1985). Arrangement of the heads of myosin in relaxed thick filaments from tarantula muscle. *Journal of Molecular Biology*, *184*(3), 429–439. https://doi.org/10.1016/0022-2836(85)90292-X

Desai, R., Geeves, M. A., & Kad, N. M. (2015). Using fluorescent myosin to directly visualize cooperative activation of thin filaments. *Journal of Biological Chemistry*, *290*(4), 1915–1925. https://doi.org/10.1074/jbc.M114.609743

Dilson E. Rassier. (2013). Encyclopedia of Biophysics. In *Encyclopedia of Biophysics*. https://doi.org/10.1007/978-3-642-16712-6

Dominguez, R., & Holmes, K. C. (2011). Actin structure and function. *Annual Review of Biophysics*, *40*(1), 169–186. https://doi.org/10.1146/annurev-biophys-042910-155359

Ebashi, S., Endo, M., & Ohtsuki, I. (1969). Control of muscle contraction. *Quarterly Reviews of Biophysics*, *2*(4), 351–384. https://doi.org/10.1017/S0033583500001190

Elzinga, M., & Collins, J. H. (1975). The Primary Structure of Actin from Rabbit Skeletal Muscle. *The Journal of Biological Chemistry*, *250*(15), 5897–5905.

Endesfelder, U., & Heilemann, M. (2014). Direct stochastic optical reconstruction microscopy (Dstorm). *Methods in Molecular Biology*, *1251*, 263–276. https://doi.org/10.1007/978-1-4939-2080-8_14

Erdmann, J., Daehmlow, S., Wischke, S., Senyuva, M., Werner, U., Raible, J., Tanis, N., Dyachenko, S., Hummel, M., Hetzer, R., & Regitz-Zagrosek, V. (2003). Mutation spectrum in a large cohort of unrelated consecutive patients with hypertrophic cardiomyopathy. *Clinical Genetics*, *64*(4), 339–349. https://doi.org/10.1034/j.1399-0004.2003.00151.x

Ervasti, J. M. (2003). Costameres: The Achilles' heel of Herculean muscle. *Journal of Biological Chemistry*, *278*(16), 13591–13594. https://doi.org/10.1074/jbc.R200021200

Farah, C. S., Miyamoto, C. A., Ramos, C. H. I., Da Silva, A. C. R., Quaggio, R. B., Fujimori, K., Smillie, L. B., & Reinach, F. C. (1994). Structural and regulatory functions of the NH2- and COOH-terminal regions of skeletal muscle troponin I. *Journal of Biological Chemistry*, *269*(7), 5230–5240. https://doi.org/10.1016/S0021-9258(17)37679-2

Flashman, E., Watkins, H., & Redwood, C. (2007). Localization of the binding site of the C-terminal domain of cardiac myosin-binding protein-C on the myosin rod. *Biochemical Journal*, *401*(1), 97–102. https://doi.org/10.1042/BJ20060500

Fukuzawa, A., Lange, S., Holt, M., Vihola, A., Carmignac, V., Ferreiro, A., Udd, B., & Gautel, M. (2008). Interactions with titin and myomesin target obscurin and obscurin-like 1 to the M-band - Implications for hereditary myopathies. *Journal of Cell Science*, *121*(11), 1841–1851. https://doi.org/10.1242/jcs.028019

Gautel, M., Zuffardi, O., Freiburg, A., & Labeit, S. (1995). Phosphorylation switches specific for the cardiac isoform of myosin binding protein-C: A modulator of cardiac contraction? *EMBO*

Journal, *14*(9), 1952–1960. https://doi.org/10.1002/j.1460-2075.1995.tb07187.x

Geeves, M. A., Chai, M., & Lehrer, S. S. (2000). Inhibition of actin-myosin subfragment 1 ATPase activity by troponin I and IC: Relationship to the thin filament states of muscle. *Biochemistry*, *39*(31), 9345–9350. https://doi.org/10.1021/bi0002232

Geeves, M. A., Fedorov, R., & Manstein, D. J. (2005). Molecular mechanism of actomyosin-based motility. *Cellular and Molecular Life Sciences*, *62*(13), 1462–1477. https://doi.org/10.1007/s00018-005-5015-5

Geeves, Michael A., & Holmes, K. C. (2005). The molecular mechanism of muscle contraction. *Advances in Protein Chemistry*, *71*(04), 161–193. https://doi.org/10.1016/S0065-3233(04)71005-0

Geier, C., Gehmlich, K., Ehler, E., Hassfeld, S., Perrot, A., Hayess, K., Cardim, N., Wenzel, K., Erdmann, B., Krackhardt, F., Posch, M. G., Bublak, A., Nägele, H., Scheffold, T., Dietz, R., Chien, K. R., Spuler, S., Fürst, D. O., Nürnberg, P., & Özcelik, C. (2008). Beyond the sarcomere: CSRP3 mutations cause hypertrophic cardiomyopathy. *Human Molecular Genetics*, *17*(18), 2753–2765. https://doi.org/10.1093/hmg/ddn160

Geisterfer-Lowrance, A. A. T., Kass, S., Tanigawa, G., Vosberg, H. P., McKenna, W., Seidman, C. E., & Seidman, J. G. (1990). A molecular basis for familial hypertrophic cardiomyopathy: A β cardiac myosin heavy chain gene missense mutation. *Cell*, *62*(5), 999–1006. https://doi.org/10.1016/0092-8674(90)90274-I

Giganti, D., Yan, K., Badilla, C. L., Fernandez, J. M., & Alegre-Cebollada, J. (2018). Disulfide isomerization reactions in titin immunoglobulin domains enable a mode of protein elasticity. *Nature Communications*, *9*(1), 1–11. https://doi.org/10.1038/s41467-017-02528-7

Gilbert, R., Cohen, J. A., Pardo, S., Basu, A., & Fischman, D. A. (1999). Identification of the A-band localization domain of myosin binding proteins C and H (MyBP-C, MyBP-H) in skeletal muscle. *Journal of Cell Science*, *112*(1), 69–79.

Goldschmidt-Clermont, P. J., Furman, M. I., Wachsstock, D., Safer, D., Nachmias, V. T., & Pollard, T. D. (1992). The control of actin nucleotide exchange by thymosinβ4 and profilin. A potential regulatory mechanism for actin polymerization in cells. *Molecular Biology of the Cell*, *3*(9), 1015–1024. https://doi.org/10.1091/mbc.3.9.1015

Gordon, A. M., Homsher, E., & Regnier, M. (2000). Regulation of contraction in striated muscle. In *Physiological Reviews* (Vol. 80, Issue 2, pp. 853–924). American Physiological Society. https://doi.org/10.1152/physrev.2000.80.2.853

Graceffa, P., & Dominguez, R. (2003). Crystal structure of monomeric actin in the ATP state: Structural basis of nucleotide-dependent actin dynamics. *Journal of Biological Chemistry*, *278*(36), 34172–34180. https://doi.org/10.1074/jbc.M303689200

Greaves, S. C., Roche, A. H. G., Neutze, J. M., Whitlock, R. M. L., & Veale, A. M. O. (1987). Inheritance of hypertrophic cardiomyopathy: A cross sectional and M mode echocardiographic study of 50 families. *Heart*, *58*(3), 259–266. https://doi.org/10.1136/hrt.58.3.259

Gustafsson, M. G. L. (2000). Surpassing the lateral resolution limit by a factor of two using structured illumination microscopy. *Journal of Microscopy*, *198*(2), 82–87. https://doi.org/10.1046/j.1365-2818.2000.00710.x

Harris, S. P., Rostkova, E., Gautel, M., & Moss, R. L. (2004). Binding of myosin binding protein-C to myosin subfragment S2 affects contractility independent of a tether mechanism.

Circulation Research, *95*(9), 930–936. https://doi.org/10.1161/01.RES.0000147312.02673.56

Hartmannova, H., Kubanek, M., Sramko, M., Piherova, L., Noskova, L., Hodanova, K., Stranecky, V., Pristoupilova, A., Sovova, J., Marek, T., Maluskova, J., Ridzon, P., Kautzner, J., Hulkova, H., & Kmoch, S. (2013). Isolated X-linked hypertrophic cardiomyopathy caused by a novel mutation of the four-and-a-half LIM domain 1 gene. *Circulation: Cardiovascular Genetics*, *6*(6), 543–551. https://doi.org/10.1161/CIRCGENETICS.113.000245

Heilemann, M., Van De Linde, S., Schüttpelz, M., Kasper, R., Seefeldt, B., Mukherjee, A., Tinnefeld, P., & Sauer, M. (2008). Subdiffraction-resolution fluorescence imaging with conventional fluorescent probes. *Angewandte Chemie - International Edition*, *47*(33), 6172–6176. https://doi.org/10.1002/anie.200802376

Hell, S. W., & Wichmann, J. (1994). Breaking the diffraction resolution limit by stimulated emission: stimulated-emission-depletion fluorescence microscopy. *Optics Letters*, *19*(11), 780. https://doi.org/10.1364/ol.19.000780

Herron, T. J., Rostkova, E., Kunst, G., Chaturvedi, R., Gautel, M., & Kentish, J. C. (2006). Activation of myocardial contraction by the N-terminal domains of myosin binding protein-C. *Circulation Research*, *98*(10), 1290–1298. https://doi.org/10.1161/01.RES.0000222059.54917.ef

Hess, S. T., Girirajan, T. P. K., & Mason, M. D. (2006). Ultra-high resolution imaging by fluorescence photoactivation localization microscopy. *Biophysical Journal*, *91*(11), 4258–4272. https://doi.org/10.1529/biophysj.106.091116

Hitchcock-DeGregori, S. E., & An, Y. (1996). Integral repeats and a continuous coiled coil are required for binding of striated muscle tropomyosin to the regulated actin filament. *Journal of Biological Chemistry*, *271*(7), 3600–3603. https://doi.org/10.1074/jbc.271.7.3600

Ho, C. Y., Mealiffe, M. E., Bach, R. G., Bhattacharya, M., Choudhury, L., Edelberg, J. M., Hegde, S. M., Jacoby, D., Lakdawala, N. K., Lester, S. J., Ma, Y., Marian, A. J., Nagueh, S. F., Owens, A., Rader, F., Saberi, S., Sehnert, A. J., Sherrid, M. V., Solomon, S. D., … Heitner, S. B. (2020). Evaluation of Mavacamten in Symptomatic Patients With Nonobstructive Hypertrophic Cardiomyopathy. *Journal of the American College of Cardiology*, *75*(21), 2649–2660. https://doi.org/10.1016/j.jacc.2020.03.064

Hooijman, P., Stewart, M. A., & Cooke, R. (2011). A new state of cardiac myosin with very slow ATP turnover: A potential cardioprotective mechanism in the heart. *Biophysical Journal*, *100*(8), 1969–1976. https://doi.org/10.1016/j.bpj.2011.02.061

Hu, L. Y. R., Ackermann, M. A., & Kontrogianni-Konstantopoulos, A. (2015). The sarcomeric M-region: A molecular command center for diverse cellular processes. *BioMed Research International*, *2015*. https://doi.org/10.1155/2015/714197

Huang, W., & Szczesna-Cordary, D. (2015). Molecular mechanisms of cardiomyopathy phenotypes associated with myosin light chain mutations. In *Journal of Muscle Research and Cell Motility* (Vol. 36, Issue 6, pp. 433–445). Springer International Publishing. https://doi.org/10.1007/s10974-015-9423-3

Huxley, A. F., & Niedergerke, R. (1954). Structural changes in muscle during contraction. *Nature*, *4412*(4412), 971–973.

Huxley, H. E., & Hanson, J. (1954). Changes in the Cross-Striations of Muscle during Contraction and Stretch and their Structural Interpretation. *Nature*.

Hypertrophic Cardiomyopathy (HCM) | American Heart Association. (n.d.). Retrieved December 14, 2020, from https://www.heart.org/en/health-topics/cardiomyopathy/what-is-cardiomyopathy-in-adults/hypertrophic-cardiomyopathy

Hypertrophic cardiomyopathy (HCM) | BHF. (n.d.). Retrieved December 14, 2020, from https://www.bhf.org.uk/informationsupport/conditions/cardiomyopathy/hypertrophic-cardiomyopathy

Hyun, S. J., Komatsu, S., Ikebe, M., & Craig, R. (2008). Head-head and head-tail interaction: A general mechanism for switching off myosin II activity in cells. *Molecular Biology of the Cell*, *19*(8), 3234–3242. https://doi.org/10.1091/mbc.E08-02-0206

Irving, T. C., & Craig, R. (2019). Getting into the thick (and thin) of it. In *Journal of General Physiology* (Vol. 151, Issue 5, pp. 610–613). Rockefeller University Press. https://doi.org/10.1085/jgp.201812307

J.R.Sellers. (2006). CONTRACTILE PROTEINS. In *Encyclopedia of Respiratory Medicine* (pp. 561–567).

Jääskeläinen, P., Miettinen, R., Kärkkäinen, P., Toivonen, L., Laakso, M., & Kuusisto, J. (2004). Genetics of hypertrophic cardiomyopathy in eastern Finland: Few founder mutations with benign or intermediary phenotypes. In *Annals of Medicine* (Vol. 36, Issue 1, pp. 23–32). Ann Med. https://doi.org/10.1080/07853890310017161

Jung, H. S., Billington, N., Thirumurugan, K., Salzameda, B., Cremo, C. R., Chalovich, J. M., Chantler, P. D., & Knight, P. J. (2011). Role of the tail in the regulated state of myosin 2. *Journal of Molecular Biology*, *408*(5), 863–878. https://doi.org/10.1016/j.jmb.2011.03.019

Kabaeva, Z., Perrot, A., Wolter, B., Dietz, R., Cardim, N., Correia, J. M., Schulte, H. D., Aldashev, A. A., Mirrakhimov, M. M., & Osterziel, K. J. (2002). Systematic analysis of the regulatory and essential myosin light chain genes: Genetic variants and mutations in hypertrophic cardiomyopathy. *European Journal of Human Genetics*, *10*(11), 741–748. https://doi.org/10.1038/sj.ejhg.5200872

Kampourakis, T., Ponnam, S., & Irving, M. (2018). Hypertrophic cardiomyopathy mutation R58Q in the myosin regulatory light chain perturbs thick filament-based regulation in cardiac muscle. *Journal of Molecular and Cellular Cardiology*, *117*(February), 72–81. https://doi.org/10.1016/j.yjmcc.2018.02.009

Kaplinsky, E., & Mallarkey, G. (2018). Cardiac myosin activators for heart failure therapy: focus on omecamtiv mecarbil. *Drugs in Context*, *7*, 1–10. https://doi.org/10.7573/dic.212518

Katzemich, A., Kreisköther, N., Alexandrovich, A., Elliott, C., Schöck, F., Leonard, K., Sparrow, J., & Bullard, B. (2012). The function of the M-line protein obscurin in controlling the symmetry of the sarcomere in the flight muscle of Drosophila. *Journal of Cell Science*, *125*(17), 4170–4170. https://doi.org/10.1242/jcs.119552

Kimura, A., Harada, H., Park, J. E., Nishi, H., Satoh, M., Takahashi, M., Hiroi, S., Sasaoka, T., Ohbuchi, N., Nakamura, T., Koyanagi, T., Hwang, T. H., Choo, J. A., Chung, K. S., Hasegawa, A., Nagai, R., Okazaki, O., Nakamura, H., Matsuzaki, M., … Sasazuki, T. (1997). Mutations in the cardiac troponin I gene associated with hypertrophic cardiomyopathy. *Nature Genetics*, *16*(4), 379–382. https://doi.org/10.1038/ng0897-379

Knöll, R., Hoshijima, M., & Chien, K. R. (2002). Z-line proteins: Implications for additional functions. *European Heart Journal, Supplement*, *4*(I), 13–17. https://doi.org/10.1016/S1520-765X(02)90105-7

Koretz, J. F. (1979). Effects of C-protein on synthetic myosin filament structure. *Biophysical Journal*, *27*(3), 433–446. https://doi.org/10.1016/S0006-3495(79)85227-3

Kubo, T., Kitaoka, H., Okawa, M., Matsumura, Y., Hitomi, N., Yamasaki, N., Furuno, T., Takata, J., Nishinaga, M., Kimura, A., & Doi, Y. L. (2005). Lifelong left ventricular remodeling of hypertrophic cardiomyopathy caused by a founder frameshift deletion mutation in the cardiac myosin-binding protein C gene among Japanese. *Journal of the American College of Cardiology*, *46*(9), 1737–1743. https://doi.org/10.1016/j.jacc.2005.05.087

Kunst, G., Kress, K. R., Gruen, M., Uttenweiler, D., Gautel, M., & Fink, R. H. A. (2000). Myosin binding protein C, a phosphorylation-dependent force regulator in muscle that controls the attachment of myosin heads by its interaction with myosin S2. *Circulation Research*, *86*(1), 51–58. https://doi.org/10.1161/01.RES.86.1.51

Labeit, S., & Kolmerer, B. (1995). Titins: Giant proteins in charge of muscle ultrastructure and elasticity. *Science*, *270*(5234), 293–296. https://doi.org/10.1126/science.270.5234.293

Landis, C. A., Bobkova, A., Homsher, E., & Tobacman, L. S. (1997). The active state of the thin filament is destabilized by an internal deletion in tropomyosin. *Journal of Biological Chemistry*, *272*(22), 14051–14056. https://doi.org/10.1074/jbc.272.22.14051

Lange, S., Pinotsis, N., Agarkova, I., & Ehler, E. (2020). The M-band: The underestimated part of the sarcomere. *Biochimica et Biophysica Acta - Molecular Cell Research*, *1867*(3). https://doi.org/10.1016/j.bbamcr.2019.02.003

Lehman, W., & Craig, R. (2008). Tropomyosin and the steric mechanism of muscle regulation. *Advances in Experimental Medicine and Biology*, *644*, 95–109. https://doi.org/10.1007/978-0-387-85766-4_8

Lehman, W., Craig, R., & Vibert, P. (1994). Ca2+-induced tropomyosin movement in Limulus thin filaments revealed by three-dimensional reconstruction. *Nature*, *368*(6466), 65–67. https://doi.org/10.1038/368065a0

Lehman, W., Vibert, P., Uman, P., & Craig, R. (1995). Steric-blocking by tropomyosin visualized in relaxed vertebrate muscle thin filaments. In *Journal of Molecular Biology* (Vol. 251, Issue 2, pp. 191–196). J Mol Biol. https://doi.org/10.1006/jmbi.1995.0425

Levine, R. J. C., Kensler, R. W., Yang, Z., Stull, J. T., & Sweeney, H. L. (1996). Myosin light chain phosphorylation affects the structure of rabbit skeletal muscle thick filaments. *Biophysical Journal*, *71*(2), 898–907. https://doi.org/10.1016/S0006-3495(96)79293-7

Li, A., Nelson, S. R., Rahmanseresht, S., Braet, F., Cornachione, A. S., Previs, S. B., O'Leary, T. S., McNamara, J. W., Rassier, D. E., Sadayappan, S., Previs, M. J., & Warshaw, D. M. (2019). Skeletal MyBP-C isoforms tune the molecular contractility of divergent skeletal muscle systems. *Proceedings of the National Academy of Sciences of the United States of America*, *116*(43), 21882–21892. https://doi.org/10.1073/pnas.1910549116

Lorenz, M., Poole, K. J. V., Popp, D., Rosenbaum, G., & Holmes, K. C. (1995). An atomic model of the unregulated thin filament obtained by X-ray fiber diffraction on oriented actin-tropomyosin gels. *Journal of Molecular Biology*, *246*(1), 108–119. https://doi.org/10.1006/jmbi.1994.0070

Lowey, S., Waller, G. S., & Trybus, B. K. M. (1993). Skeletal muscle myosin light chains are essential for physiological speeds of shortening. *Nature*, *365*(September), 454–456.

Luther, P. K. (2009). The vertebrate muscle Z-disc: Sarcomere anchor for structure and signalling. *Journal of Muscle Research and Cell Motility*, *30*(5–6), 171–185.

https://doi.org/10.1007/s10974-009-9189-6

Lymn, R. W., & Taylor, E. W. (1971). Mechanism of Adenosine Triphosphate Hydrolysis by Actomyosin. *Biochemistry*, *10*(25), 4617–4624. https://doi.org/10.1021/bi00801a004

Lynne M. Coluccio. (2008). *Myosins A Superfamily of Molecular Motors*. http://library1.nida.ac.th/termpaper6/sd/2554/19755.pdf

Mak, A. S., & Smillie, L. B. (1981). Non-polymerizable tropomyosin: Preparation, some properties and F-actin binding. *Biochemical and Biophysical Research Communications*, *101*(1), 208–214. https://doi.org/10.1016/S0006-291X(81)80032-0

Margossian, S. S. (1985). Reversible dissociation of dog cardiac myosin regulatory light chain 2 and its influence on ATP hydrolysis. *Journal of Biological Chemistry*, *260*(25), 13747–13754. https://doi.org/10.1016/S0021-9258(17)38789-6

Marian, A. J., & Braunwald, E. (2017). Hypertrophic cardiomyopathy: Genetics, pathogenesis, clinical manifestations, diagnosis, and therapy. *Circulation Research*, *121*(7), 749–770. https://doi.org/10.1161/CIRCRESAHA.117.311059

Mariano, A. C., Alexandre, G. M. C., Silva, L. C., Romeiro, A., Cameron, L. C., Chen, Y., Chase, P. B., & Sorenson, M. M. (2001). Dimethyl sulphoxide enhances the effects of Pi in myofibrils and inhibits the activity of rabbit skeletal muscle contractile proteins. *Biochemical Journal*, *358*(3), 627–636. https://doi.org/10.1042/0264-6021:3580627

Maron, B. J., Gardin, J. M., Flack, J. M., Gidding, S. S., Kurosaki, T. T., & Bild, D. E. (1995). Prevalence of hypertrophic cardiomyopathy in a general population of young adults: Echocardiographic analysis of 4111 subjects in the CARDIA study. *Circulation*, *92*(4), 785–789. https://doi.org/10.1161/01.CIR.92.4.785

McClellan, G., Kulikovskaya, I., & Winegrad, S. (2001). Changes in cardiac contractility related to calcium-mediated changes in phosphorylation of myosin-binding protein C. *Biophysical Journal*, *81*(2), 1083–1092. https://doi.org/10.1016/S0006-3495(01)75765-7

McKillop, D. F., & Geeves, M. A. (1993a). Regulation of the interaction between actin and myosin subfragment 1: evidence for three states of the thin filament. *Biophysical Journal*, *65*(2), 693–701. https://doi.org/10.1016/S0006-3495(93)81110-X

McKillop, D. F., & Geeves, M. A. (1993b). Regulation of the interaction between actin and myosin subfragment 1: evidence for three states of the thin filament. *Biophysical Journal*, *65*(2), 693–701. https://doi.org/10.1016/S0006-3495(93)81110-X

McLachlan, A. D., & Stewart, M. (1976). The 14-fold periodicity in α-tropomyosin and the interaction with actin. *Journal of Molecular Biology*, *103*(2), 271–298. https://doi.org/10.1016/0022-2836(76)90313-2

McNamara, J. W., Li, A., dos Remedios, C. G., & Cooke, R. (2014). The role of super-relaxed myosin in skeletal and cardiac muscle. *Biophysical Reviews*, *7*(1), 5–14. https://doi.org/10.1007/s12551-014-0151-5

McNamara, J. W., Singh, R. R., & Sadayappan, S. (2019). Cardiac myosin binding protein-C phosphorylation regulates the super-relaxed state of myosin. *Proceedings of the National Academy of Sciences of the United States of America*, *116*(24), 11731–11736. https://doi.org/10.1073/pnas.1821660116

Millat, G., Bouvagnet, P., Chevalier, P., Dauphin, C., Simon Jouk, P., Da Costa, A., Prieur, F., Bresson, J. L., Faivre, L., Eicher, J. C., Chassaing, N., Crehalet, H., Porcher, R., Rodriguez-

Lafrasse, C., & Rousson, R. (2010). Prevalence and spectrum of mutations in a cohort of 192 unrelated patients with hypertrophic cardiomyopathy. *European Journal of Medical Genetics*, *53*(5), 261–267. https://doi.org/10.1016/j.ejmg.2010.07.007

Millman, B. M. (1998). The filament lattice of striated muscle. *Physiological Reviews*, *78*(2), 359–391. https://doi.org/10.1152/physrev.1998.78.2.359

Mogensen, J., Klausen, I. C., Pedersen, A. K., Egeblad, H., Bross, P., Kruse, T. A., Gregersen, N., Hansen, P. S., Baandrup, U., & Børglum, A. D. (1999). α-cardiac actin is a novel disease gene in familial hypertrophic cardiomyopathy. *Journal of Clinical Investigation*, *103*(10). https://doi.org/10.1172/JCI6460

Moos, C., Mason, C. M., Besterman, J. M., Feng, I. N. M., & Dubin, J. H. (1978). The binding of skeletal muscle C-protein to F-actin, and its relation to the interaction of actin with myosin subfragment-1. *Journal of Molecular Biology*, *124*(4), 571–586. https://doi.org/10.1016/0022-2836(78)90172-9

Moss, R. L., & Fitzsimons, D. P. (2010). Regulation of contraction in mammalian striated muscles the plot thick-ens. *Journal of General Physiology*, *136*(1), 21–27. https://doi.org/10.1085/jgp.201010471

Moss, R. L., Giulian, G. G., & Greaser, M. L. (1985). The effects of partial extraction of TnC upon the tension-pCa relationship in rabbit skinned skeletal muscle fibers. *Journal of General Physiology*, *86*(4), 585–600. https://doi.org/10.1085/jgp.86.4.585

Mukund, K., & Subramaniam, S. (2020). Skeletal muscle: A review of molecular structure and function, in health and disease. *Wiley Interdisciplinary Reviews: Systems Biology and Medicine*, *12*(1), 1–46. https://doi.org/10.1002/wsbm.1462

Myosin subfragment-1: structure and function of a molecular motor. (2007). *Strength And Conditioning*, *21*(2), 500–505.

Naber, N., Cooke, R., & Pate, E. (2011). Slow myosin ATP turnover in the super-relaxed state in tarantula muscle. *Journal of Molecular Biology*, *411*(5), 943–950. https://doi.org/10.1016/j.jmb.2011.06.051

Nelson, S. R., Li, A., Beck-Previs, S., Kennedy, G. G., & Warshaw, D. M. (2020). Imaging ATP Consumption in Resting Skeletal Muscle: One Molecule at a Time. *Biophysical Journal*, *119*(6), 1050–1055. https://doi.org/10.1016/j.bpj.2020.07.036

Niimura, H., Bachinski, L. L., Sangwatanaroj, S., Watkins, H., Chudley, A. E., McKenna, W., Kristinsson, A., Roberts, R., Sole, M., Maron, B. J., Seidman, J. G., Seidman, C. E., Thierfelder, L., Jarcho, J. A., Anastasakis, A., Toutouzas, P., Elstein, E., Liew, C.-C., Liew, J., … Bjornsdottir, H. (1998). Mutations in the Gene for Cardiac Myosin-Binding Protein C and Late-Onset Familial Hypertrophic Cardiomyopathy. *New England Journal of Medicine*, *338*(18), 1248–1257. https://doi.org/10.1056/nejm199804303381802

Nogara, L., Naber, N., Pate, E., Canton, M., Reggiani, C., & Cooke, R. (2016). Piperine's mitigation of obesity and diabetes can be explained by its up-regulation of the metabolic rate of resting muscle. *Proceedings of the National Academy of Sciences of the United States of America*, *113*(46), 13009–13014. https://doi.org/10.1073/pnas.1607536113

Padrón, R., Panté, N., Sosa, H., & Kendrick-Jones, J. (1991). X-ray diffraction study of the structural changes accompanying phosphorylation of tarantula muscle. *Journal of Muscle Research and Cell Motility*, *12*(3), 235–241. https://doi.org/10.1007/BF01745112

Pandzic, E., Morkel, C. A., Li, A., Cooke, R., Whan, R. M., & dos Remedios, C. G. (2020). Nanomolar

ATP binding to single myosin cross-bridges in rigor: a molecular approach to studying myosin ATP kinetics using single human cardiomyocytes. *Biophysical Reviews*, *12*(4), 1031–1040. https://doi.org/10.1007/s12551-020-00716-2

Phillips, G. N., Fillers, J. P., & Cohen, C. (1986). Tropomyosin crystal structure and muscle regulation. *Journal of Molecular Biology*, *192*(1), 111–127. https://doi.org/10.1016/0022-2836(86)90468-7

Pirani, A., Xu, C., Hatch, V., Craig, R., Tobacman, L. S., & Lehman, W. (2005). Single particle analysis of relaxed and activated muscle thin filaments. *Journal of Molecular Biology*, *346*(3), 761–772. https://doi.org/10.1016/j.jmb.2004.12.013

Poetter, K., Jiang, H., Hassanzadeh, S., Master, S. R., Chang, A., Dalakas, M. C., Rayment, I., Sellers, J. R., Fananapazir, L., & Epstein, N. D. (1996). Mutations in either the essential or regulatory light chains of myosin are associated with a rare myopathy in human heart and skeletal muscle. *Nature Genetics*, *13*(1), 63–69. https://doi.org/10.1038/ng0596-63

Poole, K. J. V., Lorenz, M., Evans, G., Rosenbaum, G., Pirani, A., Craig, R., Tobacman, L. S., Lehman, W., & Holmes, K. C. (2006). A comparison of muscle thin filament models obtained from electron microscopy reconstructions and low-angle X-ray fibre diagrams from non-overlap muscle. *Journal of Structural Biology*, *155*(2), 273–284. https://doi.org/10.1016/j.jsb.2006.02.020

Potter, J. D., & Gergely, J. (1974). Troponin, tripomyosin, and actin interactions in the Ca2+ ion regulation of muscle contraction. *Biochemistry*, *13*(13), 2697–2703. https://doi.org/10.1021/bi00710a007

Potter, J. D., Sheng, Z., Pan, B. S., & Zhao, J. (1995). A direct regulatory role for troponin T and a dual role for troponin C in the Ca2+ regulation of muscle contraction. *Journal of Biological Chemistry*, *270*(6), 2557–2562. https://doi.org/10.1074/jbc.270.6.2557

Ratti, J., Rostkova, E., Gautel, M., & Pfuhl, M. (2011). Structure and interactions of myosin-binding protein C domain C0: Cardiac-specific regulation of myosin at its neck? *Journal of Biological Chemistry*, *286*(14), 12650–12658. https://doi.org/10.1074/jbc.M110.156646

Rayment, I., & Holden, H. M. (1993). Myosin subfragment-1: structure and function of a molecular motor. Current opinion in structural biology 1993, 3:944-952. *Current Opinion in Structural Biology*, *3*(6), 944–952. https://doi.org/10.1016/0959-440X(93)90160-M

Richard, P., Charron, P., Carrier, L., Ledeuil, C., Cheav, T., Pichereau, C., Benaiche, A., Isnard, R., Dubourg, O., Burban, M., Gueffet, J. P., Millaire, A., Desnos, M., Schwartz, K., Hainque, B., & Komajda, M. (2003). Hypertrophic cardiomyopathy: Distribution of disease genes, spectrum of mutations, and implications for a molecular diagnosis strategy. *Circulation*, *107*(17), 2227–2232. https://doi.org/10.1161/01.CIR.0000066323.15244.54

Rust, M. J., Bates, M., & Zhuang, X. (2006). Sub-diffraction-limit imaging by stochastic optical reconstruction microscopy (STORM). *Nature Methods*, *3*(10), 793–795. https://doi.org/10.1038/nmeth929

Sa, N., Tomasic, I., Gollapudi, S., Evangelista, F., Green, K., & Nag, S. (2018). Abstract 572: Role Of Human Cardiac RLC In Modulating The Super-relaxed State Of Myosin: A Cardiomyopathy Perspective. *Circulation Research*, *123*(Suppl_1). https://doi.org/10.1161/res.123.suppl_1.572

Schlossarek, S., Mearini, G., & Carrier, L. (2011). Cardiac myosin-binding protein C in hypertrophic cardiomyopathy: Mechanisms and therapeutic opportunities. In *Journal of Molecular and*

Cellular Cardiology (Vol. 50, Issue 4, pp. 613–620). J Mol Cell Cardiol. https://doi.org/10.1016/j.yjmcc.2011.01.014

Scruggs, S. B., Hinken, A. C., Thawornkaiwong, A., Robbins, J., Walker, L. A., de Tombe, P. P., Geenen, D. L., Buttrick, P. M., & Solaro, R. J. (2009). Ablation of ventricular myosin regulatory light chain phosphorylation in mice causes cardiac dysfunction in situ and affects neighboring myofilament protein phosphorylation. *Journal of Biological Chemistry*, *284*(8), 5097–5106. https://doi.org/10.1074/jbc.M807414200

Scruggs, S. B., Reisdorph, R., Armstrong, M. L., Warren, C. M., Reisdorph, N., Solaro, R. J., & Buttrick, P. M. (2010). A Novel, in-solution separation of endogenous cardiac sarcomeric proteins and identification of distinct charged variants of regulatory light chain. *Molecular and Cellular Proteomics*, *9*(9), 1804–1818. https://doi.org/10.1074/mcp.M110.000075

Shaffer, J. F., Kensler, R. W., & Harris, S. P. (2009). The myosin-binding protein C motif binds to F-actin in a phosphorylation-sensitive manner. *Journal of Biological Chemistry*, *284*(18), 12318–12327. https://doi.org/10.1074/jbc.M808850200

Sorenson, M. M., Da Silva, A. C. R., Gouveia, C. S., Sousa, V. P., Oshima, W., Ferro, J. A., & Reinach, F. C. (1995). Concerted action of the high affinity calcium binding sites in skeletal muscle troponin C. *Journal of Biological Chemistry*, *270*(17), 9770–9777. https://doi.org/10.1074/jbc.270.17.9770

Srivastava, D., & Yu, S. (2006). Stretching to meet needs: Integrin-linked kinase and the cardiac pump. *Genes and Development*, *20*(17), 2327–2331. https://doi.org/10.1101/gad.1472506

Stewart, M. A., Franks-Skiba, K., Chen, S., & Cooke, R. (2010a). Myosin ATP turnover rate is a mechanism involved in thermogenesis in resting skeletal muscle fibers. *Proceedings of the National Academy of Sciences of the United States of America*, *107*(1), 430–435. https://doi.org/10.1073/pnas.0909468107

Stewart, M. A., Franks-Skiba, K., Chen, S., & Cooke, R. (2010b). Myosin ATP turnover rate is a mechanism involved in thermogenesis in resting skeletal muscle fibers. *Proceedings of the National Academy of Sciences of the United States of America*, *107*(1), 430–435. https://doi.org/10.1073/pnas.0909468107

Sulbarán, G., Biasutto, A., Alamo, L., Riggs, C., Pinto, A., Méndez, F., Craig, R., & Padrón, R. (2013). Different head environments in tarantula thick filaments support a cooperative activation process. *Biophysical Journal*, *105*(9), 2114–2122. https://doi.org/10.1016/j.bpj.2013.09.001

Suraneni, P., Fogelson, B., Rubinstein, B., Noguera, P., Volkmann, N., Hanein, D., Mogilner, A., & Li, R. (2015). A mechanism of leading-edge protrusion in the absence of Arp2/3 complex. *Molecular Biology of the Cell*, *26*(5), 901–912. https://doi.org/10.1091/mbc.E14-07-1250

Sweeney, H. L., Brito, R. M. M., Rosevear, P. R., & Putkey, J. A. (1990). The low-affinity Ca2+-binding sites in cardiac/slow skeletal muscle troponin C perform distinct functions: Site I alone cannot trigger contraction. *Proceedings of the National Academy of Sciences of the United States of America*, *87*(24), 9538–9542. https://doi.org/10.1073/pnas.87.24.9538

Sweeney, H. Lee, Yang, Z., Zhi, G., Stull, J. T., & Trybus, K. M. (1994). Charge replacement near the phosphorylatable serine of the myosin regulatory light chain mimics aspects of phosphorylation. *Proceedings of the National Academy of Sciences of the United States of America*, *91*(4), 1490–1494. https://doi.org/10.1073/pnas.91.4.1490

Swenson, C. A., & Stellwagen, N. C. (1989). Flexibility of smooth and skletal tropomyosins. *Biopolymers*, *28*(5), 955–963. https://doi.org/10.1002/bip.360280504

Szent-Györgyi, A. G. (1975). Calcium regulation of muscle contraction. *Biophysical Journal*, *15*(7), 707–723. https://doi.org/10.1016/S0006-3495(75)85849-8

Takeda, S., Yamashita, A., Maeda, K., & Maéda, Y. (2003). Structure of the core domain of human cardiac troponin in the Ca2+-saturated form. *Nature*, *424*(6944), 35–41. https://doi.org/10.1038/nature01780

Teekakirikul, P., Zhu, W., Huang, H. C., & Fung, E. (2019). Hypertrophic cardiomyopathy: An overview of genetics and management. *Biomolecules*, *9*(12), 1–11. https://doi.org/10.3390/biom9120878

The incredible things we know about your heart and blood - BBC Future. (n.d.). Retrieved December 14, 2020, from https://www.bbc.com/future/article/20160520-the-incredible-things-we-know-about-your-heart-and-blood

Thierfelder, L., Watkins, H., MacRae, C., Lamas, R., McKenna, W., Vosberg, H. P., Seldman, J. G., & Seidman, C. E. (1994). α-tropomyosin and cardiac troponin T mutations cause familial hypertrophic cardiomyopathy: A disease of the sarcomere. *Cell*, *77*(5), 701–712. https://doi.org/10.1016/0092-8674(94)90054-X

Toepfer, C., Caorsi, V., Kampourakis, T., Sikkel, M. B., West, T. G., Leung, M. C., Al-Saud, S. A., MacLeod, K. T., Lyon, A. R., Marston, S. B., Sellers, J. R., & Ferenczi, M. A. (2013). Myosin regulatory light chain (RLC) phosphorylation change as a modulator of cardiac muscle contraction in disease. *Journal of Biological Chemistry*, *288*(19), 13446–13454. https://doi.org/10.1074/jbc.M113.455444

Tripet, B., Van Eyk, J. E., & Hodges, R. S. (1997). Mapping of a second actin-tropomyosin and a second troponin C binding site within the C terminus of troponin I, and their importance in the Ca2+-dependent regulation of muscle contraction. *Journal of Molecular Biology*, *271*(5), 728–750. https://doi.org/10.1006/jmbi.1997.1200

Van De Linde, S., Löschberger, A., Klein, T., Heidbreder, M., Wolter, S., Heilemann, M., & Sauer, M. (2011). Direct stochastic optical reconstruction microscopy with standard fluorescent probes. *Nature Protocols*, *6*(7), 991–1009. https://doi.org/10.1038/nprot.2011.336

van Eerd, J. P., & Takahashi, K. (1976). Determination of the Complete Amino Acid Sequence of Bovine Cardiac Troponin C. *Biochemistry*, *15*(5), 1171–1180. https://doi.org/10.1021/bi00650a033

Vibert, P., Craig, R., & Lehman, W. (1997). Steric-model for activation of muscle thin filaments. *Journal of Molecular Biology*, *266*(1), 8–14. https://doi.org/10.1006/jmbi.1996.0800

Von Der Ecken, J., Müller, M., Lehman, W., Manstein, D. J., Penczek, P. A., & Raunser, S. (2015). Structure of the F-actin-tropomyosin complex. *Nature*, *519*(7541), 114–117. https://doi.org/10.1038/nature14033

Wang, K., Mccarter, R., Wright, J., Beverly, J., & Ramirez-Mitchell, R. (1991). Regulation of skeletal muscle stiffness and elasticity by titin isoforms: A test of the segmental extension model of resting tension. *Proceedings of the National Academy of Sciences of the United States of America*, *88*(16), 7101–7105. https://doi.org/10.1073/pnas.88.16.7101

Wang, L., Geist, J., Grogan, A., Hu, L. Y. R., & Kontrogianni-Konstantopoulos, A. (2018). Thick filament protein network, functions, and disease association. *Comprehensive Physiology*, *8*(2), 631–709. https://doi.org/10.1002/cphy.c170023

Wendt, T., Taylor, D., Messier, T., Trybus, K. M., & Taylor, K. A. (1999). Visualization of head-head interactions in the inhibited state of smooth muscle myosin. *Journal of Cell Biology*, *147*(7),

1385–1389. https://doi.org/10.1083/jcb.147.7.1385

Wendt, T., Taylor, D., Trybus, K. M., & Taylor, K. (2001). Three-dimensional image reconstruction of dephosphorylated smooth muscle heavy meromyosin reveals asymmetry in the interaction between myosin heads and placement of subfragment 2. *Proceedings of the National Academy of Sciences of the United States of America*, *98*(8), 4361–4366. https://doi.org/10.1073/pnas.071051098

Wilson, C., Naber, N., Pate, E., & Cooke, R. (2014). The myosin inhibitor blebbistatin stabilizes the super-relaxed state in skeletal muscle. *Biophysical Journal*, *107*(7), 1637–1646. https://doi.org/10.1016/j.bpj.2014.07.075

Wittinghofer, A., & Geeves, M. A. (2016). Review: The ATPase mechanism of myosin and actomyosin. *Biopolymers*, *105*(8), 483–491. https://doi.org/10.1002/bip.22853

Woodhead, J. L., Zhao, F. Q., Craig, R., Egelman, E. H., Alamo, L., & Padrón, R. (2005). Atomic model of a myosin filament in the relaxed state. *Nature*, *436*(7054), 1195–1199. https://doi.org/10.1038/nature03920

Xu, C., Craig, R., Tobacman, L., Horowitz, R., & Lehman, W. (1999). Tropomyosin positions in regulated thin filaments revealed by cryoelectron microscopy. *Biophysical Journal*, *77*(2), 985–992. https://doi.org/10.1016/S0006-3495(99)76949-3

Xu, J., Ma, H., & Liu, Y. (2017). Stochastic optical reconstruction microscopy (STORM). *Current Protocols in Cytometry*, *2017*, 12.46.1-12.46.27. https://doi.org/10.1002/cpcy.23

Yamada, Y., Namba, K., & Fujii, T. (2020). Cardiac muscle thin filament structures reveal calcium regulatory mechanism. *Nature Communications*, *11*(1), 1–3. https://doi.org/10.1038/s41467-019-14008-1

Yuan, C. C., Muthu, P., Kazmierczak, K., Liang, J., Huang, W., Irving, T. C., Kanashiro-Takeuchi, R. M., Hare, J. M., & Szczesna-Cordary, D. (2015). Constitutive phosphorylation of cardiac myosin regulatory light chain prevents development of hypertrophic cardiomyopathy in mice. *Proceedings of the National Academy of Sciences of the United States of America*, *112*(30), E4138–E4146. https://doi.org/10.1073/pnas.1505819112

Zhao, F. Q., Padrón, R., & Craig, R. (2008). Blebbistatin stabilizes the helical order of myosin filaments by promoting the switch 2 closed state. *Biophysical Journal*, *95*(7), 3322–3329. https://doi.org/10.1529/biophysj.108.137067

Zoghbi, M. E., Woodhead, J. L., Moss, R. L., & Craig, R. (2008). Three-dimensional structure of vertebrate cardiac muscle myosin filaments. *Proceedings of the National Academy of Sciences of the United States of America*, *105*(7), 2386–2390. https://doi.org/10.1073/pnas.0708912105

Ackermann, Maegen A., and Aikaterini Kontrogianni-Konstantopoulos. 2011. “Myosin Binding Protein-C Slow Is a Novel Substrate for Protein Kinase A (PKA) and C (PKC) in Skeletal Muscle.” *Journal of Proteome Research* 10 (10): 4547–55.

Brito, Reicy, Lorenzo Alamo, Ulf Lundberg, José R. Guerrero, Antonio Pinto, Guidenn Sulbarán, Mary Ann Gawinowicz, Roger Craig, and Raúl Padrón. 2011. “A Molecular Model of Phosphorylation-Based Activation and Potentiation of Tarantula Muscle Thick Filaments.” *Journal of Molecular Biology* 414 (1): 44–61.

Carrara, Serena. 2017. “Towards New Efficient Nanostructured Hybrid Materials for ECL Applications,” April. http://dx.doi.org/.

Colson, Brett A., Jitandrakumar R. Patel, Peter P. Chen, Tanya Bekyarova, Mohamed I. Abdalla, Carl W. Tong, Daniel P. Fitzsimons, Thomas C. Irving, and Richard L. Moss. 2012. “Myosin Binding Protein-C Phosphorylation Is the Principal Mediator of Protein Kinase A Effects on Thick Filament Structure in Myocardium.” *Journal of Molecular and Cellular Cardiology* 53 (5): 609–16.

“File:G-Actin Subdomains.Png.” n.d. Accessed November 29, 2021. https://commons.wikimedia.org/wiki/File:G-actin_subdomains.png.

Hooijman, Pleuni, Melanie A. Stewart, and Roger Cooke. 2011. “A New State of Cardiac Myosin with Very Slow ATP Turnover: A Potential Cardioprotective Mechanism in the Heart.” *Biophysical Journal* 100 (8): 1969–76.

Huxley, A. F., and R. Niedergerke. 1954. “Structural Changes in Muscle during Contraction.” *Nature* 4412 (4412): 971–73.

Lim, M. S., and M. P. Walsh. 1986. “Phosphorylation of Skeletal and Cardiac Muscle C-Proteins by the Catalytic Subunit of CAMP-Dependent Protein Kinase.” *Biochemistry and Cell Biology = Biochimie et Biologie Cellulaire* 64 (7): 622–30.

McNamara, James W., Amy Li, Cristobal G. dos Remedios, and Roger Cooke. 2014. “The Role of Super-Relaxed Myosin in Skeletal and Cardiac Muscle.” *Biophysical Reviews* 7 (1): 5–14.

“Muscle Types.” n.d. Accessed November 29, 2021. https://socratic.org/questions/is-the-diaphragm-a-smooth-muscle-or-a-skeletal-muscle.

Nelson, Shane R., Amy Li, Samantha Beck-Previs, Guy G. Kennedy, and David M. Warshaw. 2020. “Imaging ATP Consumption in Resting Skeletal Muscle: One Molecule at a Time.” *Biophysical Journal* 119 (6): 1050–55.

“Origin 2022 Feature Highlights.” n.d. Accessed December 8, 2021. https://www.originlab.com/index.aspx?go=Products/Origin/2022&pid=4418.

Russell, Alan J., and Edgewise Therapeutics. 2021. “Selective Inhibition of Fast Skeletal Muscle Myosin as a Novel Therapeutic Strategy for Muscular Dystrophy.” June 28, 2021. https://edgewisetx.com/wp-content/uploads/2021/07/2021_06_28_New_Directions_Presentation_EDGEWISE-V2.pdf.

Samanthi. 2017. “Difference Between Myofibril and Muscle Fiber.” Differencebetween.com. July 17, 2017. https://www.differencebetween.com/difference-between-myofibril-and-vs-muscle-fiber/.

Sulbarán, Guidenn, Antonio Biasutto, Lorenzo Alamo, Claire Riggs, Antonio Pinto, Franklin Méndez, Roger Craig, and Raúl Padrón. 2013. “Different Head Environments in Tarantula Thick Filaments Support a Cooperative Activation Process.” *Biophysical Journal* 105 (9): 2114–22.

Wikipedia contributors. 2021. “Sarcomere.” Wikipedia, The Free Encyclopedia. October 8, 2021. https://en.wikipedia.org/w/index.php?title=Sarcomere&oldid=1048826422.

Woodhead, John L., Fa Qing Zhao, Roger Craig, Edward H. Egelman, Lorenzo Alamo, and Raúl Padrón. 2005. “Atomic Model of a Myosin Filament in the Relaxed State.” *Nature* 436 (7054): 1195–99.

Yamada, Yurika, Keiichi Namba, and Takashi Fujii. 2020. “Cardiac Muscle Thin Filament Structures Reveal Calcium Regulatory Mechanism.” *Nature Communications* 11 (1): 1–3.